

# FIELD VERIFICATION OF GEOGRID PROPERTIES FOR BASE COURSE REINFORCEMENT APPLICATIONS

FINAL REPORT ~ FHWA-OK-13-11  
ODOT SP&R ITEM NUMBER 2244

**Submitted to:**

John R. Bowman, P.E.  
Planning & Research Division Engineer  
Oklahoma Department of Transportation

**Submitted by:**

Kianoosh Hatami, Ph.D., P.Eng.  
Tahsina Mahmood, Ph.D.  
Juan Pereira-Villarroel, M.Sc. Candidate  
School of Civil Engineering and Environmental Science (CEES)  
University of Oklahoma



November 2013

## TECHNICAL REPORT DOCUMENTATION PAGE

|   |  |   |                  |
|---|--|---|------------------|
| 1. REPORT NO.<br>FHWA-OK- 13-11   | 2. GOVERNMENT ACCESSION NO.                          | 3. RECIPIENT'S CATALOG NO.  |                  |
| 4. TITLE AND SUBTITLE<br>Field Verification of Geogrid Properties for Base Course Reinforcement Applications  |  | 5. REPORT DATE<br>Nov 2013  |                  |
|   |  | 6. PERFORMING ORGANIZATION CODE   |                  |
| 7. AUTHOR(S)<br>Kianoosh Hatami, Ph.D., P.Eng., Tahsina Mahmood, Ph.D., Juan Pereira-Villarroel, M.Sc. Candidate  |  | 8. PERFORMING ORGANIZATION REPORT<br><a href="#">Click here to enter text.</a>  |                  |
| 9. PERFORMING ORGANIZATION NAME AND ADDRESS<br>University of Oklahoma<br>School of Civil Engineering and Environmental Science<br>202 W. Boyd Street, Room 334, Norman, OK 73019  |  | 10. WORK UNIT NO.   |                  |
|   |  | 11. CONTRACT OR GRANT NO.<br>ODOT SP&R Item Number 2244   |                  |
| 12. SPONSORING AGENCY NAME AND ADDRESS<br>Oklahoma Department of Transportation<br>Planning and Research Division<br>200 N.E. 21st Street, Room 3A7<br>Oklahoma City, OK 73105  |  | 13. TYPE OF REPORT AND PERIOD COVERED<br>Final Report<br>Oct 2012 - Sep 2013  |                  |
|   |  | 14. SPONSORING AGENCY CODE  |                  |
| 15. SUPPLEMENTARY NOTES<br><a href="#">Click here to enter text.</a>  |  |   |                  |
| 16. ABSTRACT<br>The proposed field study is a continuation of a recently concluded, ODOT-funded project titled: Development of ODOT Guidelines for the Use of Geogrids in Aggregate Bases, which is aimed at addressing the need for improved guidelines for base reinforcement applications. One important objective of this long-term study is to develop a correlation between the index properties of geogrids and their field performance for base reinforcement applications. The index properties that will be studied include the junction strength, low-strain rib strength (i.e. strength at 2%-strain and 5%-strain) and the ultimate rib strength of selected geogrids. The project will involve the selection of a full-depth roadway construction project authorized by ODOT. During the construction of the road subgrade, one test section will be used to examine and compare the performance of selected base course reinforcement geogrid products. The field performance of different geogrids will be monitored using different instruments and monitoring techniques and compared with one another as a function of their index properties. Selected instruments include Earth Pressure Cells (EPC) to measure the stress on the subgrade underneath the geogrid, pore pressure transducers to measure the pore pressure in the subgrade and strain gauges to measure the tensile strength of the different geosynthetics. The results of this study will help ODOT to develop an improved and expanded set of materials specification guidelines for the use of geogrids in aggregate base reinforcement applications. The outcome of this study will help ODOT and other transportation agencies in the U.S. develop more durable and economical aggregate base designs which will result in longer service life and reduced maintenance costs for the roadways in Oklahoma and across the United States. |  |   |                  |
| 17. KEY WORDS<br>Geogrid, geotextile, geosynthetics, subgrade, aggregate, strength, field test section, cyclic plate load   |  | 18. DISTRIBUTION STATEMENT<br>No restrictions. This publication is available from the Planning & Research Div., Oklahoma DOT. |                  |
| 19. SECURITY CLASSIF. (OF THIS REPORT)<br>Unclassified  | 20. SECURITY CLASSIF. (OF THIS PAGE)<br>Unclassified | 21. NO. OF PAGES<br>215   | 22. PRICE<br>N/A |

The contents of this report reflect the views of the author(s) who is responsible for the facts and the accuracy of the data presented herein. The contents do not necessarily reflect the views of the Oklahoma Department of Transportation or the Federal Highway Administration. This report does not constitute a standard, specification, or regulation. While trade names may be used in this report, it is not intended as an endorsement of any machine, contractor, process, or product.

## SI\* (MODERN METRIC) CONVERSION FACTORS

| APPROXIMATE CONVERSIONS TO SI UNITS                                |                            |                             |                             |                   |
|--|----------------------------|-----------------------------|-----------------------------|-------------------|
| SYMBOL   | WHEN YOU KNOW              | MULTIPLY BY                 | TO FIND                     | SYMBOL            |
| <b>LENGTH</b>  |                            |                             |                             |                   |
| in   | inches                     | 25.4                        | millimeters                 | mm                |
| ft   | feet                       | 0.305                       | meters                      | m                 |
| yd   | yards                      | 0.914                       | meters                      | m                 |
| mi   | miles                      | 1.61                        | kilometers                  | km                |
| <b>AREA</b>  |                            |                             |                             |                   |
| in <sup>2</sup>  | square inches              | 645.2                       | square millimeters          | mm <sup>2</sup>   |
| ft <sup>2</sup>  | square feet                | 0.093                       | square meters               | m <sup>2</sup>    |
| yd <sup>2</sup>  | square yard                | 0.836                       | square meters               | m <sup>2</sup>    |
| ac   | acres                      | 0.405                       | hectares                    | ha                |
| mi <sup>2</sup>  | square miles               | 2.59                        | square kilometers           | km <sup>2</sup>   |
| <b>VOLUME</b>  |                            |                             |                             |                   |
| fl oz  | fluid ounces               | 29.57                       | milliliters                 | mL                |
| gal  | gallons                    | 3.785                       | liters                      | L                 |
| ft <sup>3</sup>  | cubic feet                 | 0.028                       | cubic meters                | m <sup>3</sup>    |
| yd <sup>3</sup>  | cubic yards                | 0.765                       | cubic meters                | m <sup>3</sup>    |
| NOTE: volumes greater than 1000 L shall be shown in m <sup>3</sup> |                            |                             |                             |                   |
| <b>MASS</b>  |                            |                             |                             |                   |
| oz   | ounces                     | 28.35                       | grams                       | g                 |
| lb   | pounds                     | 0.454                       | kilograms                   | kg                |
| T  | short tons (2000 lb)       | 0.907                       | megagrams (or "metric ton") | Mg (or "t")       |
| <b>TEMPERATURE (exact degrees)</b>                                 |                            |                             |                             |                   |
| °F   | Fahrenheit                 | 5 (F-32)/9<br>or (F-32)/1.8 | Celsius                     | °C                |
| <b>ILLUMINATION</b>  |                            |                             |                             |                   |
| fc   | foot-candles               | 10.76                       | lux                         | lx                |
| fl   | foot-Lamberts              | 3.426                       | candela/m <sup>2</sup>      | cd/m <sup>2</sup> |
| <b>FORCE and PRESSURE or STRESS</b>                                |                            |                             |                             |                   |
| lbf  | poundforce                 | 4.45                        | newtons                     | N                 |
| lbf/in <sup>2</sup>  | poundforce per square inch | 6.89                        | kilopascals                 | kPa               |

| APPROXIMATE CONVERSIONS FROM SI UNITS |                             |             |                            |                     |
|---------------------------------------|-----------------------------|-------------|----------------------------|---------------------|
| SYMBOL                                | WHEN YOU KNOW               | MULTIPLY BY | TO FIND                    | SYMBOL              |
| <b>LENGTH</b>                         |                             |             |                            |                     |
| mm                                    | millimeters                 | 0.039       | inches                     | in                  |
| m                                     | meters                      | 3.28        | feet                       | ft                  |
| m                                     | meters                      | 1.09        | yards                      | yd                  |
| km                                    | kilometers                  | 0.621       | miles                      | mi                  |
| <b>AREA</b>                           |                             |             |                            |                     |
| mm <sup>2</sup>                       | square millimeters          | 0.0016      | square inches              | in <sup>2</sup>     |
| m <sup>2</sup>                        | square meters               | 10.764      | square feet                | ft <sup>2</sup>     |
| m <sup>2</sup>                        | square meters               | 1.195       | square yards               | yd <sup>2</sup>     |
| ha                                    | hectares                    | 2.47        | acres                      | ac                  |
| km <sup>2</sup>                       | square kilometers           | 0.386       | square miles               | mi <sup>2</sup>     |
| <b>VOLUME</b>                         |                             |             |                            |                     |
| mL                                    | milliliters                 | 0.034       | fluid ounces               | fl oz               |
| L                                     | liters                      | 0.264       | gallons                    | gal                 |
| m <sup>3</sup>                        | cubic meters                | 35.314      | cubic feet                 | ft <sup>3</sup>     |
| m <sup>3</sup>                        | cubic meters                | 1.307       | cubic yards                | yd <sup>3</sup>     |
| <b>MASS</b>                           |                             |             |                            |                     |
| g                                     | grams                       | 0.035       | ounces                     | oz                  |
| kg                                    | kilograms                   | 2.202       | pounds                     | lb                  |
| Mg (or "t")                           | megagrams (or "metric ton") | 1.103       | short tons (2000 lb)       | T                   |
| <b>TEMPERATURE (exact degrees)</b>    |                             |             |                            |                     |
| °C                                    | Celsius                     | 1.8C+32     | Fahrenheit                 | °F                  |
| <b>ILLUMINATION</b>                   |                             |             |                            |                     |
| lx                                    | lux                         | 0.0929      | foot-candles               | fc                  |
| cd/m <sup>2</sup>                     | candela/m <sup>2</sup>      | 0.2919      | foot-Lamberts              | fl                  |
| <b>FORCE and PRESSURE or STRESS</b>   |                             |             |                            |                     |
| N                                     | newtons                     | 0.225       | poundforce                 | lbf                 |
| kPa                                   | kilopascals                 | 0.145       | poundforce per square inch | lbf/in <sup>2</sup> |

\*SI is the symbol for the International System of Units. Appropriate rounding should be made to comply with Section 4 of ASTM E380.

## Table of Contents

|  |            |
|--|------------|
| <b>1. Introduction</b> .....   | <b>1</b>   |
| <b>2. Literature Review</b> .....  | <b>2</b>   |
| <b>3. Field Test Section</b> .....   | <b>113</b> |
| 3.1 Field Project Selection.....   | 113        |
| 3.1.1 Choice of Road Category.....   | 113        |
| 3.1.2 Location .....   | 114        |
| 3.1.3 Annual Average Daily Traffic (AADT).....                                       | 115        |
| 3.1.4 Percentage of Truck Traffic.....   | 116        |
| 3.1.5 Pavement Type.....   | 118        |
| 3.1.6 Proposed Location of the Field Test Section .....                              | 118        |
| 3.2. Selection of Geosynthetic Samples.....  | 122        |
| 3.2.1 Pavement Type.....   | 122        |
| 3.2.2 Reinforced Base Design Methods and Software Available in Practice .....        | 124        |
| 3.3. Test Section Layout.....  | 131        |
| 3.4. Instrumentation Plan .....  | 133        |
| <b>4. Material Characterization</b> .....  | <b>137</b> |
| 4.1 Testing Plan .....   | 137        |
| 4.2 Laboratory Testing on Aggregates .....   | 137        |
| 4.2.1 Los Angeles (LA) Abrasion Test .....   | 137        |
| <b>5. Laboratory Testing of Geosynthetics</b> .....                                  | <b>139</b> |
| <b>6. In Aggregate Laboratory Tests of Geosynthetics for Base Reinforcement.....</b> | <b>149</b> |
| 6.1 Pullout Test .....   | 149        |
| 6.2 Large-Scale Cyclic Plate Load Tests.....   | 151        |
| <b>7. Overall Summary of Work Performed</b> .....                                    | <b>168</b> |
| <b>References</b> .....  | <b>172</b> |
| <b>Appendix A</b> .....  | <b>177</b> |
| <b>Appendix B</b> .....  | <b>187</b> |
| <b>Appendix C</b> .....  | <b>191</b> |

**Appendix D ..... 194**

## List of Figures

|  |    |
|--|----|
| Figure 1. Plan view of the full-scale test section by Black and Holtz (1999) .....   | 3  |
| Figure 2. Average permittivity results in the study by Black and Holtz (1999).....   | 6  |
| Figure 3. Comparison of FWD test results (Northbound lane) in the study by Black and Holtz (1999).....   | 9  |
| Figure 4. Equation proposed by Yu (2000) to relate PRM and the change in base course thickness to the permanent deformation of an aggregate base flexible pavement system..... | 19 |
| Figure 5. Three cases considered for permanent deformation calculations (Yu 2000).....   | 19 |
| Figure 6. Permanent deformation generated by wheel loading passes under unreinforced conditions (Yu 2000) .....  | 20 |
| Figure 7. Permanent deformation generated by wheel loading passes with geogrid at the middle of base layer (Yu 2000) .....   | 21 |
| Figure 8. Permanent deformation generated by wheel loading passes with geogrid at the base-subgrade interface (Yu 2000).....   | 21 |
| Figure 9. Base Damage Index over the life of pavement in the study by Al-Qadi and Appea (2003) .....   | 27 |
| Figure 10. Surface Condition Index over the life of pavement in the study by Al-Qadi and Appea (2003).....   | 27 |
| Figure 11. Rut depths of the 4-inch Base course sections in the study by Al-Qadi and Appea (2003) .....  | 29 |
| Figure 12. Rutting progress over the testing period of the 4-inch base course sections in the study by Al-Qadi and Appea (2003) .....  | 30 |
| Figure 13. Rut depth progression in Sections 1-3 in the study by Al-Qadi and Appea (2003) .....  | 31 |
| Figure 14. Equation for estimating the required base thickness by Giroud and Han (2004a).....  | 34 |

|   |    |
|---|----|
| Figure 15. Calibrated equation for biaxial geogrids in the study by Giroud and Han (2004b).....   | 35 |
| Figure 16. Nomenclature for equation in Figure 15 (Giroud and Han 2004). .....  | 36 |
| Figure 17. Plan view of the full-scale test section (in inches) by Chehab et al. (2007) .....   | 38 |
| Figure 18. Plan view, indicating the instrumented test sections (numbered rectangles) where traffic load was applied in the study by Henry et al. (2008) ...                                | 40 |
| Figure 19. Plan view indicating the locations of instruments in a geogrid test section in the study by Henry et al. (2008).....   | 42 |
| Figure 20. Cross sectional view indicating the locations of instruments in a geogrid test section in the study by Henry et al. (2008) .....   | 42 |
| Figure 21. Orientation of pressure cells in the study by Henry et al. (2008).....   | 43 |
| Figure 22. Wheatstone bridge configuration used for strain gauge measurement in the study by Henry et al. (2008) .....  | 45 |
| Figure 23. Measured pavement layer profiles after excavation (Al-Qadi et al. 2008).....   | 48 |
| Figure 24. Geosynthetic instrumentation layout and gauge protection methods in test sections reported by Warren et al. (2008) .....   | 51 |
| Figure 25. Strain gauge protection methods in the study by Warren et al. (2008): (a) sand cushion; (b) edge-protected PVC pipe; (c) geosynthetic strip drain; (d) neoprene mouse pads. .... | 52 |
| Figure 26. Schematic cross-section of the field test section in Cuelho and Perkins's study (2009) .....   | 57 |
| Figure 27. General layout of test sections (Cuelho and Perkins 2009) .....  | 57 |
| Figure 28. Plan and profile views of the full-scale test section layout in the study by Tingle and Jersey (2009) .....  | 60 |
| Figure 29. Laboratory cyclic plate load test layout in the study by Abu-Farsakh and Chen (2010) .....   | 64 |

|  |    |
|--|----|
| Figure 30. Measured permanent deformation at the base/subgrade interface for tests with different types of geogrids used in the study by Abu-Farsakh and Chen (2010) ..... | 70 |
| Figure 31. Surface permanent deformation for tests with GG3 and GG4 geogrids placed at different locations in the study by Abu-Farsakh and Chen (2010) .....               | 71 |
| Figure 32. Summary of permanent surface deformation profiles for all cyclic plate load tests after 30,000 cycles in the study by Abu-Farsakh and Chen (2010) ....          | 73 |
| Figure 33. Layout of the field cyclic plate load and rolling wheel load test sections in the study by Abu-Farsakh and Chen (2010) .....                                    | 74 |
| Figure 34. Summary of rut depths measured in rolling wheel load test sections in the study by Abu-Farsakh and Chen (2010) .....  | 78 |
| Figure 35. Summary of rut depths measured in cyclic plate load test sections in the study by Abu-Farsakh and Chen (2010) .....   | 79 |
| Figure 36. Comparison of field and laboratory cyclic plate load tests in the study by Abu-Farsakh and Chen (2010).....   | 79 |
| Figure 37. Test section layout in the study by Oh (2011).....  | 81 |
| Figure 38. Falling Weigh Deflectometer results in the study by Oh (2011) .....   | 82 |
| Figure 39. Ground Penetrating Radar data from snapshot at control Section 2 and reinforced Section 3 in the study by Oh (2011) .....                                       | 83 |
| Figure 40. Generated mesh for geogrid reinforced pavement using Plaxis program in the study by Oh (2011) .....   | 87 |
| Figure 41. Profile of test section (Jersey et al. 2012) (CH = High-plasticity Clay; CBR = California Bearing Ratio) .....  | 90 |
| Figure 42. Pavement cross sections during post traffic forensic investigation (Jersey et al. 2012) (a) Item A, (b) Item B, (c) Item C .....                                | 92 |
| Figure 43. Test section layout in the study by Mishra and Tutumluer (2013).....  | 97 |
| Figure 44. Plan (top) and cross-sectional views of the full-scale pavement test sections in the study by Mishra and Tutumluer (2013).....                                  | 98 |

Figure 45. Example of a cell performance after failure in the study by Mishra and Tutumluer (2013) (a) Ground-Penetrating Radar (GPR) scan (b) excavated trench (c) surface rut profile. .... 100

Figure 46. Rut deformation in Cell 6, Section 2 resulting from unidirectional ATLAS loading in the study by Mishra and Tutumluer (2013)..... 101

Figure 47. Pavement structure layout of the test lanes in the study by Wu (2013) ..... 104

Figure 48. Elastic deformation profiles obtained from MDD in the study by Wu (2013) ..... 106

Figure 49. Plastic deformations from MDD in Section 3 in the study by Wu (2013) ..... 107

Figure 50. Dynaflect pavement structure number results in the study by Wu (2013) ..... 108

Figure 51. Map of Oklahoma counties and ODOT divisions (adopted and revised; Source: <http://www.okladot.state.ok.us/aadtcnt/>) ..... 114

Figure 52. Proposed location of a test section located on the Dolese Bros. Co. Prairie Park Sand Plant in Oklahoma City (Hall 2013)..... 120

Figure 53. Cross-section of the unpaved road design proposed by Dolese Bros. Co. Engineering Department..... 121

Figure 54. Design equation for flexible pavements (AASHTO 1993) ..... 126

Figure 55. Structural Number equation for geosynthetic reinforced pavement (AASHTO 1993)..... 127

Figure 56. Tensor design software SpectraPave4 PRO trial results for this study ..... 128

Figure 57. TenCate design software MiraSpec Design Solutions trial results for this study..... 129

Figure 58. Proposed layout of the field road test section for this study (scale: 1:600)..... 133

|   |     |
|---|-----|
| Figure 59. Plan view of a tentative instrumentation plan for different test sections in this project (Scale 1:60) .....   | 135 |
| Figure 60. Typical instrumentation plan intended for each segment of the field test section (Not to scale) .....  | 136 |
| Figure 61. Los Angeles abrasion machine after the test of ODOT Type-A aggregate at Ray Broce Materials Laboratory .....   | 138 |
| Figure 62. A 3-inch-wide specimen of the Mirafi RS580i geotextile at the end of a tensile strength test using the new universal testing machine (model United "Smart-1" STM) at the OU Geosynthetics laboratory ..... | 140 |
| Figure 63. 8-inch-wide specimen of the Mirafi RS580i geotextile subjected to a tensile strength test using the Baldwin hydraulic universal testing machine at the Fears engineering laboratory .....                  | 141 |
| Figure 64. Tensile test results for the Mirafi RS580i geotextile (3 inch-wide specimens) in machine direction.....  | 142 |
| Figure 65. Tensile test results for the Mirafi RS580i geotextile (3-inch-wide specimens)in cross-machine direction .....  | 143 |
| Figure 66. Comparison of geotextile RS580i tensile strength test results in machine direction.....  | 144 |
| Figure 67. Comparison of geotextile RS580i tensile strength test results in cross-machine direction.....  | 144 |
| Figure 68. Tensile test results on Mirafi RS380i geotextile (3 inch-wide specimens) in machine direction.....   | 146 |
| Figure 69. Tensile test results on Mirafi RS380i geotextile (3-inch-wide specimens) in cross-machine direction .....  | 147 |
| Figure 70. A pullout test in progress on Tensar TX 160 geogrid at the OU Geosynthetics laboratory .....   | 150 |
| Figure 71. Pullout response results for TX 160 geogrid in ODOT Type-A aggregate subjected to 69 psf overburden pressure.....  | 150 |
| Figure 72. Cyclic plate load test on Mirafi SR580i geotextile at Donald G. Fears Structural Engineering Laboratory .....  | 152 |

|   |     |
|---|-----|
| Figure 73. Layout of the cyclic plate load tests performed on Mirafi RS580i and RS380i geotextiles (units: inches).....   | 154 |
| Figure 74. Instrumentation layout for the cyclic plate load tests (units: inches)   | 156 |
| Figure 75. Load pulse applied in the cyclic plate load tests .....  | 157 |
| Figure 76. Plate load settlement response during cyclic plate load test on the model with Mirafi RS580i geotextile .....  | 158 |
| Figure 77. Plate load settlement response during cyclic plate load test on the model with Mirafi RS380i geotextile .....  | 158 |
| Figure 78. Total cumulative deflection at the top surface during cyclic plate load test using Mirafi RS580i geotextile.....   | 159 |
| Figure 79. Total cumulative deflection at the top of subgrade during cyclic plate load test using Mirafi RS580i geotextile .....  | 159 |
| Figure 80. Total cumulative deflection at the top surface during cyclic plate load test using Mirafi RS380i geotextile.....   | 160 |
| Figure 81. Total cumulative deflection at the top of subgrade during cyclic plate load test using Mirafi RS380i geotextile .....  | 160 |
| Figure 82. Comparison of top surface deflections between different cyclic plate load tests .....  | 161 |
| Figure 83. Comparison of subgrade deflections at the top between different cyclic plate load tests.....   | 161 |
| Figure 84. Dynamic settlement of the loading plate as measured in different cyclic plate load tests (inches) .....  | 163 |
| Figure 85. Dynamic Settlement Reduction Factors (SRF) from different cyclic plate load tests.....   | 164 |
| Figure 86. Dynamic settlement performance of different test models sorted according to their SRF values (W: woven geogrid, E: extruded geogrid, K: knitted geogrid, GT: geotextile) ..... | 164 |
| Figure 87. Traffic Benefit Ratio (TBR) on different cyclic plate load tests .....   | 165 |

|  |     |
|--|-----|
| Figure 88. Traffic Benefit Ratio from high to low (W: woven geogrid, E: extruded geogrid, K: knitted geogrid, GT: geotextile)..... | 165 |
| Figure 89. AADT data for Canadian County (2011) .....  | 178 |
| Figure 90. AADT data for Cleveland County (2010).....  | 179 |
| Figure 91. AADT data for Garvin County (2011).....   | 180 |
| Figure 92. AADT data for Grady County (2010).....  | 181 |
| Figure 93. AADT data for Lincoln County (2011) .....   | 182 |
| Figure 94. AADT data for Logan County (2011).....  | 183 |
| Figure 95. AADT data for McClain County (2007).....  | 184 |
| Figure 96. AADT data for Oklahoma County (2006-2010) .....   | 185 |
| Figure 97. AADT data for Pottawatomie County (2007).....   | 186 |
| Figure 98. Map representing the locations of candidate roads based on their AADT values .....                                      | 195 |
| Figure 99. Subgrade soil properties along East Robinson Street, Norman, Oklahoma (Source: USDA-WSS).....                           | 197 |
| Figure 100. Subgrade soil properties along Alameda Street, Norman, Oklahoma (Source: USDA-WSS).....                                | 198 |

## List of Tables

|  |    |
|--|----|
| Table 1. Laboratory test results in the study by Black and Holtz (1999) .....  | 4  |
| Table 2. Wide-width test results in the study by Black and Holtz (1999).....   | 7  |
| Table 3. Summary of added-value benefit from previous aggregate base reinforcement projects surveyed by Berg et al. (2000).....                            | 12 |
| Table 4. Qualitative summary of potential geosynthetic reinforcement applications based upon previous research studies reported by Berg et al. (2000)..... | 16 |
| Table 5. Tensile strength and elongation of geosynthetics used in the study by Al-Qadi and Appea (2003).....   | 25 |
| Table 6. Maximum rut depth measured in October 2001 in the study by Al-Qadi and Appea (2003) .....   | 28 |
| Table 7. Service life for Sections 1-3 in the study by Al-Qadi and Appea (2003)  | 31 |
| Table 8. Properties of the geogrid used in the test sections in the study by Henry et al. (2008).....  | 41 |
| Table 9. Pavement test cells and sections (Al-Qadi et al. 2008; 1 inch = 25.4 mm; 1 ft = 0.305 m).....   | 47 |
| Table 10. Survivability of gauge protection methods in the study by Warren et al. (2008) (NA= not applicable) .....  | 54 |
| Table 11. Methodology and findings of the study by Cuelho and Perkins (2009)   | 57 |
| Table 12. Pavement material specifications in the study by Abu-Farsakh and Chen (2010).....  | 65 |
| Table 13. Physical and mechanical properties of geogrids used in the study by Abu-Farsakh and Chen (2010).....   | 66 |
| Table 14. Summary of TBR results from the laboratory cyclic plate load tests in the study by Abu-Farsakh and Chen (2010) .....                             | 69 |
| Table 15. Base and sub-base materials for the pavement test section in the study by Abu-Farsakh and Chen (2010).....                                       | 76 |

|   |     |
|---|-----|
| Table 16. Severity of distresses observed in the field visual survey by Oh (2011)<br>.....  | 84  |
| Table 17. Average resilient modulus from every layer of each test section in the<br>study by Oh (2011) .....                        | 84  |
| Table 18. Subgrade soil properties from each test section in the study by Oh<br>(2011) .....  | 85  |
| Table 19. Input parameters for the numerical simulation in the study by Oh (2011)<br>.....  | 86  |
| Table 20. Summary of output of the numerical simulation in the study by Oh<br>(2011) .....  | 88  |
| Table 21. ESALs at Various levels of surface deformation (Jersey et al. 2012)..   | 92  |
| Table 22. Traffic Benefit Ratios at various rut depths (Jersey et al. 2012).....  | 93  |
| Table 23. Effect of geosynthetic on pavement performance (Jersey et al. 2012)   | 93  |
| Table 24. Vertical compressive stress results in the study by Wu (2013) .....   | 105 |
| Table 25. Summary of instrumentation plans used in previous field test sections<br>.....  | 109 |
| Table 26. Candidate roads in Central Oklahoma for this study based on their<br>AADT data .....                                      | 115 |
| Table 27. Location of industrial parks within a 35-mile radius from Norman .....  | 117 |
| Table 28. Summary of tentative geosynthetics intended for use in the field test<br>section .....                                    | 123 |
| Table 29. Predicted aggregate thickness results in this study using selected<br>methods available in the geosynthetic industry..... | 131 |
| Table 30. Summary of test section dimensions in previous field studies .....  | 132 |
| Table 31. Description of the instruments planned for the proposed test section in<br>this study.....                                | 134 |

|   |     |
|---|-----|
| Table 32. Mirafi RS580i geotextile tensile strength test results in machine direction .....                 | 141 |
| Table 33. Mirafi RS580i geotextile tensile strength test results in cross-machine direction .....           | 142 |
| Table 34. Mirafi RS380i geotextile tensile strength test results in machine direction (MD) .....            | 145 |
| Table 35. Mirafi RS380i geotextile tensile strength test results in cross-machine direction (XD) .....      | 146 |
| Table 36. Comparison of Mirafi RS580i and RS380i tensile strength properties (MD) .....                     | 148 |
| Table 37. Comparison of Mirafi RS580i and RS380i tensile strength properties (XD) .....                     | 148 |
| Table 38. Maximum earth pressure measured at three different locations during cyclic plate load tests ..... | 162 |
| Table 39. Identification of the maximum AADT per county .....   | 188 |
| Table 40. Candidate road with high truck traffic (Industrial park directory) .....                          | 192 |
| Table 41. Locations of high AADT candidate roads in Central Oklahoma .....                                  | 196 |

## **1. Introduction**

Use of geogrids for aggregate base reinforcement, with proper installation, can result in increased service life, superior performance and major reduction in repair and maintenance costs. A primary objective of the current study is to help ODOT expand its selection of approved geosynthetic products for base reinforcement applications. This report describes the background work to select a suitable test section to carry out a comparative study of different geosynthetics performance in the field. The report includes a comprehensive literature review of previous field and laboratory studies, selection of geosynthetic products and instrumentation plan for the proposed field project based on the authors' recently concluded laboratory study (Hatami et al. 2012) and in-isolation and in-aggregate laboratory testing of new base reinforcement products.

The full-scale instrumented test section is designed to quantify the comparative performance of selected geosynthetic products and measure their long term response to vehicular loading and environmental conditions. The outcome of the study will provide ODOT and other departments of transportation with field data on current base reinforcement products for their possible use in roadway projects.

## **2. Literature Review**

A comprehensive literature survey was carried out to collect information on the construction practice, instrumentation plans, test methods and data reported in the published literature as related to the field reinforced roadway test sections. Major findings of the literature survey are described in this section as follows.

Black and Holtz (1999) studied the performance of geotextile separators five years after installation. For this purpose, a full-scale test section was established during the reconstruction of Washington State Highway SR-507 in Bucoda, WA by the Washington State Department of Transportation (WSDOT) in June 1991. This site was ideal for application of geotextile separators because of long history of poor pavement performance in conjunction with the soft, silty clay subgrade soils, a seasonally high ground-water table and heavy logging truck traffic. Black and Holtz (1999) concluded that geotextile separators were effective in preserving the integrity of the pavement system, to increase the strength of the base course and to improve the subgrade consolidation process.

The first phase of the project focused on constructability and installation survivability. The test section consisted of the installation of five separator geotextiles plus a control section. The six test sections were 25 feet long and were constructed in each lane of the roadway. The dimensions of the test section are shown in Figure 1. The test sections were reinforced with the following geotextiles: HB (Reemay Inc. 3401), NP4 (Polyfelt TS500), NP6 (Polyfelt TS600), NP8 (Polyfelt TS700), SF (Exxon GTF 300). The total thicknesses of the base

course in the northbound and southbound lanes were 1.5 feet and 2 feet, respectively. The roadway was paved with 6.7 inches of asphalt concrete, relatively thick by WSDOT standards, due to the history of poor pavement performance at the site. Traffic volumes were generally moderate but with a high percentage of heavy trucks.

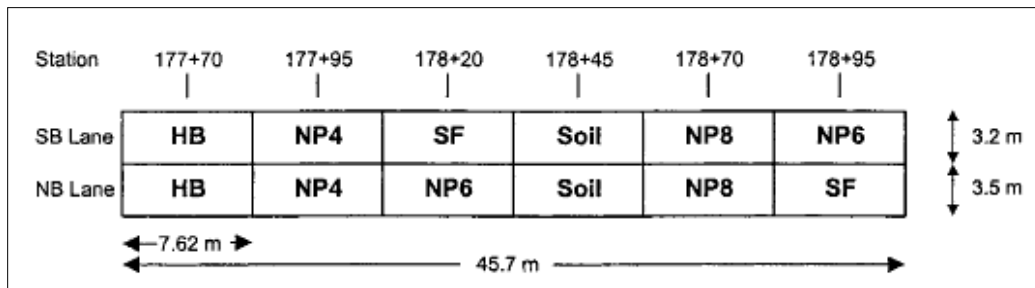


Figure 1. Plan view of the full-scale test section by Black and Holtz (1999)

Samples of geotextiles, subgrade and base course materials were exhumed for visual observation and laboratory tests after five years of installation. The excavations, 4 ft x 6 ft in size, were made on the inside wheel paths of every test section. Several samples of the base course were collected for laboratory analysis. The geotextile samples were carefully removed and visual observations were recorded. Then, the subgrade soil conditions were observed and a series of in-situ tests were performed. Additionally, samples of the subgrade were collected for laboratory tests. Results from laboratory and in-situ tests on the subgrade soils were compared with similar tests performed when the geotextiles were installed in 1991 (Phase 1 study). After sampling was completed, geotextile

patches were placed over the removed areas before the test pits were backfilled, compacted and patched with asphalt.

Black and Holtz (1999) found that exhumed geotextiles contained a minimal amount of damage due to construction. However, angular aggregates did partially penetrate isolated areas of the lighter-weight nonwoven geotextiles (HB and NP4). The holes created by the partially penetrated aggregates varied in size but were generally < 0.04-0.08 inches in diameter. Table 1 presents the number of holes greater than or equal to 0.08 inches in size resulting from aggregate puncture (construction damage) recorded for each exhumed geotextile. Table 1 also shows that the northbound lane geotextile samples generally contained more construction damage than geotextiles exhumed from the southbound lane. As the subgrade conditions in both lanes were similar, this difference was attributed to the differing initial base course thicknesses that were 6 inches in the northbound lane and 12 inches in the southbound lane. Aggregate indentations were detected on all of the geotextiles.

Table 1. Laboratory test results in the study by Black and Holtz (1999)

| Geotextile | Sample Size (cm x cm) | Number of Holes >2mm caused by agg puncture (mm) | Size of Holes >2mm caused by agg puncture (mm) | Percent Blinding/Clogging | Percent Cacking | Percent Iron-Oxide Staining |
|------------|-----------------------|--|--|---------------------------|-----------------|-----------------------------|
| HB-NB      | 61 x 91               | 1  | 5  | 65-80                     | 15-30           | 55-65                       |
| NP4-NB     | 61 x 112              | 9  | 3,3,3,4,4,7,8,13,22                            | 60-80                     | 15-30           | 90-95                       |
| NP6-NB     | 58 x 91               | 2  | 3,3  | 65-80                     | <5              | 90                          |
| NP8-NB     | 76 x 107              | 1  | 8  | 50-65                     | <5              | <5                          |
| SF-NB      | 66 x 102              | 1  | 7  | 15-30                     | >75             | 5-10                        |

| Geotextile | Sample Size (cm x cm) | Number of Holes >2mm caused by agg puncture (mm) | Size of Holes >2mm caused by agg puncture (mm) | Percent Blinding/Clogging | Percent Cacking | Percent Iron-Oxide Staining |
|------------|-----------------------|--|--|---------------------------|-----------------|-----------------------------|
| HB-SB      | 56 x 97               | None   | -  | 85-95                     | 15-30           | 95                          |
| NP4-SB     | 66 x 112              | 2  | 3,3  | 90-95                     | 30-60           | 90                          |
| NP6-SB     | 76 x 99               | None   | -  | 80-90                     | 60-75           | 10-25                       |
| NP8-SB     | 64 x 86               | None   | -  | 95                        | >75             | 25-30                       |
| SF-SB      | 84 x 137              | None   | -  | 15-25                     | 60-75           | 20-30                       |

Note: Percentages of blinding/clogging, caking and iron-oxide staining estimated visually

Black and Holtz (1999) conducted permittivity tests on both virgin and exhumed geotextiles to evaluate their degree of blinding and clogging by comparing the permittivity values before and after the soil particles were washed from the specimens. Control tests performed on virgin geotextiles resulted in permittivity changes between 0.5% and 5.4% due to the washing process. These results indicated that the effects of the washing process were relatively minor in comparison with the increase in permittivity of the exhumed geotextiles. As shown in Figure 2, heat-bonded geotextiles had the largest average increases in permittivity after washing, compared to the needle-punched and slit-film geotextiles, which had comparable increases in permittivity with each other. These results suggest that heat-bonded geotextiles experienced significantly more clogging than the other geotextiles even though the visual estimates of blinding/clogging for the heat-bonded geotextiles were not substantially different than those for the needle-punched geotextiles (Table 1). The slit-film permittivity values were less representative of the in-situ conditions than the other geotextiles

because soil particles blinding the bottom and caked on the top of the slit films may have been removed during the exhumation or handling procedures.

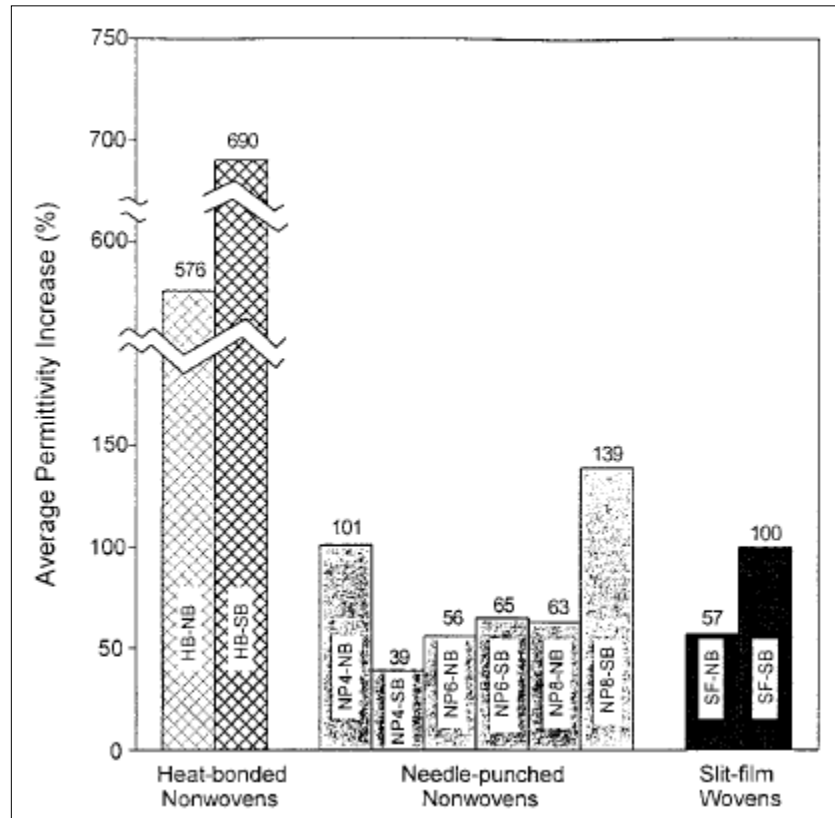


Figure 2. Average permittivity results in the study by Black and Holtz (1999)

Black and Holtz (1999) conducted wide-width tests to evaluate the retained strength and elongation at failure by comparing the exhumed test results with the control results. In addition, comparisons were made between the northbound and southbound lane to evaluate the effect of different initial base course lift thicknesses on the survivability of the geotextiles. The results of Black and Holtz's wide-width tests are shown in Table 2. When compared with the control

specimens, the slit-film geotextiles suffered the greatest reductions in retained strength but had the highest retained elongations at failure. Black and Holtz speculated that the slit-films might have experienced the greatest strength reductions because of their high stiffness. The needle-punched geotextiles presented more changes as they suffered the greatest reductions in retained elongation at failure.

Table 2. Wide-width test results in the study by Black and Holtz (1999)

| Geotextile   | Average Exhumed Strength (kN/m) | Average Control Strength (kN/m) | Average Exhumed Elongation at Failure (%) | Average Control Elongation at Failure (%) |
|--|---------------------------------|---------------------------------|---|---|
| HB-NB  | 5.7                             | 6.1                             | 27  | 55  |
| NP4-NB   | 7.3                             | 7.5                             | 22  | 79  |
| NP6-NB   | 9.7                             | 10.9                            | 24  | 84  |
| NP8-NB   | 13.0                            | 15.6                            | 28  | 96  |
| SF-NB  | 29.0                            | 37.6                            | 12  | 21  |
| HB-SB  | 7.4                             | 6.1                             | 35  | 55  |
| NP4-SB   | 9.0                             | 7.5                             | 28  | 79  |
| NP6-SB   | 11.9                            | 10.9                            | 35  | 84  |
| NP8-SB   | 14.4                            | 15.6                            | 31  | 96  |
| SF-SB  | 31.7                            | 37.6                            | 14  | 21  |
| Note: Control (virgin) geotextile tested were from different lots than those installed at test site. Test results were intended to be compared with results of tests performed on same geotextile lots, but data have been lost. |                                 |                                 |   |   |

Results from laboratory and in-situ tests on the subgrade soils were compared to similar tests performed when the geotextiles were installed in 1991. Included were laboratory moisture content, field Torvane (a hand-held vane shear device for rapid determination of shear strength in cohesive soils), pocket penetrometer, nuclear densometer and Falling Weight Deflectometer (FWD) tests.

The Torvane test results indicated that there was a general increase in subgrade shear strength in both lanes since the geotextiles were installed, but the pocket penetrometer test results overall showed an opposite trend. Black and Holtz (1999) attributed the possible reason for these differences to the variability they observed in these tests. The nuclear densometer test results were compared to the Phase I study, which indicated a general increase in density (wet and dry) at all test locations except at the control sections. The increases in dry density in the sections containing geotextiles ranged from 0.7% at the HB-NB location to 39.0% at the SF-SB location. These results suggested that the subgrade had consolidated more in the areas containing geotextiles than in the control sections.

WSDOT personnel carried out FWD tests at the test site on April 29, 1991 just before the road reconstruction started. Additional tests were carried out on July 24, 1991, November 25, 1991 and March 25, 1996. The output values were normalized to a 9-kip (40-kN) load and adjusted for pavement thickness and temperature. The subgrade modulus values determined from the FWD tests showed a steady increase in the subgrade modulus throughout the test section since April 1991 (Figure 3). The subgrade conditions during the installation of the geotextiles (1991) were generally noted to be soft and saturated. In the field investigations performed five years later, the subgrade conditions were generally observed to be medium stiff to stiff at all test pits. With the exception of the pocket penetrometer tests, the in-situ tests and observations indicated the subgrade under the geotextiles was consolidated during the 5 years after construction.

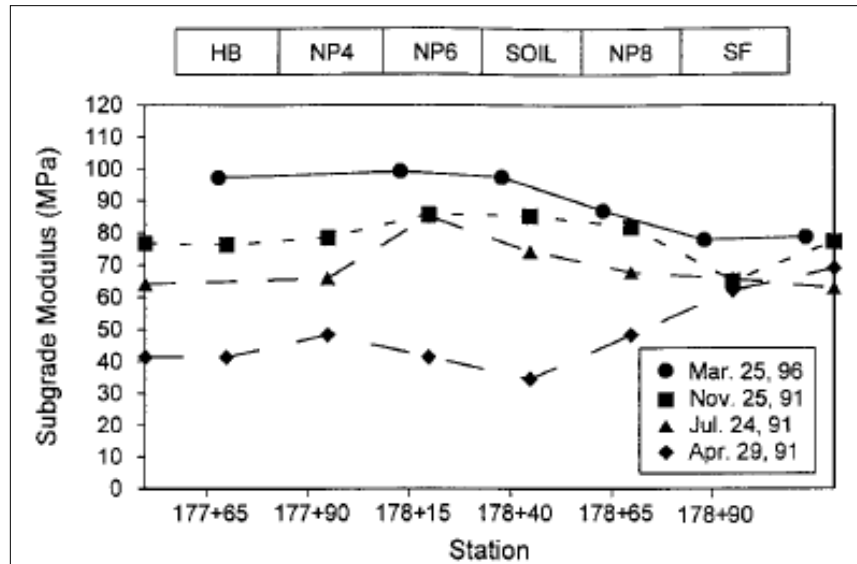


Figure 3. Comparison of FWD test results (Northbound lane) in the study by Black and Holtz (1999)

Black and Holtz (1999) drew the following conclusions:

- The road that was constructed using different geotextile separators at a site with a history of poor pavement performance was in good condition five years after construction.
- Permittivity tests revealed that heat-bonded geotextiles were significantly more vulnerable to clogging than needle-punched or slit-film geotextiles.
- Different geotextiles used in the test road all survived the construction reasonably well, except for the NP4 geotextile in the northbound lane. Aggregate puncture caused geotextile damage mostly under thinner initial base course lifts.

- Visual inspections indicated that lighter-weight geotextiles (HB and NP4) sustained more construction damage. However, this damage was not reflected in the results of the wide-width tensile laboratory tests.
- The thickness of the base course first lift showed a notable influence on the strength and elongation at failure of the separator geotextiles used. The elongation at failure was particularly more influenced than strength.
- Density tests indicated that the subgrade in the sections containing geotextiles consolidated more than the subgrade in the sections without geotextiles.
- The long-term separation performance of geotextiles may not be critical in many cases because due to consolidation over time, subgrade strength typically increases and its compressibility decreases.

Berg et al. (2000) conducted a study on the use of geosynthetic reinforcement in the aggregate base and sub-base courses of pavement structures. Their study was along the efforts of the AASHTO Committee 4E to develop specifications for geosynthetic base course reinforcement applications. Specific objectives of the study were to:

- Define geosynthetic reinforcement applications in roads,
- Carry out a survey of related literature
- Define the value added to pavement structures by the use of reinforcement,

- Provide a recommended design practice, and
- Provide design and material specifications

Berg et al. (2000) identified the following benefits of using geosynthetics in roadways, which demonstrate the value-added to pavement structure:

- Reduction of stress intensity on the subgrade (function: separation)
- Prevention of subgrade fines filtration into the base (function: filtration)
- Preventing contamination of base materials allowing more open-graded, free-draining aggregates to be considered in the design (function: filtration).
- Reduction of excavation depth required for the removal of unsuitable subgrade materials (function: separation and reinforcement).
- Reduction of the aggregate thickness required to stabilize the subgrade (function: separation and reinforcement).
- Reduction of subgrade disturbance during construction (function: separation and reinforcement).
- Increase of subgrade strength over time (function: filtration).
- Minimize the differential settlement of the roadway, which helps maintain pavement integrity and uniformity (function: reinforcement).
- Minimize maintenance and extending the life of the pavement (functions: all).

Berg et al. (2000) expressed the benefit or value-added in terms of "life extension" or "savings in base course thickness". Extension of life was defined in terms of a Traffic Benefit Ratio (TBR). TBR is the ratio of the number of cycles necessary to reach a given rut depth for a test section containing reinforcement to the number of cycles necessary to reach this same rut depth for an unreinforced section with the same section thickness and subgrade properties. The Base Course Reduction (BCR) is expressed as a percentage savings of the unreinforced base thickness.

Berg et al. (2000) evaluated previous laboratory and full-scale geosynthetic-reinforced studies. They found that there are many variables that may affect the performance results of a particular test including geosynthetic type and properties, subgrade strength, loading conditions, and base course thickness and properties. A summary of added-value benefit from laboratory and field test sections based on previous studies is given in Table 3.

Table 3. Summary of added-value benefit from previous aggregate base reinforcement projects surveyed by Berg et al. (2000)

| Study           | Geotextile Product - Location | AC/Base Thickness (mm) | Subgrade CBR | Rut Depth (mm) | Value-Added Benefits  |                             |
|-----------------|-------------------------------|------------------------|--------------|----------------|-----------------------|-----------------------------|
|                 |                               |                        |              |                | Extension of Life TBR | Base Course Reduction BCR % |
| Al-Qadi (lab)   | B-B                           | 70/150 and 200         | 2-4          | 25             | 1.7-3                 | CTNC                        |
| Al-Qadi (field) | A-B                           | 90/100                 | 7            | 17             | 1.6                   | CTNC                        |
| Al-Qadi (field) | A-B                           | 90/150                 | 7            | 17             | CTNC                  | <33                         |
| Anderson        | L-B                           | 105/450                | NR           | NR             | CTNC                  | 22                          |

| Study  | Geotextile Product - Location | AC/Base Thickness (mm) | Subgrade CBR | Rut Depth (mm) | Value-Added Benefits  |                             |
|--|-------------------------------|------------------------|--------------|----------------|-----------------------|-----------------------------|
|  |                               |                        |              |                | Extension of Life TBR | Base Course Reduction BCR % |
| Barksdale  | C-B                           | 25/150                 | 2.9          | 12.5           | 2.8                   | CTNC                        |
| Barksdale  | C-B                           | 38/200                 | 2.7          | 12.5           | 1.0                   | CTNC                        |
| Barksdale  | C-M                           | 38/200                 | 2.7          | 12.5           | 4.7                   | CTNC                        |
| Barksdale  | C-M                           | 38/200                 | 3.2          | 12.5           | 2.2                   | CTNC                        |
| Cancelli (lab)   | E-B                           | 75/300                 | 3            | 25             | 1.7                   | CTNC                        |
| Cancelli (field)   | E-B                           | 75/400                 | 3            | 10             | 220                   | CTNC                        |
| Perkins  | I-B                           | 75/300                 | 1.5          | 22             | 8.5                   | CTNC                        |
| Notes: <ul style="list-style-type: none"> <li>- For Product Code: A=Amoco 2002, B=Amoco 2016, C=Nicolon HP570, D=NR, E=Amoco 6070, G=Terram 7M7, H=Terram 1000, I=Amoco 2006, J=Nicolon HP67809, K=TC Mirafi 180N, L=Terrafix 270R</li> <li>- For Location Code: B=Bottom, M=Middle.</li> <li>- NR=Not Reported, NTD=None To Date, CTNC=Comparative Test not Conduct.</li> </ul> |                               |                        |              |                |                       |                             |

A summary of Berg et al.'s (2000) conclusions with respect to the benefit of geosynthetic reinforcement in different laboratory and full-scale studies is presented as follows:

- Several studies indicated an optimum benefit when the geosynthetic was placed at the bottom of an 8-12 inch-thick base layer.
- For thicker base sections, the most beneficial reinforcement location appeared to be in the middle of the base, where geogrids were found to perform best.

- For thin bases (less than 8 inches), lack of separation was noted as a potential problem for geogrids. Geotextiles or geocomposites tend to perform better for the thin bases, especially where subgrade strengths were lower than  $\text{CBR} = 3$ .
- Reinforcement benefits were observed with subgrade strengths up to  $\text{CBR} = 8$ . In at least one study, some benefit was found at even greater subgrade strengths. However, there does appear to be a relation between decreasing reinforcement benefits with increasing subgrade strength.

Berg et al. (2000) stated that the mechanisms of geosynthetic base reinforcement are not fully understood. Therefore, performance of geosynthetics in base reinforcement applications must be determined by testing specific reinforcement products. Laboratory and/or field tests with specific products, similar pavement materials and cross-sections, and similar subgrade conditions are required to quantify the contribution of the geosynthetic reinforcement to the pavement performance.

Berg et al. (2000) specified the following steps for base reinforcement design: 1) assess applicability, 2) design an unreinforced roadway section, 3) select the target benefit in terms of service life improvement and/or reduced structural section, 4) evaluate the benefit offered by various geosynthetics in terms of TBR, BCR or Layer Coefficient Ratio (LCR), 5) design a reinforced base course section, and 6) perform life-cycle cost analysis.

Berg et al. (2000) stated that subgrade restraint design is essentially the same as stabilization design, except that a reinforcement modulus value may be required in addition to the properties of interest in stabilization, which are related to filtration and survivability.

A qualitative summary of potential geosynthetic reinforcement applications in relation to project conditions and geosynthetic type based upon previous research studies is given in Table 4.

Table 4. Qualitative summary of potential geosynthetic reinforcement applications based upon previous research studies reported by Berg et al. (2000)

| Roadway Design Conditions               |                             | Geosynthetic Type |       |          |                  |                  |                  |
|---|-----------------------------|-------------------|-------|----------|------------------|------------------|------------------|
| Subgrade                                | Base/Subbase Thickness (mm) | Geotextile        |       | Geogrid  |                  | GG-GT Composite  |                  |
|   |                             | Nonwoven          | Woven | Extruded | Knitted or Woven | Open-graded Base | Well Graded Base |
| Low (CBR<3) (MR<30 MPa)                 | 150-300                     | 7                 | 1     | 1        | 4                | 1                | 5                |
|   | >300                        | 7                 | 7     | 2        | 2                | 2                | 5                |
| Firm to Very Stiff (3<CBR<8) (30<Mr<80) | 150-300                     | 6                 | 2     | 1        | 4                | 1                | 5                |
|   | >300                        | 6                 | 6     | 2        | 4                | 4                | 5                |
| Firm (CBR>8) (Mr>80 MP)                 | 150-300                     | 3                 | 3     | 2        | 4                | 4                | 5                |
|   | >300                        | 3                 | 3     | 3        | 3                | 3                | 5                |

Note:  
 1. Usually applicable, 2. Applicable for some conditions, 3. Usually not applicable, 4. Insufficient information at this time, 5. Geotextile component of composite likely is not required for filtration with a well graded base course; therefore, composite reinforcement usually not applicable, 6. Separation and filtration application; reinforcement usually not applicable, 7. Reinforcement usually applicable, but typically addressed as a subgrade stabilization application.

With respect to material properties, Berg et al. (2000) concluded that the influences of geosynthetic index properties on the reinforcement benefit, defined by TBR, BCR and LCR are not fully understood. Therefore, TBR, BCR and LCR values must be developed through product-specific testing in each unique environment. These ratios are considered to be product-specific for base and

sub-base reinforcement applications. However, the following properties are believed to influence performance: tensile strength at 1%, 2% and 5% strain, coefficients of pullout and direct shear, aperture size (in geogrids) and percent open area (in geotextiles). More recent tests indicate a possible correlation between aggregate confinement and performance. Junction strength is viewed as an index property which is specific to the manufacturing method of a given product. For subgrade restraint applications, the properties of tensile strength at 2% and 5% strain are primarily related to geosynthetic performance.

Yu (2000) studied flexible reinforced pavement structure by conducting a sensitivity analysis. He performed a series of triaxial tests in order to identify geosynthetics various functions in flexible pavements. Two parameters were studied, permanent deformation and elastic modulus. The confining pressure varied from 10 psi to 20 psi and the layers included in different test specimens increased from non-reinforced to specimens with three layers of reinforcement. The data was recorded by the program 'Test Control Software' (TCS) and a one-dimensional numerical analysis using the finite element method (FEM) package ABAQUS was employed to analyze the data. Yu (2000) demonstrated that geogrids would be more effective in reinforcing the base layer if placed in the middle of the layer as compared to the base-subgrade interface. Furthermore, his numerical results indicated that a reinforced section was indeed stiffer than an unreinforced section.

Yu (2000) used plastic strain rather than recoverable elastic strain to measure resilient modulus, referred to here as the permanent resilient modulus (PRM). He determined the PRM value for different soil layers as a result of a change in their geometry. The PRM parameter was introduced because an elastic analysis was used to analyze the permanent deformation of the pavement structure, in which the subsequent deformation was based on the deformed geometry of the pavement system in the previous stage. In his study, Yu (2000) examined the magnitudes of permanent deformation at the surface of the asphalt layer and at the asphalt-base and base-subgrade interfaces in his flexible pavement model.

Yu (2000) validated his calculated PRM values from ABAQUS by using them in the multi-layer analysis package KENLAYER to predict the corresponding pavement deformations. He used regression analysis to correlate PRM with the number of wheel load passes.

Yu (2000) carried out a sensitivity analysis to study the variation of permanent deformation with the PRM value of the base layer. It was assumed that the PRM values of the asphalt layer and the subgrade remained constant when subjected to tire load, whereas that of the base layer would be changed as a function of the number of passes. An equation, presented in Figure 4, was used to evaluate the sensitivity of permanent deformation to the thickness and PRM values of pavement layers. This equation indicated that the variations of the base layer resilient modulus and thickness were coupled. Yu (2000) carried out his

sensitivity analysis of the change in permanent deflection for the three different conditions shown in Figure 5.

$$\delta E + \delta H = \frac{\delta v_{pi}^1 * E}{2\pi \int_r (\bar{\sigma}_z \epsilon_z + \bar{\sigma}_r \epsilon_r + \bar{\sigma}_\theta \epsilon_\theta + \bar{\tau}_{rc} \gamma_{rc}) r dr}$$

in which

- $\delta E$ : the variation of permanent resilient modulus
- $\delta H$ : the variation of thickness of base layer
- $\delta v_{pi}^1$ : the variation of permanent deformation
- $E$ : the modulus of base layer
- $\bar{\sigma}_z, \bar{\sigma}_r, \bar{\sigma}_\theta$ : the normal stresses generated in adjoint structures
- $\bar{\tau}_{rc}$ : the shear stress generated in adjoint structures
- $\epsilon_z, \epsilon_r, \epsilon_\theta$ : the direct strains generated in primary structures
- $\gamma_{rc}$ : the shear strain generated in primary structures

Figure 4. Equation proposed by Yu (2000) to relate PRM and the change in base course thickness to the permanent deformation of an aggregate base flexible pavement system

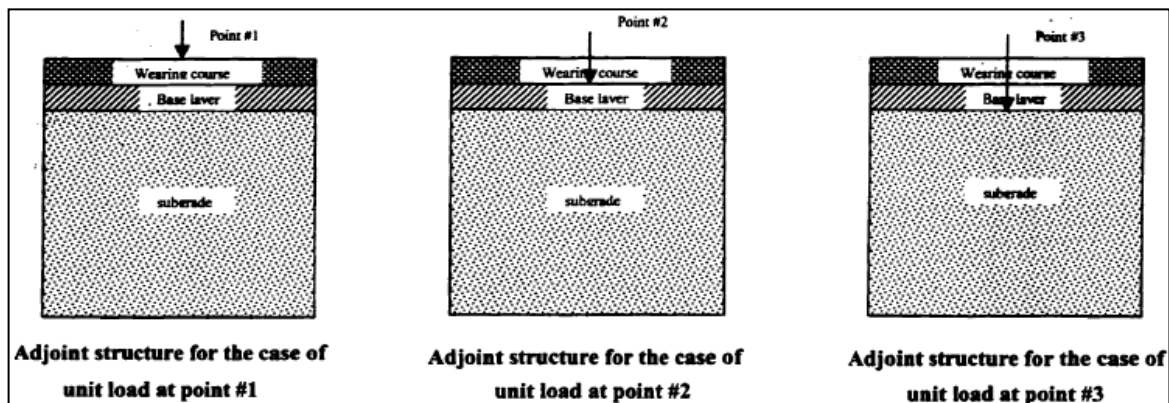


Figure 5. Three cases considered for permanent deformation calculations (Yu 2000)

Figure 6, Figure 7 and Figure 8 describe three different cases in which permanent deformation was plotted as a function of the number of wheel load passes. Case 1 was the unreinforced case, in Case 2 the geogrid reinforcement was placed in the middle of the base layer and in Case 3, the geogrid reinforcement was placed at the base-subgrade interface.

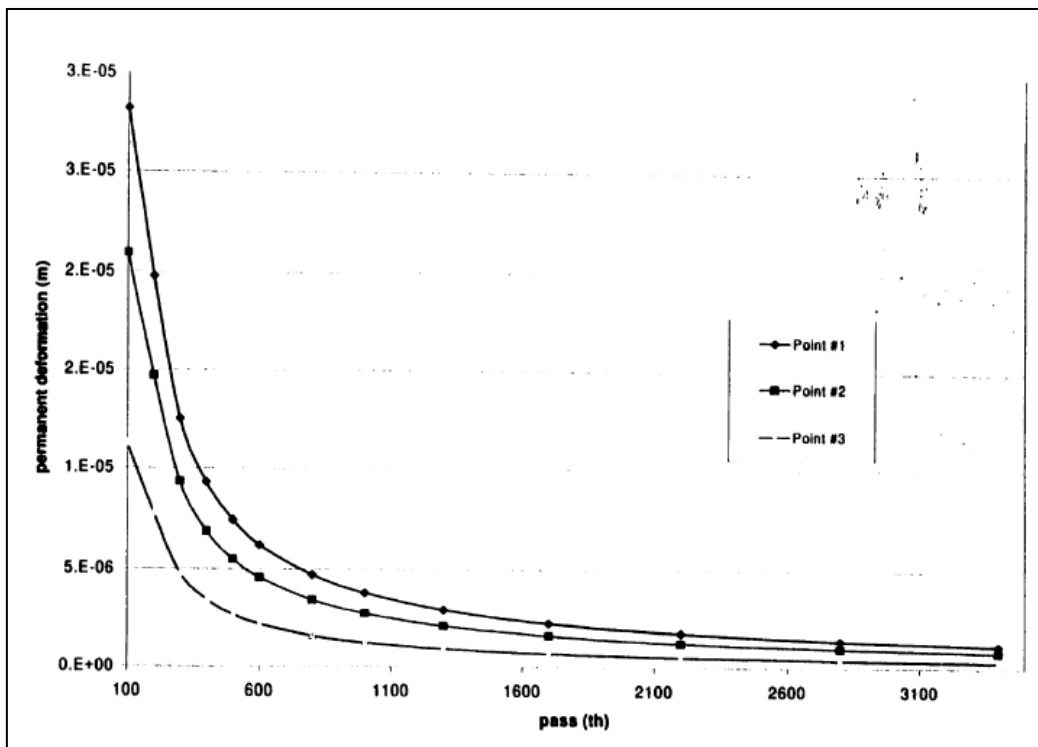


Figure 6. Permanent deformation generated by wheel loading passes under unreinforced conditions (Yu 2000)

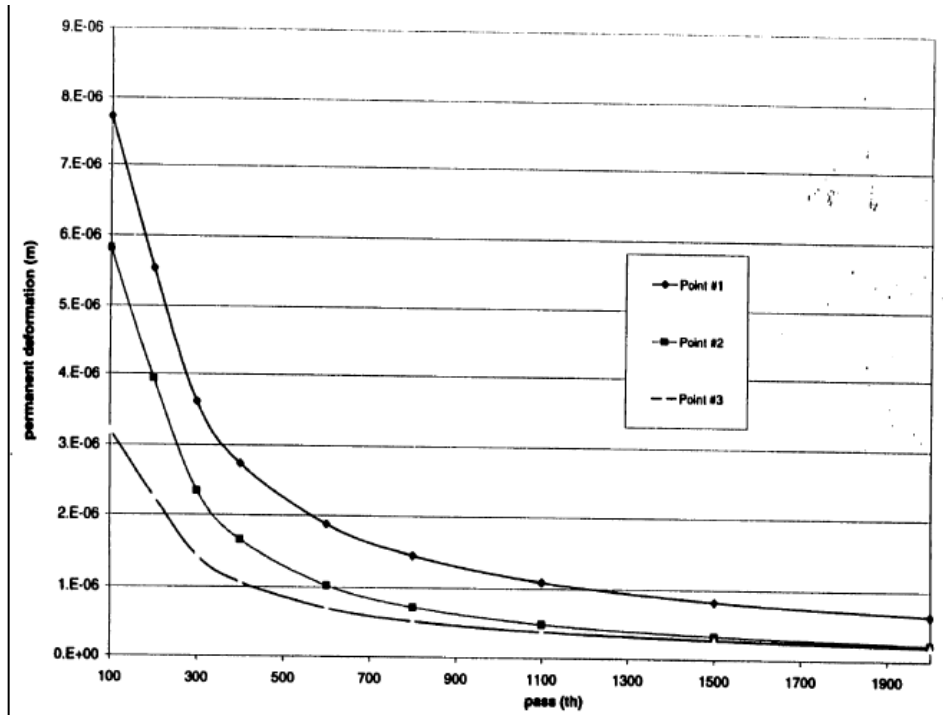


Figure 7. Permanent deformation generated by wheel loading passes with geogrid at the middle of base layer (Yu 2000)

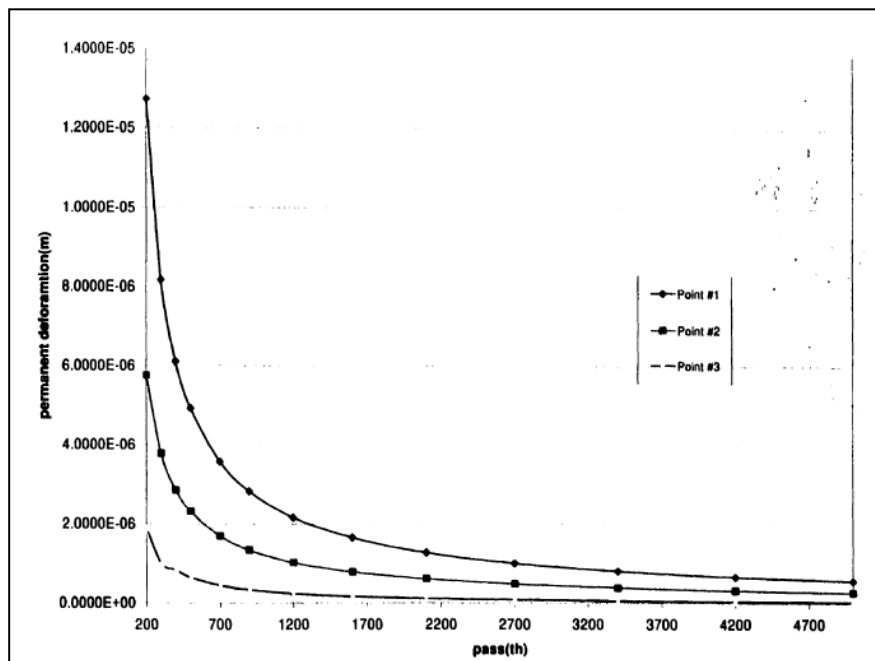


Figure 8. Permanent deformation generated by wheel loading passes with geogrid at the base-subgrade interface (Yu 2000)

Based on his studies, Yu (2000) made the following observations:

- a) The inclusion of geotextiles improved the performance of base material, both in terms of yielding stress and secant modulus.
- b) Both the yielding stress and secant modulus increased with the number of geotextile layers and/or the confining pressure. However, the extent of increase in the yielding stress and secant modulus resulting from confining pressure was not as significant as that caused by the number of geotextiles used.
- c) When the geotextiles were used as reinforcement and separator in two separate layers, the deformed shape of the part between the two layers of geotextiles was the same as that of unreinforced soil sample. When the soil sample was reinforced with merely one layer of geotextile which divided the sample into two parts, one part deformed and the other part kept its original shape. It was unpredictable to know which part was going to deform. This observation indicates an uncertainty in the measured behavior of reinforced test sections when simulated using triaxial tests.

The following conclusions were made based on the numerical analysis associated with the experimental results regarding the effect of geogrids:

- a) The FEM analysis was found to be very sensitive to the model set-up. A fine numerical mesh led to better results, especially to capture stress concentrations in the model.
- b) Analysis results from the multi-layer elastic theory agreed with those from FEM.
- c) Numerical analysis showed permanent deformation of up to 0.8 inches after 3400 passes when the pavement was unreinforced. Most of this deformation took place during the first several hundred passes. Therefore, it was concluded that the inclusion of geogrids increased the gradual stiffening of the aggregate layer when subjected to repeated loads.
- d) Test results indicated that geogrids placed in the middle of the base layer are more effective in increasing the PRM of the layer than when they are installed at the base-subgrade interface.
- e) During the stiffening period, the permanent deformation of the base layer was sensitive to a combination of change in its thickness and its PRM value. Assuming that the layer thickness remained practically constant, it was concluded that PRM increased linearly with the number of wheel load passes.
- f) On the contrary, the variation of permanent deformation was essentially independent of the change in the thickness of the base layer. The same amount of variation of permanent deformation that could be obtained by a layer of

geogrid, could be achieved by a thicker base layer. This demonstrated the cost effectiveness of geogrids in reinforcing flexible pavements.

Al-Qadi and Appea (2003) studied the field performance of geosynthetic-reinforced pavements on a secondary road over the course of eight years. The study involved the construction of an instrumented secondary road pavement in Bedford County, Virginia. The objective of the study was to validate a previous laboratory evaluation of geosynthetics-reinforced pavement sections (Al-Qadi et al. 1994). In the previous study, Al-Qadi found that geosynthetics could be effective in improving the performance of flexible pavements and determined the extent of their benefit by testing eighteen reinforced and unreinforced test sections with a computer-controlled pneumatic system. However, there was still a need to monitor the long-term performance of geosynthetically stabilized pavement sections so that the benefits of geosynthetics could be quantified in terms of lifecycle-cost analysis and service life prediction.

Al-Qadi and Appea's (2003) test section consisted of nine 49.2 ft-long segments. The entire test section was divided into three groups with aggregate base layer thicknesses of 4, 6 and 8 inches. Three sections, one from each group, were stabilized with geotextiles and three were stabilized with geogrids at the base course-subgrade interface. The remaining three sections were kept as control sections. Table 5 shows the tensile properties of the geosynthetics used before and after excavation, respectively.

Table 5. Tensile strength and elongation of geosynthetics used in the study by Al-Qadi and Appea (2003)

| Material (before installation) | Direction | Ultimate        |            |
|--------------------------------|-----------|-----------------|------------|
|                                |           | Strength (kN/m) | Elong. (%) |
| Geotextile                     | Warp      | 27              | 23.6       |
|                                | Fill      | 25              | 9.9        |
| Geogrid                        | Machine   | 19              | 8.9        |
|                                | X-Mach    | 33              | 9.3        |
| After Excavation               |           |                 |            |
| Geotextile                     | Warp      | 18              | 14.8       |
|                                | Fill      | 25              | 12.5       |
| Geogrid                        | Machine   | 19              | 12.4       |
|                                | X-Mach    | 32              | 14.1       |

Al-Qadi and Appea (2003) performed Falling Weight Deflectometer (FWD) tests and evaluated the rutting progress during the eight years of the study. The FWD tests were conducted on the pavement to estimate its structural capacity and service life. All nine sections in both lanes were subjected to five FWD drops, each at different nominal load levels: 5, 7, 9, 11 and 13 kips. The locations of the FWD testing points were carefully marked in the wheel path away from the instrumented locations.

The FWD tests allowed the calculation of deflection parameters, such as the Surface Curvature Index (SCI) and the Base Damage Index (BDI). These parameters were calculated for all deflection measurements obtained during the study period (1994-2001). A deteriorated base layer is proportionally related to the BDI and the SCI of the pavement system is a measure of its stiffness. A strong pavement (i.e. a pavement with a low SCI) is likely to have a better load

distributing system than a weak pavement system. Results of SCI and BDI for all nine sections were analyzed and corrected to a standard temperature (25°C). Figure 9 and Figure 10 show the BDI and SCI values over the life of the pavement, respectively. From the 1995 data, the relative strengths of the 4-inch base course sections (i.e. Sections 1 through 3) appeared to be the same, which was expected during the early age of the project. The sections with 6 inches and 8 inches of base course layers were also relatively stronger than the ones with a 4-inch base course. Further analysis of data given in Figure 10 and Table 6 show that the geotextile-stabilized, 4-inch base course section (Section 2) was stronger than both the geogrid-stabilized and control test sections (Sections 1 and 3). The BDI for Sections 1, 2 and 3 were 150, 80 and 90, respectively for the last measurements, while the SCI was calculated to be 1252, 500 and 570, respectively, for the same measurements. In general, the determination of the BDI over the seven-year period of FWD testing among the stabilized and non-stabilized sections confirmed the phenomenon of a weakened base layer over time when a separator is not utilized. The geosynthetic stabilized sections had BDI values less than half that of the unstabilized section in the first three sections.

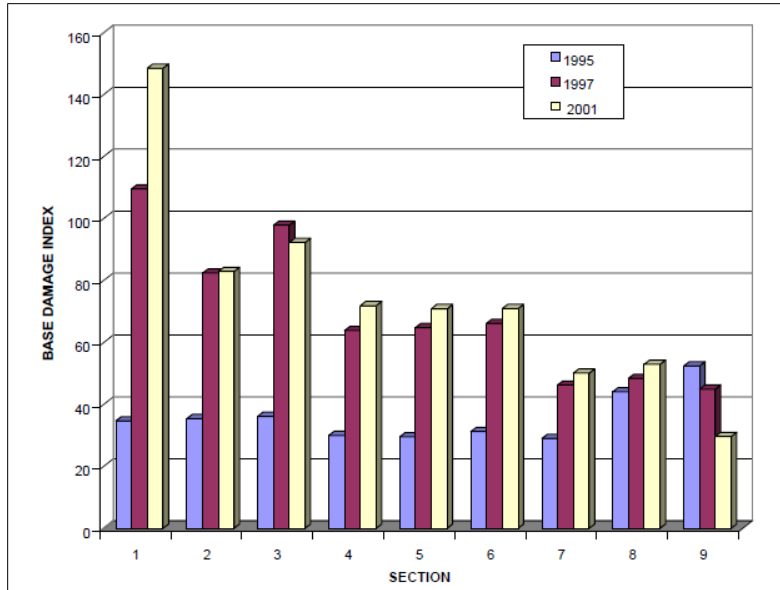


Figure 9. Base Damage Index over the life of pavement in the study by Al-Qadi and Appea (2003)

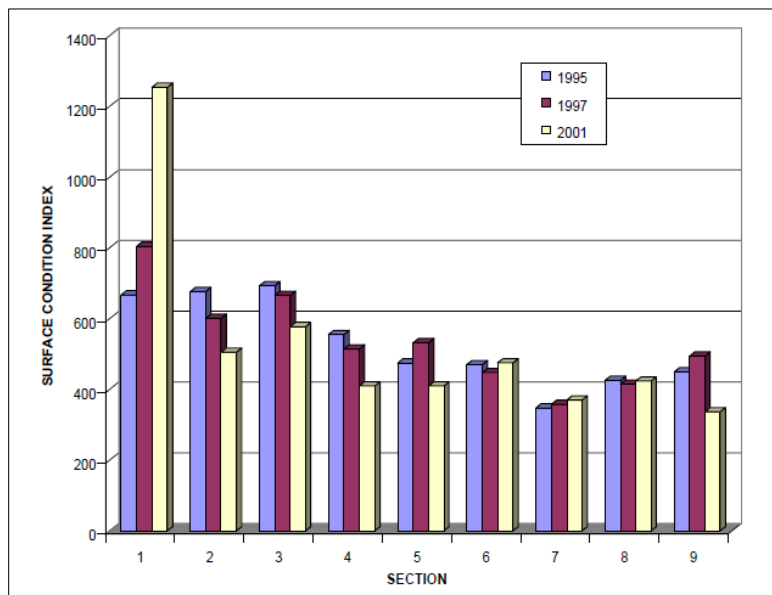


Figure 10. Surface Condition Index over the life of pavement in the study by Al-Qadi and Appea (2003)

Table 6. Maximum rut depth measured in October 2001 in the study by Al-Qadi and Appea (2003)

| Section | Stabilization Type | Northbound (mm)* | Southbound (mm)* |
|---------|--------------------|------------------|------------------|
| 1       | Control            | 45.9             | 29.2             |
| 2       | Geotextile         | 18.8             | 15.9             |
| 3       | Geogrid            | 23.2             | 16.4             |
| 4       | Control            | 12.              | 10.1             |
| 5       | Geotextile         | 12.1             | 8.3              |
| 6       | Geogrid            | 12.7             | 6.8              |
| 7       | Control            | 11.5             | 9.4              |
| 8       | Geotextile         | 11.7             | 9.6              |
| 9       | Geogrid            | 12.0             | 7.8              |

\*Variation in rutting between lanes is caused by different traffic pattern (heavier trucks in northbound)

Al-Qadi and Appea (2003) related the development of an intermixing area at the subgrade-aggregate base layer with the loss in the aggregate support. This intermixing area was observed during a forensic excavation in 1997. Observed weakness of the pavement system was attributed to an increase in the fines content of the aggregate base layer. In the 1997 excavation, the fines content exceeded 12% in the control section, especially in the first 2 inches above the aggregate-subgrade interface. The reduction in the pavement structural capacity due to fines increase in the aggregate layer is supported by Jorenby and Hicks (1986) who reported a dramatic drop in aggregate resilient modulus when the fines content exceeded 12%.

With respect to rutting, Al-Qadi and Appea (2003) conducted rut depth measurements on both lanes of the pavement test sections using a straight edge, in accordance with ASTM E 1703. These measurements were carried out since construction. Table 6 presents the maximum rut depth at each section for both

lanes. The geotextile-stabilized section (Section 2) continued to have less rutting than the geogrid section (Section 3) and the control section (Section 1). Figure 11 and Figure 12 show the latest rut depth profile along the pavement cross-section for the 4-inch base section and the rutting depth progress over the life of the pavement, respectively. The rut depths reported in Figure 12 also show a definite contribution of geosynthetics in improving the performance of the stabilized sections. The increase in rutting for the other design test sections was less pronounced. For this reason, Al-Qadi and Appea (2003) focused their study on Sections 1 through 3.

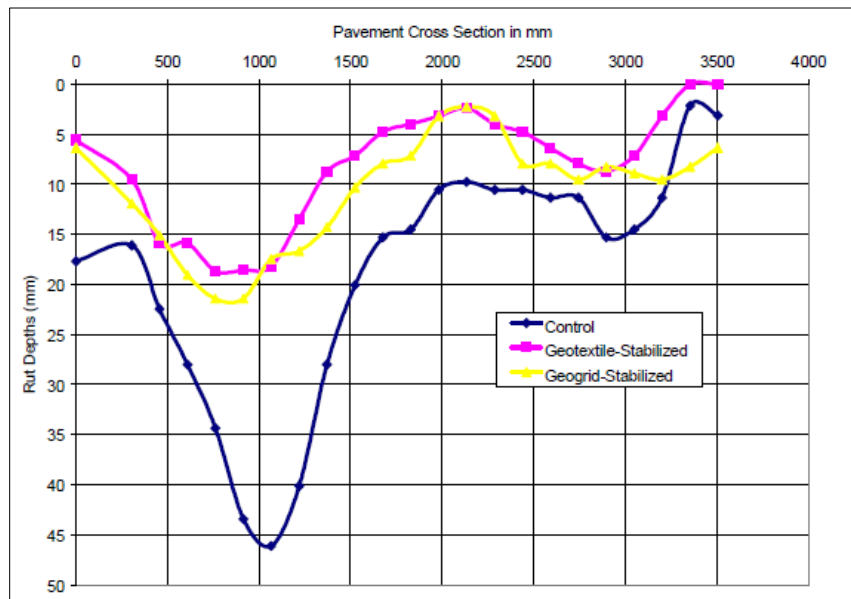


Figure 11. Rut depths of the 4-inch Base course sections in the study by Al-Qadi and Appea (2003)

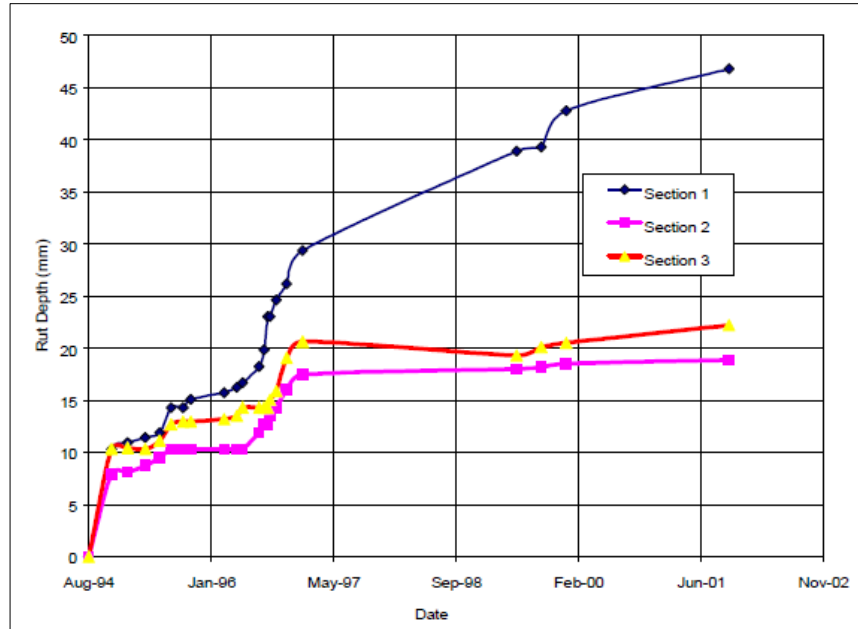


Figure 12. Rutting progress over the testing period of the 4-inch base course sections in the study by Al-Qadi and Apea (2003)

The normal traffic on the test sections was monitored using a traffic counter and piezoelectric sensors. In addition, a controlled research traffic load was applied using a truck with a 30-lb axle load and a tire pressure of 101.5 psi over a period of two weeks. The cumulative ESALs over the period between the end of construction and when the last rut depth was measured (October 2001) are shown in Figure 13. A terminal rut depth of 0.8 inch was specified for the first three test sections to determine their service life. Figure 13 shows the plots of total rutting versus ESALs for Sections 1 through 3. Table 7 presents the service life calculated for the three sections based on the terminal rutting depth of 0.8 inch. After eight years of monitoring, the geotextile-stabilized section with 4 inches of aggregate base course carried 195% more traffic than the non-

stabilized section, while the geogrid-stabilized section carried 187% more traffic than the non-stabilized section (Table 7).

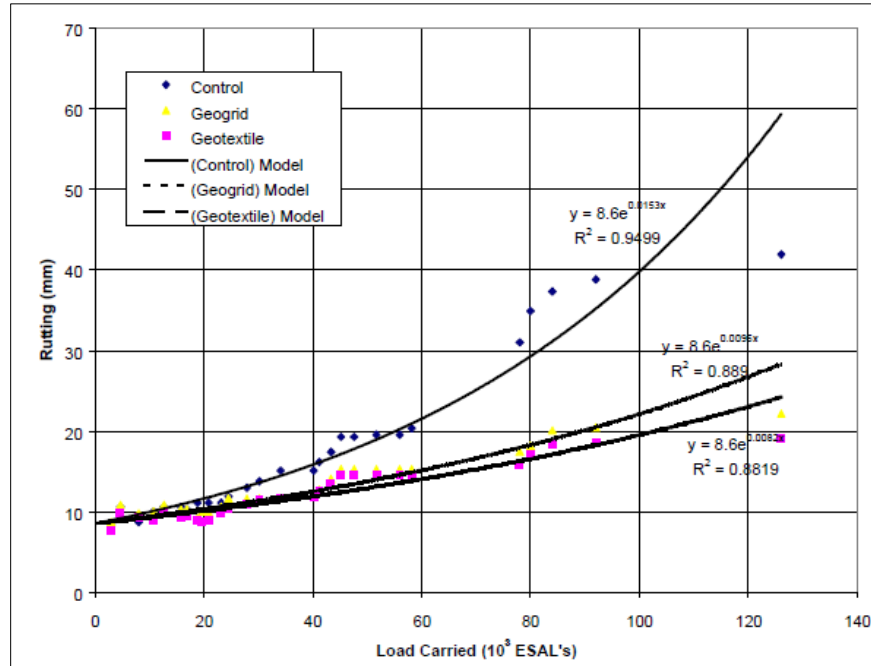


Figure 13. Rut depth progression in Sections 1-3 in the study by Al-Qadi and Appea (2003)

Table 7. Service life for Sections 1-3 in the study by Al-Qadi and Appea (2003)

| Section    | Service Life (ESAL's) | Increase (%) | Service Life (years) |
|------------|-----------------------|--------------|----------------------|
| Control    | 67,033                | -            | 4                    |
| Geotextile | 130,972               | 195          | 7.5                  |
| Geogrid    | 125,780               | 187          | 6.8                  |

Al-Qadi and Appea (2003) results showed that geosynthetically stabilized sections for the 4-inch base course segments can increase the life of a pavement

system by almost two folds. However this increase in service life would be smaller for stronger pavements (e.g. 6- and 8-inch-thick aggregate base layers).

The control (unreinforced) section had the greatest amount of rutting, followed by the geogrid- and geotextile-stabilized sections, which respectively, had the least amount of rutting. Rutting rate, vertical compressive stresses and surface deflections was used as performance criteria to compare the performance of different test sections. Analysis of rutting rate results confirmed that the separation function of geosynthetics used prevented the migration of fines from the subgrade to the base course layer.

Analysis of Falling Weight Deflectometer (FWD) data suggested that the base course sections stabilized with geotextiles had a lower Base Damage Index (BDI), almost half that of the unstabilized section. The BDI is directly related to the pumping of fines from the subgrade to the base course, causing intermixing, which reduces the base course strength.

Giroud and Han (2004a) developed a theoretical design method for the base course thickness in unpaved roads. In addition to the conditions considered in earlier design methods, they took into account other factors such as distribution of stresses, strength of base course material, interlock between geosynthetic and base course material and geosynthetic stiffness. They proposed an equation to calculate the required base course thickness for given input parameters such as traffic load, subgrade strength and geogrid aperture stability modulus. The

equation could be implemented using different geosynthetics with appropriate calibration.

Giroud and Han (2004a) estimated the stresses at the interface between the base and subgrade using a stress distribution angle. The effect of base stiffness on the stress distribution angle is quantified using an approximate relationship between the stress distribution angle and the base to subgrade modulus ratio based on the Burmister's two-layer elastic solution (Burmister 1958).

Giroud and Han (2004a) analyzed laboratory tests performed by Gabr (2001) on unreinforced base and on base reinforced with biaxial geogrids. Their study led to a linear relationship involving the stress distribution angle and  $\log N$ , where  $N$  is the number of load applications (number of axle passes in the field). The stress distribution angle decreased progressively because of the progressive deterioration of the base due to cyclic loading resulting from trafficking. As the stress distribution angle decreases, the maximum vertical stress at the base/subgrade interface increases. Bearing capacity failure of the subgrade occurs when the stress distribution angle decreases to a point where the stress at the interface exceeds the mobilized bearing capacity of the subgrade. The bearing capacity of the subgrade depends on the undrained shear strength of the subgrade, the surface deformation or rut depth, the tire contact area and the base thickness (Giroud and Han 2004a).

Figure 14 shows Giroud and Han's proposed equation, which takes into account the progressive decrease of the stress distribution angle with the term  $k \log N$ ,

where  $k$  is a dimensionless parameter that depends on the radius of tire contact area, base thickness and reinforcement type. The inclusion of geosynthetic reinforcement between the base and subgrade interface reduces the deterioration rate of the base. As a result, the rate of decrease of the stress distribution angle is reduced.

$$h = \frac{1 + k \log N}{\tan \alpha_0 [1 + 0.204(R_E - 1)]} \times \left[ \sqrt{\frac{P}{\pi r^2 \left(\frac{s}{f_s}\right) \left\{ 1 - \xi \exp\left[-\omega \left(\frac{r}{h}\right)^n\right]\right\} N_c c_u}} - 1 \right] r$$

Figure 14. Equation for estimating the required base thickness by Giroud and Han (2004a)

The presence of a properly selected geosynthetic at the base/subgrade interface results in a stabilization effect, which decreases subgrade deformation and allows for a higher bearing capacity factor than if there was no geosynthetic. Giroud and Noiray (1981) suggested bearing capacity factors of 3.14 and 5.14 in the case of unreinforced and geotextile reinforced unpaved roads, respectively. In the case of a geogrid reinforced base, the lateral restraint due to geogrid aggregate interlock results in an inward shear stress on the subgrade, which increases the bearing capacity factor from 5.14 to 5.71. These bearing capacity factors have been adopted for Giroud and Han equation (Figure 14).

Giroud and Han (2004b) proposed that the deterioration rate correlates with the aperture stability modulus of geogrids in reinforced unpaved roads. They established this relationship based on the interpretation of laboratory cyclic plate loading tests on geogrid reinforced unpaved roads by Gabr (2001). Figure 15 shows a calibrated equation for the thickness of base layers reinforced with biaxial geogrids.

$$h = \frac{0.868 + (0.661 - 1.006J^2) \left(\frac{r}{h}\right)^{1.5} \log N}{1 + 0.204[R_E - 1]} \times \left[ \sqrt{\frac{\frac{P}{\pi r^2}}{\left(\frac{s}{f_s}\right) \left\{ 1 - 0.9 \exp\left[-\left(\frac{r}{h}\right)^2\right]\right\} N_c c_u} - 1} \right] r$$

Figure 15. Calibrated equation for biaxial geogrids in the study by Giroud and Han (2004b)

|            |  |
|------------|--|
| $h$        | = base course thickness  |
| $N$        | = number of passes of axle;  |
| $\alpha_0$ | = reference stress distribution angle, i.e., stress distribution angle derived from laboratory studies when $E_{bc} = E_{sg}$ ;                    |
| $R_E$      | = limited modulus ratio of base course to subgrade soil;   |
| $P$        | = load applied by one of the wheels in the case of single-wheel axles and the load applied by a set of two wheels in the case of dual-wheel axles; |
| $r$        | = radius of equivalent tire contact area;  |
| $s$        | = rut depth and, generally, allowable rut depth;   |
| $f_S$      | = factor equal to 75 mm rut depth;   |
| $c_u$      | = undrained cohesion of subgrade soil;   |
| $N_c$      | = bearing capacity factor;   |
| $J$        | = aperture stability modulus of geogrid;   |
| $\xi$      | = constant;  |
| $\omega$   | = constant.  |

Figure 16. Nomenclature for equation in Figure 15 (Giroud and Han 2004).

Giroud and Han (2004) determined the three unknown parameters  $\xi$ ,  $\omega$  and  $n$  by using the field data published by Hammitt (1970) for unpaved roads constructed with unreinforced unbound aggregate. The values  $\xi = 0.9$ ,  $\omega = 1.0$  and  $n = 2.0$  were found to provide the best correlation between the measured base thickness values and the values calculated using the equation in Figure 14. Figure 16 presents a list of notations used by Giroud and Han (2004a,b) in their study.

In conclusion, the design method for geogrid reinforced unpaved roads presented by Giroud and Han (2004a,b) includes parameters that were not accounted for in methods published previously such as interlock between geogrid and base course aggregate, in-plane aperture stability modulus of the geogrid and base course aggregate resilient modulus. In addition, their design method accounts for parameters that were accounted for in methods published previously, such as:

traffic volume, wheel loads, tire pressure, subgrade strength and rut depth. Moreover, Giroud and Han calculate the required base course thickness for a reinforced unpaved road using a single equation. This is an advantage over earlier methods where base course thickness for reinforced unpaved roads was determined in two steps: first the required base course thickness for an unreinforced unpaved road had to be calculated and the difference between the required base course thickness for the unreinforced and the reinforced unpaved roads on the same subgrade soil could be determined.

Chehab et al. (2007) studied the effects of aperture size, tensile strength at 2% strain, ultimate tensile strength, junction strength and flexural rigidity of geogrids on rutting performance of small-scale roadway models. For this purpose, they implemented an Accelerated Pavement Tests (APT) section. Figure 1 shows the dimensions and layout of the four segments. Geogrids Synteen SF11, Huesker Fornit 30, Tensar BX1200 and Mirafi BXG11 were placed in segments R1, R2, R3 and R4, respectively (Figure 17).

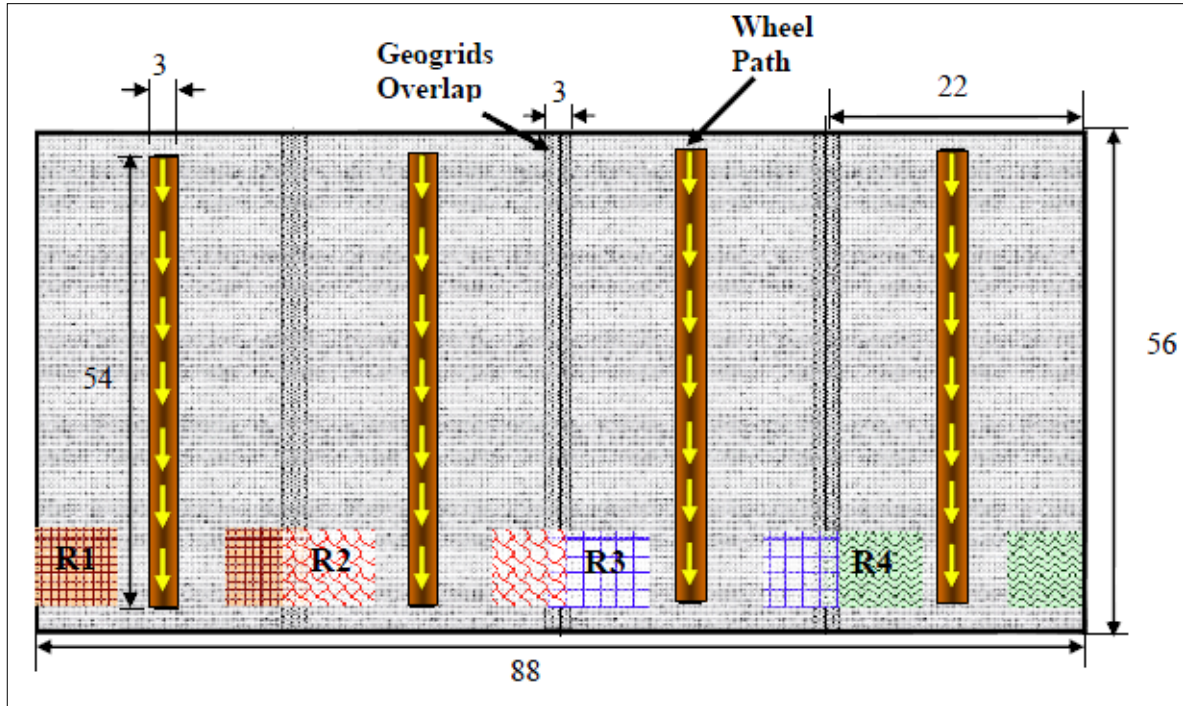


Figure 17. Plan view of the full-scale test section (in inches) by Chehab et al. (2007)

Chehab et al. (2007) proposed a series of correlations between the geogrid index properties and the rutting performance of their reinforced models. Important geogrid characteristics that can influence reinforcing effectiveness were recognized. They concluded that ultimate junction strength is an important property of geogrids to attain high pullout resistance. It was also found that geogrid junction strength contributes to the interface resistance significantly. Overall, a good correlation was found between the combined geogrid tensile strength and junction strength properties and the results of their direct shear and pullout tests. They concluded that wide-width tensile strength and junction

strength contributed to the characterization of geogrids in a complex manner, influencing the interaction properties of the reinforcement interface.

Henry et al. (2008) constructed and instrumented a set of full-scale pavement test sections to evaluate the reinforcing effect of a geogrid placed between the base and subgrade layers of pavement typically constructed by state transportation agencies. Prior studies reported significant benefits related to the presence of a geogrid layer with soft subgrades and relatively thin asphalt layers compared to typical state highways. The test sections were constructed for this study to help evaluate the potential benefits of geogrid reinforcement in pavement structures representative of modern highways. The testing of the pavement test sections included accelerated pavement testing by means of a heavy vehicle simulator under controlled temperature and moisture conditions.

The test sections were constructed in the Frost Effects Research Facility (FERF) of the U.S. Army Engineer Research and Development Center's Cold Regions Research and Engineering Laboratory (ERDC-CRREL) in Hanover, New Hampshire. The FERF maintains moisture and temperature conditions during construction and traffic testing. The temperature inside the FERF was kept at approximately 73°F (23°C) during construction. The ERDC/CRREL TR-08-6 report documents in detail, the construction and instrumentation of the test sections which are essential data interpretation and analysis.

The test sections were constructed in a test pit with concrete walls that was 110 ft (33.5 m) long, 21 ft (6.4 m) wide and 8 ft (2.44 m) deep below the pavement

surface (Figure 18). The thickness of the base course was 12 inches (0.30 m) for Test Sections 1 through 4, and 24 inches (0.61 m) for Test Sections 5 through 8. The asphalt thickness for the east lane (Test Sections 2, 4, 6 and 8) was 4 inches (102 mm). The asphalt thickness for the west lane (Test Sections 1, 3, 5 and 7) was 6 in (152 mm).

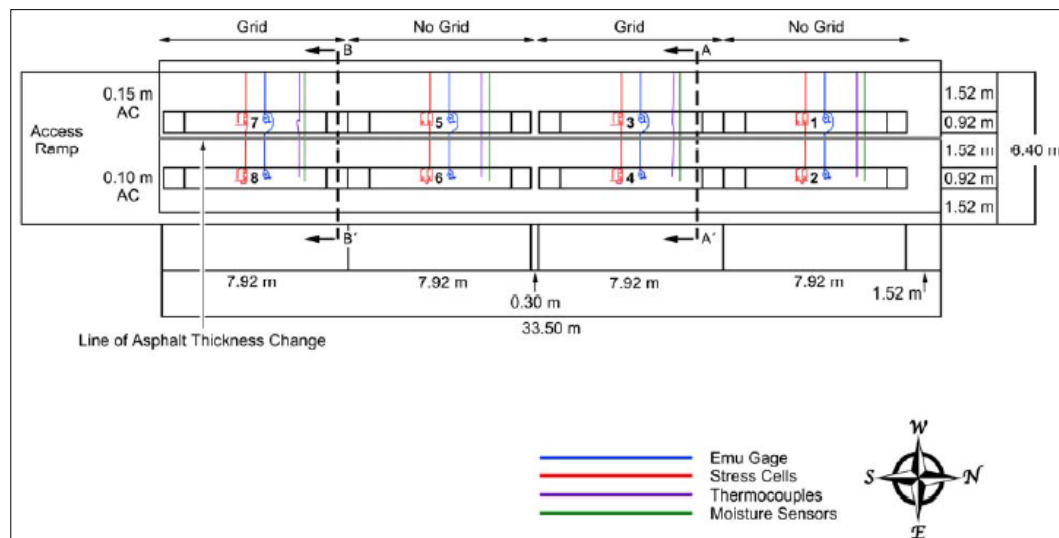


Figure 18. Plan view, indicating the instrumented test sections (numbered rectangles) where traffic load was applied in the study by Henry et al. (2008)

The geogrid used in these experiments was Tensar BX1200 and was chosen because it had been used in similar studies in the past and it was relatively easy to instrument with strain gauges. This allowed a comparison between the test results generated by Henry et al.'s study and others reported in the literature. The mechanical properties provided by the manufacturer for the geogrid are listed in Table 8.

Table 8. Properties of the geogrid used in the test sections in the study by Henry et al. (2008)

| Aperture size (mm; in.) |                         | Wide-width tensile strength at 2% strain* (kN/m; lb/ft) |                         |
|-------------------------|-------------------------|---|-------------------------|
| Machine direction       | Cross-machine direction | Machine direction                                       | Cross-machine direction |
| 25; 1.0                 | 33; 1.3                 | 6.0; 410  | 9.0; 620                |

\*Determined according to ASTM D6637

Each test section was instrumented with moisture and temperature sensors, triaxial strain gauges ( $\epsilon$ mu coils) and pressure cells. In addition to the installed coils, a hand-held  $\epsilon$ mu coil was placed over the asphalt surface to measure the vertical deformation of the asphalt layer when deformation readings were made. Figure 19 and Figure 20 show a typical plan view and cross section of the portion of a geogrid test section in which instrumentation was installed, respectively.

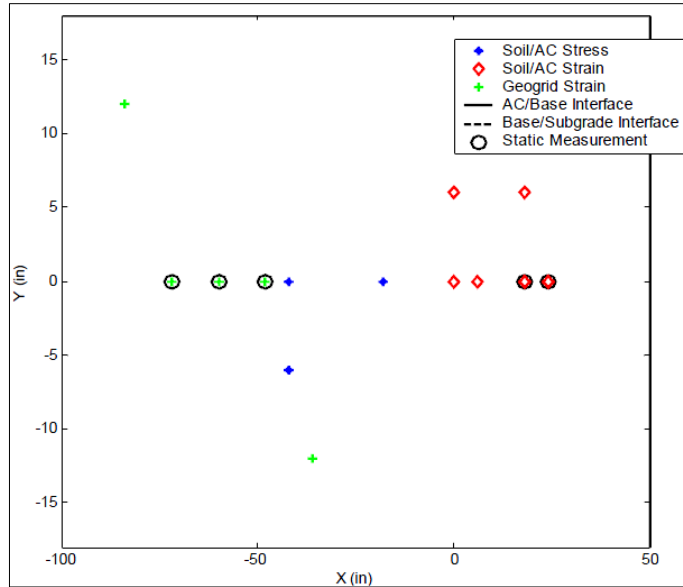


Figure 19. Plan view indicating the locations of instruments in a geogrid test section in the study by Henry et al. (2008)

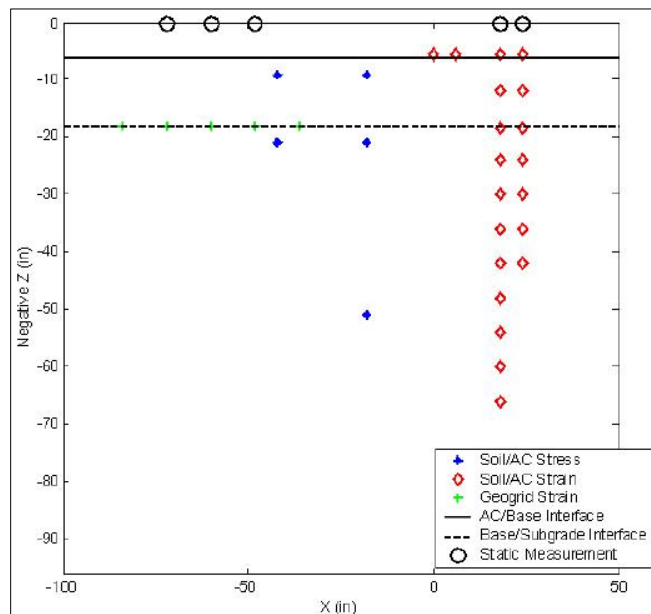


Figure 20. Cross sectional view indicating the locations of instruments in a geogrid test section in the study by Henry et al. (2008)

Henry et al. (2008) provided a detailed description of their instrumentation and test setup which is summarized below:

### Pressure Cells

Geokon® soil pressure cells were installed in the base course and subgrade of each test section for the purpose of measuring stresses in the soil (Figure 21). The pressure cells consist of two circular stainless steel plates welded together around their edge and enclosing a fluid connected to a pressure transducer through a high-pressure stainless steel tube. The pressure transducer outputs a voltage that is calibrated to measure stress.

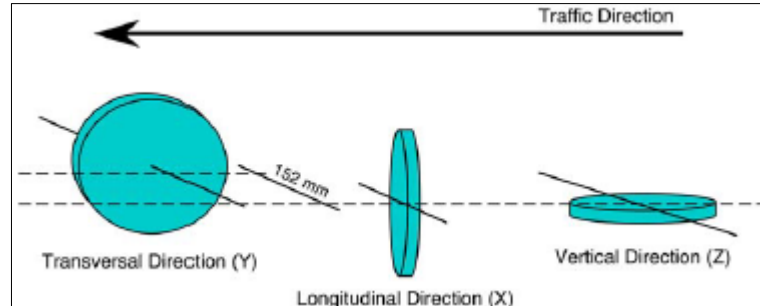


Figure 21. Orientation of pressure cells in the study by Henry et al. (2008)

The pressure cells were installed in three perpendicular directions: vertical, longitudinal (in the direction of traffic) and transverse (perpendicular to the direction of traffic). The pressure cells in the transverse direction were offset 6

inches (152 mm) to avoid pressure measurement directly beneath the wheel load.

### Soil and Asphalt Strain Sensors

Henry et al. (2008) installed electromagnetic induction ( $\epsilon\mu$ ) coils to measure static deformations in the soil in the vertical and horizontal directions. The  $\epsilon\mu$  coils were manufactured and calibrated at the ERDC-CRREL. The  $\epsilon\mu$  coils work in pairs which are not in contact with each other. One coil (sender) is energized by an external power supply. The nearest coil (receiver) is located within the electromagnetic field of the sender and produces an induced current proportional to the distance between the coils.

### Geogrid Strain Gauges

Ten electrical resistance strain gauges were attached to the geogrid in each test section to measure longitudinal and transverse strain. Five strain gauges were placed at the top and other five at the bottom of the grid. The strain gauges used were Texas Measurements model FLA-5-23, which are capable of measuring up to 3% strain and have a gauge factor of 2.16. The gauges had a copper-nickel alloy foil element, which was attached to the geogrid ribs using a two-part epoxy. Each gauge had pre-soldered lead wires that were connected to a data

acquisition system. Readings were taken by applying an excitation voltage of approximately 2500 mV using a Wheatstone bridge (Figure 22).

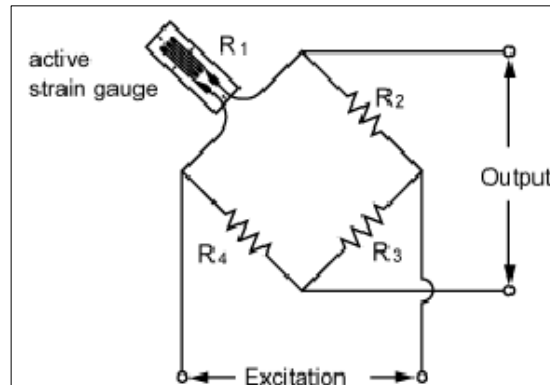


Figure 22. Wheatstone bridge configuration used for strain gauge measurement in the study by Henry et al. (2008)

### Data Acquisition System

The data acquisition in Henry et al.'s project consisted of four subsystems. The moisture and temperature sensors were connected to a system of Campbell Scientific CR10X data loggers, which were networked with a computer located in the FERF facility. The CR10X is a fully programmable datalogger/controller with non-volatile memory and a battery-backed clock. It has an input voltage range of  $\pm 2500$  mV to  $\pm 2.5$  mV. In addition, three multi-channel relay board Campbell Scientific AM416 multiplexers were used to handle the large number of sensors,

The second subsystem used consisted of the sensors within the heavy vehicle simulator. This system was an integral part of the HVS. It kept records of the number of traffic passes, traffic wander and average load intensity for each pass.

The third data acquisition subsystem was the laser profilometer developed by Dynatests to accurately measure ruts developed by HVS traffic. This system automatically logged data related to rut depth measurement whenever the profilometer was operating.

The fourth subsystem was a high-speed data acquisition system developed by ERDC-CRREL electronic engineers to collect and preprocess the signals from the stress and strain sensors. National Instruments LabVIEW was used in conjunction with an NI 6033E data acquisition card to read the outputs of the  $\epsilon$ mu coils and the strain gauges.

Al-Qadi et al. (2008) carried out a series of full-scale accelerated pavement tests to determine the effectiveness of geogrids in improving the performance of low-volume flexible pavement roads. Their study also examined the methods to maximize the benefits and cost-effectiveness of geogrids. Three flexible pavement test cells (i.e. A, B/C and D, as shown in Table 9) were constructed at the University of Illinois Advanced Transportation Research and Engineering Laboratories (ATREL).

Table 9. Pavement test cells and sections (Al-Qadi et al. 2008; 1 inch = 25.4 mm; 1 ft = 0.305 m)

| Pavement Test Cell Name | Section | Base Thickness (mm) | HMA Thickness (mm) | Length (m) | Geogrid (GG) Type and Location                             |
|-------------------------|---------|---------------------|--------------------|------------|--|
| A                       | A-1     | 203                 | 76                 | 6.1        | GG1 @ subgrade-base interface                              |
|                         | A-2     |                     |                    |            | GG2 @ subgrade-base interface                              |
|                         | A-3     |                     |                    |            | Control  |
| B/C                     | B-1     | 305                 | 76                 | 6.1        | Control  |
|                         | B-2     |                     |                    | 7.6        | GG2 @ subgrade-base interface                              |
|                         | C-1     |                     |                    | 127        | Control  |
| D                       | D-1     | 457                 | 76                 | 6.1        | GG2 @ 152 mm from top base                                 |
|                         | D-2     |                     |                    |            | GG2 @ subgrade-base interface & GG2 @ 152 mm from top base |
|                         | D-3     |                     |                    |            | Control  |

A total of 173 instruments were embedded during the pavement construction. These instruments were used to monitor the environmental (temperature, moisture and pore-water pressure) and tire loading effects (stress, strain and deflection) in the test sections. The load-associated instruments were installed along the pavement centerline to collect dynamic responses underneath the tire. The instruments used to measure environmental effect were installed 3 ft away from the centerline to collect static data.

Two types of field testing were conducted: 1) response testing and 2) traffic loading (performance). Germane to response testing, environmental responses included: a) Temperature measurements, in which data were collected over a period of 20 days and b) Moisture content measurements, in which data were

collected over a period of 8 months. Response testing was primarily conducted at various load levels, speeds, offsets and tire inflation pressures. Traffic loading was applied at the centerline of the test section. A 10-kip load at 5 mph and 100 psi tire pressure was applied to the pavement test sections. The ATLAS (Accelerated Testing Loading Assembly System) loading was applied in one direction to simulate field loading conditions. ATALS was used to load the three pavement test sections of each cell at the same time. Figure 23 shows the pavement layer profiles after excavation.

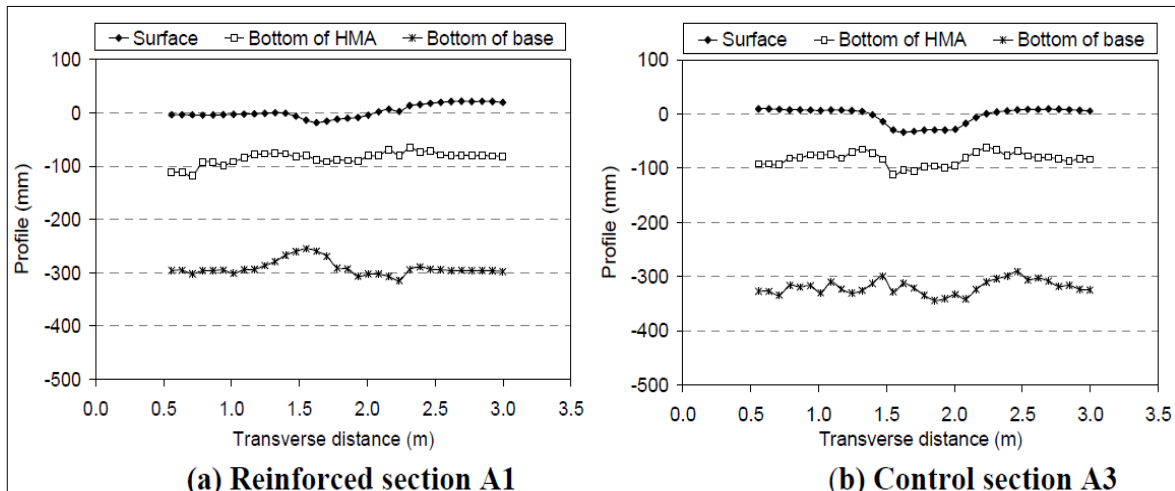


Figure 23. Measured pavement layer profiles after excavation (Al-Qadi et al. 2008)

Al-Qadi et al. (2008) found that pavement structure composition and layer thickness were crucial to the pavement performance and to the distress type developed. They observed that geogrid was effective in reducing pavement distresses, especially when properly installed at an optimal location. Al-Qadi et al. (2008) also concluded that the optimal geogrid location in a thin aggregate layer

was at the unbound aggregate-subgrade interface. However, they suggested that it was optimal to install a single geogrid at the upper third of thicker base layers, in which case another geogrid at the subgrade-base layer interface might be needed for stability.

Based on the measured pavement responses as well as the visual observations of the pavement cross sections after excavation, their study showed that geogrid was very effective in reducing the horizontal shear deformation of the aggregate layer, especially in the traffic direction.

Warren et al. (2008) studied the strain gauge survivability on both geogrid and geotextiles in a full-scale unpaved test section. Five protection methods were implemented on five geogrid and five geotextile products. The objective of this study was to compare different strain gauge protection techniques under construction and traffic loads, in order to identify the preferred method for use during the field construction of a geosynthetic-reinforced test section in an actual road.

Warren et al. (2008) reinforced the first test section with a 15 ft-wide and 25 ft-long high-strength woven geotextile (Amoco Fabrics Propex 2044). The second test section was reinforced using a 13 ft-wide and 25 ft-long, biaxial geogrid (Tensar BX1200). An 8-inch-deep test area was excavated and a trash pump was used to dewater the site which had received a significant amount of rain, resulting in poor subgrade conditions. Instrumented geosynthetics were placed at

the top of the subgrade and 8 inches of aggregate was placed to bring the base course layer to surface grade.

Geosynthetic specimens were instrumented with five groups of strain gauges. To ensure repeatability, each group consisted of three strain gauges. Figure 24 shows the strain gauge layout in both test sections. Geogrid specimens were instrumented using 0.23-inch-long EP-08-230DS-120 strain gauges (by Micro-Measurements) together with the AE-10 adhesive. Geotextile specimens were instrumented using 1.9-inch-long model EP-08-19CDZ-350 strain gauges. The wires and gauges were coated and/or wrapped with a combination of protective products (i.e. Micro-Measurements M-Coat, Gagekote No. 8, Aquaseal and electrical tape) to protect them from moisture. However, the use of above products was not suitable for geotextile specimens because it would alter their stiffness. As an alternative, high-grade silicone (Dow Corning RTV 3145) was used as for the adhesive and waterproofing agent.

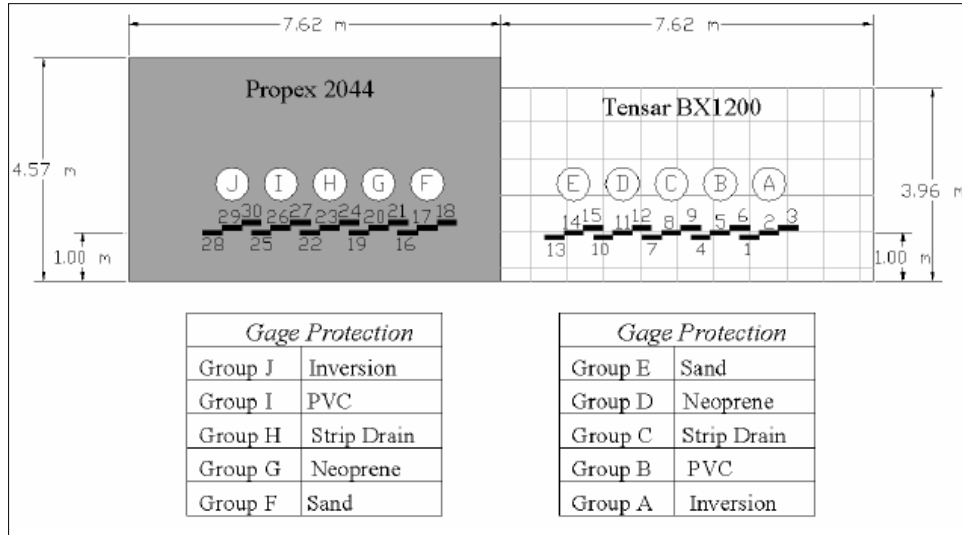


Figure 24. Geosynthetic instrumentation layout and gage protection methods in test sections reported by Warren et al. (2008)

Each group of strain gauges was protected using one of five methods as applicable to each geosynthetic material: (1) strain gauges in groups A and J were attached to the bottom of each geosynthetic material and a sand cushion was placed underneath the material adjacent to the gauges; (2) schedule 40 PVC pipe was sliced in half to create a hemispherical section that could be placed on top of gauge groups B and I and flexible vinyl tubing was wrapped around the edges to protect them from sharp edges; (3) geosynthetic strip drains (distributed by American Wick Drain Corporation) were placed over gauge groups C and H, ensuring that the pressure points of the polymeric core were facing downward between gauges; (4) gauge groups D and G were protected using neoprene mouse pads connected in a floating mat formation; and (5) a sand cushion was

placed on gauge groups E and F. Figure 25 shows each protection method adjacent to the corresponding strain gauge.

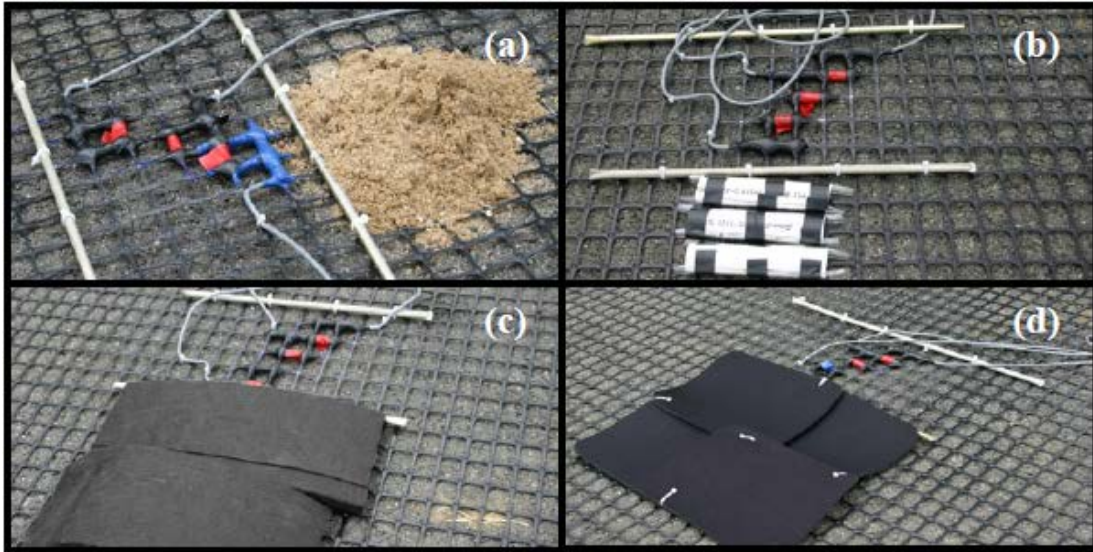


Figure 25. Strain gauge protection methods in the study by Warren et al. (2008): (a) sand cushion; (b) edge-protected PVC pipe; (c) geosynthetic strip drain; (d) neoprene mouse pads.

Groups A-F each consisted of three strain gauges. The resistance of the first two gauges was manually measured with a multi-meter and the third gauge was wired to a data acquisition system to continuously monitor the voltage. Measurements from gauges that were inactive were dismissed. A gauge was considered active as long as the multi-meter read a value close to the initial gauge resistance or a voltage jump was measured from the data acquisition system as the test sections were loaded.

Following geosynthetic installation, Warren et al. (2008) carried out a two-phase field test: Phase 1 - aggregate placement and compaction using a tracked bulldozer and vibratory compaction roller and Phase 2 - loaded construction traffic. During Phase 1, the base course aggregate was placed on the geosynthetic materials using a John Deere Bulldozer (750B Long Track) with 24 inch-wide tracks, to minimize the overburden pressure on the strain gauges. Then, a compaction roller with roller drum widths equal to 6.9 ft and an operating weight equal to 8.27 ton-force was used to complete 74 single passes over each geosynthetic specimen. The base course layer was approximately 8 inches thick at the completion of this phase. Average dry unit weight, total unit weight and water content measurements at the completion of the compaction phase using a Troxler nuclear gauge were found equal to 132 lb/ft<sup>3</sup>, 137 lb/ft<sup>3</sup> and 4%, respectively. During Phase 2, a 517 ft<sup>3</sup>-capacity dump truck with a 110 psi tire pressure was loaded with 73 kips of soil. The dump truck completed 70 single passes before it malfunctioned and the study was forced to terminate. However, most gauges had already failed by the end of Phase 2.

Table 10 shows a summary of the survivability success of the protection methods for each group of gauges in the two geosynthetic test sections. The cause of failure and the number of passes at failure are summarized for each strain gauge.

Table 10. Survivability of gauge protection methods in the study by Warren et al. (2008) (NA= not applicable)

| Group | Gage No. | Material   | Protection Method        | Cause of Failure | No. Total Passes |
|-------|----------|------------|--------------------------|------------------|------------------|
| A     | 1        | Geogrid    | Inversion with Sand      | NA               | NA               |
|       | 2        |            |                          | Compaction       | 66               |
|       | 3        |            |                          | NA               | NA               |
| B     | 4        | Geogrid    | PVC                      | Transition       | 74               |
|       | 5        |            |                          | Truck Traffic    | 84               |
|       | 6        |            |                          | NA               | NA               |
| C     | 7        | Geogrid    | Geosynthetic Strip Drain | NA               | NA               |
|       | 8        |            |                          | Transition       | 74               |
|       | 9        |            |                          | Truck Traffic    | 94               |
| D     | 10       | Geogrid    | Neoprene                 | Truck Traffic    | 96               |
|       | 11       |            |                          | NA               | NA               |
|       | 12       |            |                          | Compaction       | 20               |
| E     | 13       | Geogrid    | Sand                     | Transition       | 74               |
|       | 14       |            |                          | Compaction       | 68               |
|       | 15       |            |                          | Compaction       | 40               |
| F     | 16       | Geotextile | Sand                     | Truck Traffic    | 104              |
|       | 17       |            |                          | Truck Traffic    | 94               |
|       | 18       |            |                          | Truck Traffic    | 92               |
| G     | 19       | Geotextile | Neoprene                 | Compaction       | 64               |
|       | 20       |            |                          | Truck Traffic    | 84               |
|       | 21       |            |                          | Truck Traffic    | 124              |
| H     | 22       | Geotextile | Geosynthetic Strip Drain | Compaction       | 64               |
|       | 23       |            |                          | Compaction       | 52               |
|       | 24       |            |                          | Truck Traffic    | 92               |
| I     | 25       | Geotextile | PVC                      | Truck Traffic    | 114              |
|       | 26       |            |                          | Compaction       | 30               |
|       | 27       |            |                          | Truck Traffic    | 110              |
| J     | 28       | Geotextile | Inversion                | NA               | NA               |

| Group | Gage No. | Material | Protection Method | Cause of Failure | No. Total Passes |
|-------|----------|----------|-------------------|------------------|------------------|
|       | 29       |          | with Sand         | Truck Traffic    | 144              |
|       | 30       |          |                   | NA               | NA               |

Warren et al. (2008) concluded that the preferred method of gauge protection depends on the geosynthetic. The sand cushion method (group E) was the only group that failed to have an operating gauge at the end of the study. All PVC and geosynthetic strip drain gauges remained operational through the compaction phase. The geosynthetic strip drain and PVC tube protection methods performed similarly. However, the geosynthetic strip drain was selected as the preferred method because it is more readily available, the specifications are consistent to ensure quality control, the core is relatively flexible in comparison to hemispherical PVC and the polymeric core design easily fits within the apertures of the geogrid to develop an interlocking feature for this protection method during construction.

On the other hand, all geotextile gauges failed to remain operational at the end of the study. Even though the gauges in group F (i.e. sand protection) performed the best overall, a solid protection layer would still be necessary to prevent sharp aggregate particles from puncturing the gauges during construction. The method involving neoprene mouse pads was selected as the most suitable method to protect geotextile strain gauges because the alternative methods either did not perform as well or were not fabricated as easily. To examine this choice further, a

separate area was constructed as part of the main geosynthetic research project. A woven geotextile was instrumented with 20 strain gauges and all but one gauge survived using neoprene mouse pad protection.

Cuelho and Perkins (2009) constructed field test sections to evaluate the performance of several geosynthetics (8 geogrids and 2 geotextiles) in subgrade stabilization. Their research was aimed at understanding which geogrid properties were most relevant to their field performance in order to update the Montana Department of Transportation (MDT) materials specifications to include a broader range of geosynthetic materials for reinforcement applications.

Figure 26 shows a schematic cross-section of the field test section studied by Cuelho and Perkins (2009). Each test section was 4 m wide, 1 m deep and 15 m long (195 m long in total) (Figure 27). A 1-m (40 in) deep subgrade soil (CBR approximately 1.8) was placed followed by geosynthetic specimens and a 20 cm (8 in)-thick aggregate layer. Table 11 presents the methodology and findings of Cuelho and Perkins study.

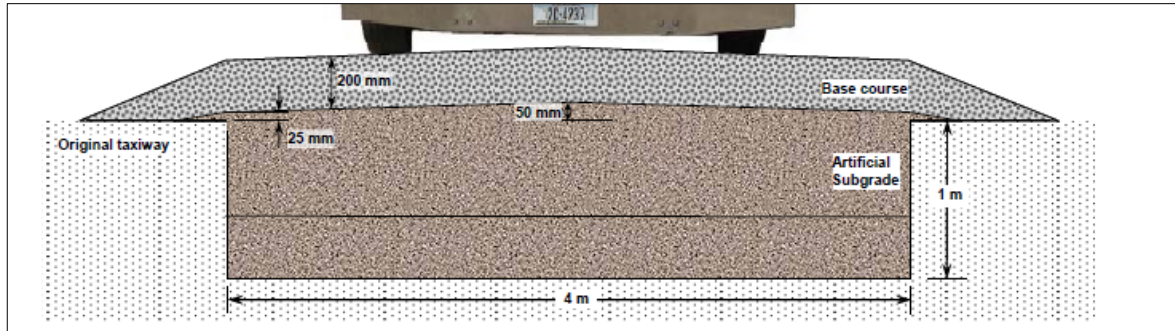


Figure 26. Schematic cross-section of the field test section in Cuelho and Perkins's study (2009)

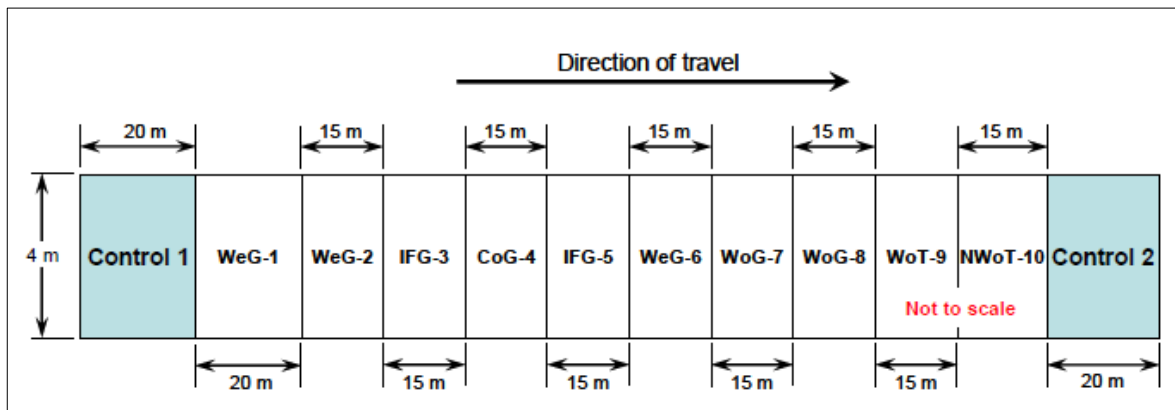


Figure 27. General layout of test sections (Cuelho and Perkins 2009)

Table 11. Methodology and findings of the study by Cuelho and Perkins (2009)

|                                    |   |
|------------------------------------|---|
| Date, location, size and objective | <p>The final report was submitted in July 2009.</p> <p>The field test was done at the 'Transcend' research facility in Lewistown, Montana, in a decommissioned taxiway.</p> <p>The study was aimed at understanding which geogrid properties were most relevant to their field performance</p>                |
| Instrumentation plan               | <p>12 test sections. 8 with geogrids, 2 with geotextiles and 2 control sections.</p> <p>Each section: Three measurement of transverse displacement of the geosynthetics in the vicinity of rut bowl, using three LVDTs. A single measurement of pore pressure with a stainless steel pressure transducer.</p> |

|                         |  |
|-------------------------|--|
| <p>Testing programs</p> | <p><u>Laboratory tests:</u></p> <ol style="list-style-type: none"> <li>1. Tests to relate CBR to vane shear</li> </ol> <p><u>Subgrade soil:</u></p> <ol style="list-style-type: none"> <li>1. Atterberg limit tests</li> <li>2. Sieve Analysis tests</li> <li>3. Standard Proctor tests (AASHTO T-99)</li> <li>4. Unsaturated CBR tests were run to laboratory prior to construction to determine the relationship between CBR (subgrade strength) and moisture content</li> <li>5. Vane shear tests were also conducted on the laboratory CBR samples to relate CBR to vane shear strength.</li> </ol> <p><u>Aggregate:</u></p> <ol style="list-style-type: none"> <li>1. Atterberg limit tests</li> <li>2. Sieve Analysis tests</li> <li>3. Modified Proctor tests (ASTM D1557)</li> </ol> <p><u>Geogrid:</u></p> <ol style="list-style-type: none"> <li>1. Wide-width tensile strength tests (ASTM D4595) both in MD and XD</li> <li>2. Junction strength (GRI GG2) tests both in MD and XD</li> </ol> <p>These tests were done by WTI (Western Transportation Institute).</p> <ol style="list-style-type: none"> <li>3. Rib and junction damage assessments</li> </ol> <p><u>Field tests:</u></p> <ol style="list-style-type: none"> <li>1. Vane shear tests to monitor in-place shear strength of the subgrade as it was being constructed.</li> <li>2. Dynamic cone penetrometer (DCP) tests to monitor subgrade strength before and after trafficking</li> <li>3. Moisture content of subgrade soil was monitored</li> <li>4. Installation damage tests</li> <li>5. Air and vacuum removal of base course and subgrade removal</li> <li>6. Rut analysis</li> <li>7. Pore water pressure analysis</li> </ol> |
|-------------------------|--|

|                              |   |
|------------------------------|---|
| Findings and recommendations | The results showed that the welded geogrids, woven geogrids and the stronger integrally-formed geogrid seemed to provide the best overall performance. The two geotextile products and the weaker integrally-formed geogrid provided significantly less stabilization benefit based on the normalized rutting performance at 50 mm, 75 mm and 100 mm of longitudinal rut data. This performance was likely directly related to the tensile strength of the materials in the cross-machine direction. Based on the comparative analysis used during this study, tensile strength in the cross-machine direction of the geosynthetics (especially at 2 percent axial strain) likely plays a large role in suppressing rut formation under these conditions. |
| Final remarks                | Additional research is needed to determine other material tests and to relate these results to field performance.   |

Tingle and Jersey (2009) constructed and trafficked a full-scale roadway test section with a heavy truck to evaluate the strength and deformation performance of the unreinforced and reinforced sections. The investigation involved eight instrumented aggregate road sections, including three different aggregate base materials and two different geosynthetic products. The objective of this investigation was to evaluate the performance of geosynthetic-reinforced aggregate road sections constructed with marginal base materials over a typical subgrade. The experiment was conducted under the Lines-of-Communication program of the U.S. Army Corps of Engineers by the U.S. Army Engineering Research and Development Center, Waterways Experiment Station.

The design of the full-scale aggregate road test section depicted in Figure 28 was divided into eight individual test items (i.e. segments), each consisting of an aggregate base course placed over a high-plasticity clay (CH) subgrade. Items 4

through 8 included a geosynthetic layer installed at the interface between the base and subgrade. Three different base materials were used: a crushed limestone, a crushed chert aggregate and a clay gravel. The crushed limestone aggregate (SW-SM) with nonplastic fines was used for the higher-quality base aggregate material. The crushed chert aggregate base (GW) with nonplastic fines was used to evaluate a more uniformly graded base material with crushed particles. The clay gravel base (GP-GM) with rounded aggregate and plastic fines was used to evaluate the performance of the geosynthetic reinforcement in a marginal base material. For this study, only one type of geotextile and geogrid were selected, based on guidance in the U.S. Army Corps of Engineers (2003).

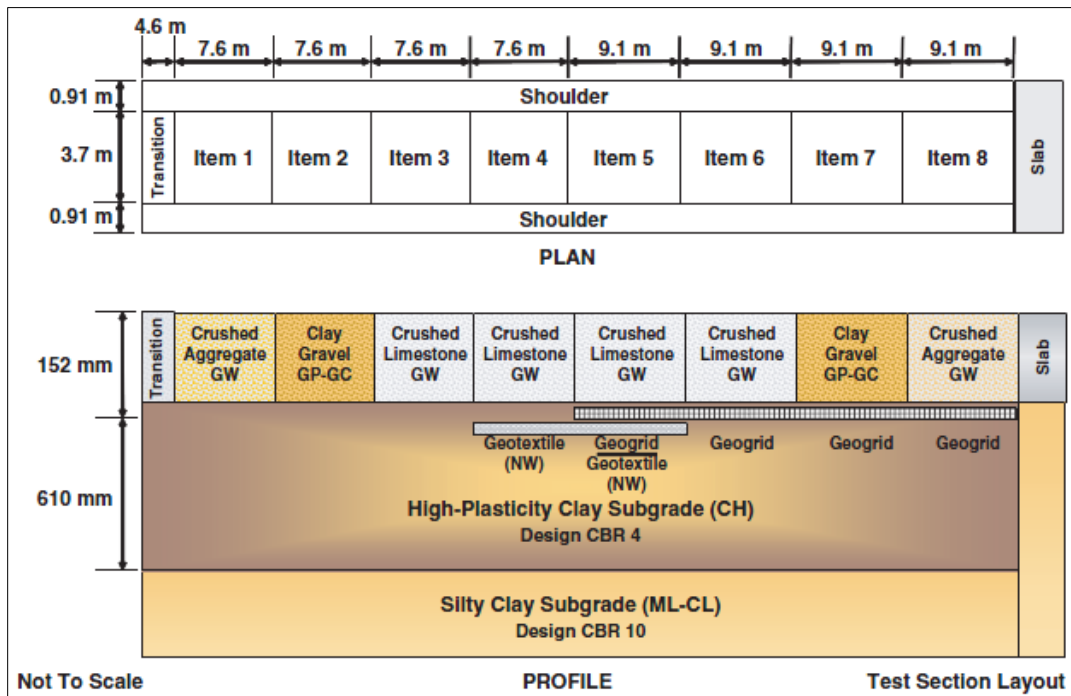


Figure 28. Plan and profile views of the full-scale test section layout in the study by Tingle and Jersey (2009)

Instruments were installed in the test section to measure the response of each test item to the applied loading. Eight 9-inch-diameter Geokon earth pressure cells (EPCs), one per test item, were placed in the wheel path approximately 2 inches below the base–subgrade interface to measure the vertical stress near the top of the subgrade. Eight single-depth deflectometers (SDDs) consisting of a linear variable differential transformer (LVDT) were installed in Items 2 through 7 at the surface of subgrade to measure the deflection at the top of the subgrade. Each LVDT was mounted in a tube on a rod anchored in concrete at a depth of 10 ft below the subgrade surface. Items 1 and 8 did not include SDDs because of projections of early item failure. Two SDDs were installed in Items 4 and 6 for redundancy because these items were deemed essential to the analysis. Four Geokon vibrating wire pore pressure transducers (VW-PPT) were placed in the wheel path of Items 3 through 6 at a depth of 2 in below the top of the subgrade to measure the relative change in pore pressure near the top of the subgrade. Campbell Scientific time domain reflectometry (TDR) moisture and temperature probes were placed near the top of the subgrade in Item 3 and the bottom of the aggregate base in Item 6 to monitor environmental changes. Eight foil strain gauges were mounted in half-bridge arrangements: two gauges on each of the geotextile in Item 4 and the geogrid in Item 6 were perpendicular to each other. Two data acquisition systems were used to filter and amplify the sensors output. A computer-controlled OPTIM system was used to measure the static and dynamic responses of the EPCs, SDDs and geosynthetic strain gauges. A Campbell Scientific data logger recorded soil temperature, volumetric moisture

and relative pore pressure every hour throughout testing to monitor changes in subgrade conditions.

The test section was trafficked with a dual-wheel tandem axle truck loaded to a gross weight of approximately 21.83 US tons with an equivalent axle load factor of approximately 0.98 based on a terminal serviceability index of 2.5 and an initial structural number of 5. The individual tires were inflated to a 50 psi tire pressure and produced a contact area of approximately 50 in<sup>2</sup>. The test vehicle was driven forward over the test items and then backed the length of the traffic lane in the same wheel path, resulting in two load applications or two passes. Static and dynamic response data and rut depth measurements for each test item were collected at selected traffic intervals. Data were also collected at the failure point of the test item, typically at 3 inches of permanent surface deformation.

The analysis of the results produced several conclusions regarding the benefit of incorporating geosynthetics into aggregate road sections and the effect on marginal base materials as follows:

1. Different aggregates provide different strength and deformation behavior as evidenced by the deflection, stress and deformation measurements presented for the unreinforced test items. The crushed chert aggregate performed the worst, followed by the crushed limestone and then the clay gravel. The clay gravel's performance was mostly attributed to natural cementation, presumably because of its high plastic fines content, because moisture susceptibility was not a test variable.

2. Reinforced pavement sections demonstrated an improved resistance to permanent deformation or rutting. Thus, geosynthetics are effective in reinforcing both high-quality and marginal base materials.

3. The initial stiffness of the reinforced test items was not a good indicator of performance. However, as the test items densified and mobilized the reinforcement, the stiffness of the reinforced test items increased rapidly and became better indicators of performance. Thus, initial pavement stiffness should not be used to evaluate reinforcement effectiveness. Stiffness may be used as a performance indicator only after a sufficient conditioning period to ensure that initial densification of the aggregate has occurred and the reinforcement has been mobilized.

Abu-Farsakh and Chen (2010) evaluated the performance of base and subgrade soil in flexible pavement under repeated loading test conditions. For this purpose, they performed indoor and full-scale field cyclic plate load tests on several pavement sections. The study was conducted for the Louisiana Department of Transportation in order to investigate the potential benefits of using geogrids as base reinforcement.

A series of large-scale cyclic plate load tests were conducted inside a test box [with dimensions 6.5-ft (L) x 6.5-ft (W) x 5.5-ft (H)], using a servo-hydraulic actuator, on flexible pavement sections with and without geogrid base reinforcement (Figure 29). The maximum applied load was 9 kips, which represents a loading pressure of 80 psi and simulates dual wheels under an

equivalent 18 kips single-axle load. The load pulse, had a linear load increase from 0.5 kips to 9 kips in 0.3 second, followed by a 0.2-second period where the load was held constant at 9 kips, then the linear load decreased to 0.5 kips over a 0.3-seconds period, followed by a 0.5-second period of 0.5 kips before the next loading cycle. This load pulse resulted in a frequency of 0.77 Hz. The parameters studied by the authors included selected properties of geogrids (including their aperture shape, tensile modulus and embedment depth). Measured responses in the tests included stress distribution, permanent vertical strain and pore water pressure in the subgrade and the strain distribution in the geogrids.

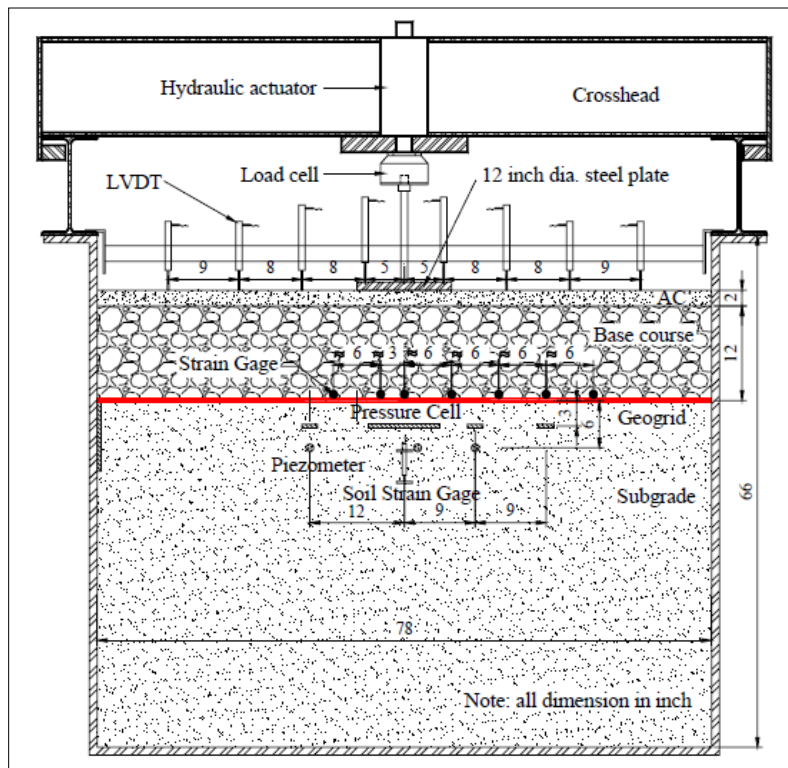


Figure 29. Laboratory cyclic plate load test layout in the study by Abu-Farsakh and Chen (2010)

With respect to the pavement layer materials, Abu-Farsakh and Chen (2010) used a super pavement Hot Mix Asphalt (HMA), a Kentucky crushed limestone as base course material and silty clay as subgrade material. Table 12 presents a brief description of the pavement materials used. Four different geogrids were used in the base course of the reinforced test sections. These geogrids had a punched structure (extruded) and were made from polypropylene with different geometries. The physical and mechanical properties of these geogrids are provided in Table 13.

Table 12. Pavement material specifications in the study by Abu-Farsakh and Chen (2010)

| Pavement materials    | Description  |
|-----------------------|--|
| Hot Mix Asphalt (HMA) | 19-mm designed for intermediate volume roads [i.e., 3-30 million equivalent single axis loads (ESALS)] Optimum asphalt binder content = 4.1 percent, classified as PG 76-22M. Theoretical maximum specific gravity of the HMA = 2.51.          |
| Base course           | Kentucky crushed limestone classified as GW (USCS) and A-1 (AASHTO). Maximum dry density = 140 lb/ft <sup>3</sup> (ASTM D698 Standard Proctor test) Optimum moisture content = 6.6 %   |
| Subgrade              | Silty clay classified as CL (USCS) and A-6 (AASHTO). Liquid limit (LL) of 31, plasticity index (PI) of 15.72 percent silt and 19 percent clay. Maximum dry density was 104 lb/ft <sup>3</sup> . Optimum moisture content of 18.75% (ASTM D698) |

Table 13. Physical and mechanical properties of geogrids used in the study by Abu-Farsakh and Chen (2010)

| Reinforcement       | Aperture Shape | T <sup>a</sup> , lb/ft |                 | J <sup>b</sup> , lb/ft |                 | Aperture Stability<br>kg-cm/deg | Aperture Size, in. |
|---------------------|----------------|------------------------|-----------------|------------------------|-----------------|---------------------------------|--------------------|
|                     |                | MD <sup>c</sup>        | CD <sup>d</sup> | MD <sup>c</sup>        | CD <sup>d</sup> |                                 |                    |
| GG1 biaxial geogrid | Squared        | 280                    | 450             | 14,000                 | 22,500          | 3.2                             | 1.0 x 1.3          |
| GG2 biaxial geogrid |                | 410                    | 620             | 20,500                 | 31,000          | 6.5                             | 1.0 x 1.3          |
| GG3 biaxial geogrid | Triangular     | 590 <sup>e</sup>       |                 | 29,500 <sup>e</sup>    |                 | 3.6                             | 1.6 x 1.6<br>x 1.6 |
| GG4 biaxial geogrid |                | 650 <sup>e</sup>       |                 | 32,500 <sup>e</sup>    |                 | 7.8                             | 1.6 x 1.6<br>x 1.6 |

<sup>a</sup>Tensile Strength (at 2% strain) (in accordance with ASTM D6637 for GG1 and ISO 10319:1996 for GG2), <sup>b</sup>Tensile Modulus (at 2% strain), <sup>c</sup>Machine Direction, <sup>d</sup>Cross Machine Direction, <sup>e</sup>Radial Direction

Abu-Farsakh and Chen (2010) prepared their indoor cyclic plate load tests with silty clay subgrade placed and compacted in lifts inside a steel box. The target dry density and water content was 100 lb/ft<sup>3</sup> and 22%, respectively, to achieve a weak subgrade of CBR = 0.5. In addition, an unreinforced test with subgrade compacted at optimum moisture content (CBR = 8%) was prepared to check the performance difference between a weak and a strong subgrade. The final thickness of the subgrade layer was approximately 46 inches. After the completion of subgrade preparation, the instrumentation and the geogrid layer were installed. The instrumentation plan included a soil strain gauge in the subgrade beneath the center of the loading plate. It consisted of a 4 inch-long LVDT fitted with two steel plates. The pore water pressure was measured using Model 4500AL Vibrating Wire (VW) piezometers from Geokon Inc. which were installed 6 inches beneath the top of the subgrade by excavating with a hand

trowel. In the same way, four pressure cells were installed 3 inches beneath the subgrade surface. Three type 0234 pressure cells from Kulite and one Model 3500-1 earth pressure cell from Geokon Inc. were positioned as shown in Figure 29. The strain distribution along the geogrid was measured using electrical resistance strain gauges model EP-08-250BG-120 from Vishay Micro-Measurements that were placed at different locations along the geogrid as shown in Figure 29. After the installation of the geogrids, the base course layer was prepared by placing the crushed limestone in 6 inch-thick lifts, mixing with desired water and then compacting to the final thickness of 12 inches. The target dry density and water content of base course layer were 138 lb/ft<sup>3</sup> (i.e., 98 percent degree of standard proctor compaction) and 6.0 %, respectively. The surface asphalt concrete (AC) layer was consequently prepared by placing prime coat on the top of the base layer, followed by placing cold-mix asphalt concrete along the sides of the box with a width of 12 inches. The remaining center area of the test box (a 54 inch-wide square) was left for the HMA. The cold mix asphalt at the boundary area of two mixes was covered with a tack coat. Then the HMA was placed over the reserved central area in the test box and immediately compacted to the predetermined height using the Bosch Brute breaker hammer. After the HMA was compacted, eight LVDTs from RDP Electronics were used to monitor surface deformation of the HMA layer. The LVDTs were mounted on a steel reference beam and installed on both sides of the actuator in a straight line as shown in Figure 29.

The main data acquisition system consisted of a Strain Gauge Amplifier (SGA) digital signal conditioning module and a FlexTest GT test controller connected to a desktop computer running the Station Manage Software package supplied by the MTS Systems Corporation. The magnitudes of output signals from the pressure cells and strain gauges were too small to be read by the controller, therefore they were connected to the signal conditioners first. A separate data acquisition system was used to read the vibration wire piezometers. This system consisted of Geokon Model 8032 16/32 channel multiplexers and a Geokon Model 8020 MICRO-10 Data logger connected to a laptop computer running a Multi-logger Software package.

A total of 10 tests were conducted on different pavement sections. Three unreinforced sections were constructed, one was placed on strong subgrade (CBR = 8%) and the other two were placed on a weak subgrade (CBR = 0.5%). Four reinforced sections with one geogrid layer were placed at the base/subgrade interface. Two reinforced sections with one geogrid layer were placed at the middle of the base layer. Finally, one reinforced section with one geogrid layer was placed at the upper one third of the base layer on the weak subgrade. The traffic benefit ratio (TBR), which is defined as the number of load cycles carried by a reinforced section at a specific rut depth divided by that of an otherwise identical unreinforced section, was calculated to evaluate the benefit of geogrid base reinforcement. The TBR results for unreinforced and reinforced pavement sections are summarized in Table 14. Figure 30 shows surface permanent deformations for different types of geogrids placed at the

base/subgrade interface. Figure 31 shows surface permanent deformations for test items in which GG3 and GG4 geogrids were placed at different locations.

Table 14. Summary of TBR results from the laboratory cyclic plate load tests in the study by Abu-Farsakh and Chen (2010)

| Reinforcement configuration        | Base Thickness inch (mm)  | HMA Thickness inch (mm) | Rut depth = 0.75 inch (19.1 mm) |                  |                  |                  | Rut depth = 1 inch (25 mm) |                  |                  |                  |
|------------------------------------|---------------------------|-------------------------|---------------------------------|------------------|------------------|------------------|----------------------------|------------------|------------------|------------------|
|                                    |                           |                         | Cycles                          | TBR <sub>c</sub> | TBR <sub>d</sub> | TBR <sub>e</sub> | Cycles                     | TBR <sub>c</sub> | TBR <sub>d</sub> | TBR <sub>e</sub> |
| Unreinforced -1 (CBR = 0.5%)       | 12 (305) <sup>a</sup>     | 2 (51) <sup>a</sup>     | 1601                            | -                | -                | -                | 14014                      | -                | -                | -                |
| Unreinforced -2 (CBR = 0.5%)       | 12.7 (323) <sup>b</sup>   | 2.1 (52.8) <sup>b</sup> | 7536                            | -                | -                | -                | 32962                      | -                | -                | -                |
| Unreinforced avg (CBR = 0.5%)      | -                         | -                       | 3887                            | -                | -                | -                | 23340                      | -                | -                | -                |
| Unreinforced (CBR = 8%)            | 12 (305) <sup>b</sup>     | 2 (51) <sup>a</sup>     | -                               | -                | -                | -                | -                          | -                | -                | -                |
| GG1 (interface) (CBR = 0.5%)       | 12.6 (319) <sup>b</sup>   | 2.4 (60) <sup>b</sup>   | 2148 <sub>2</sub>               | 5.5              | 13.4             | 2.9              | 49145                      | 2.1              | 3.5              | 1.5              |
| GG2 (interface) (CBR = 0.5%)       | 12.5 (317.5) <sup>b</sup> | 2.2 (55.6) <sup>b</sup> | 2362 <sub>8</sub>               | 6.1              | 14.8             | 3.1              | 70427                      | 3.0              | 5.0              | 2.1              |
| GG3 (interface) (CBR = 0.5%)       | 12.8 (325) <sup>b</sup>   | 2.2 (56) <sup>b</sup>   | 2487 <sub>2</sub>               | 6.4              | 15.5             | 3.3              | 81362                      | 3.5              | 5.8              | 2.5              |
| GG4 (interface) (CBR = 0.5%)       | 12.2 (311) <sup>b</sup>   | 2.2 (57) <sup>b</sup>   | 2873 <sub>5</sub>               | 7.4              | 17.9             | 3.8              | 10422 <sub>3</sub>         | 4.55             | 7.4              | 3.2              |
| GG3 (middle) (CBR = 0.5%)          | 12 (305) <sup>b</sup>     | 2.2 (57) <sup>b</sup>   | 2295 <sub>2</sub>               | 5.9              | 14.3             | 3.0              | 50663                      | 2.2              | 3.6              | 1.5              |
| GG4 (middle) (CBR = 0.5%)          | 11.9 (302) <sup>b</sup>   | 2.3 (59) <sup>b</sup>   | 2668 <sub>1</sub>               | 6.9              | 16.7             | 3.5              | 59621                      | 2.6              | 4.3              | 1.8              |
| GG4 (upper one third) (CBR = 0.5%) | 12.2 (310) <sup>b</sup>   | 2.2 (57) <sup>b</sup>   | 5956 <sub>0</sub>               | 15.3             | 37.2             | 7.9              | - <sup>f</sup>             | -                | -                | -                |
| GG4 (middle)                       | 12.3                      | 2.2 (57) <sup>b</sup>   | 4722                            | 12.1             | 29.5             | 6.3              | - <sup>f</sup>             | -                | -                | -                |

| Reinforcement configuration   | Base Thickness inch (mm) | HMA Thickness inch (mm) | Rut depth = 0.75 inch (19.1 mm) |                  |                  |                  | Rut depth = 1 inch (25 mm) |                  |                  |                  |
|-------------------------------|--------------------------|-------------------------|---------------------------------|------------------|------------------|------------------|----------------------------|------------------|------------------|------------------|
|                               |                          |                         | Cycles                          | TBR <sub>c</sub> | TBR <sub>d</sub> | TBR <sub>e</sub> | Cycles                     | TBR <sub>c</sub> | TBR <sub>d</sub> | TBR <sub>e</sub> |
| with prime coat) (CBR = 0.5%) | (312) <sup>b</sup>       |                         | 5                               |                  |                  |                  |                            |                  |                  |                  |

<sup>a</sup>Nominal thickness (measured actual thickness is not available for those sections); <sup>b</sup>Measured actual thickness; <sup>c</sup>Compared to unreinforced (average) (CBR=0.5%); <sup>d</sup>Compared to unreinforced-1 (CBR=0.5%); <sup>e</sup>Compared to unreinforced-2 (CBR=0.5%); <sup>f</sup>Rut depth in these test did not reach 1 inch; -: N/A.

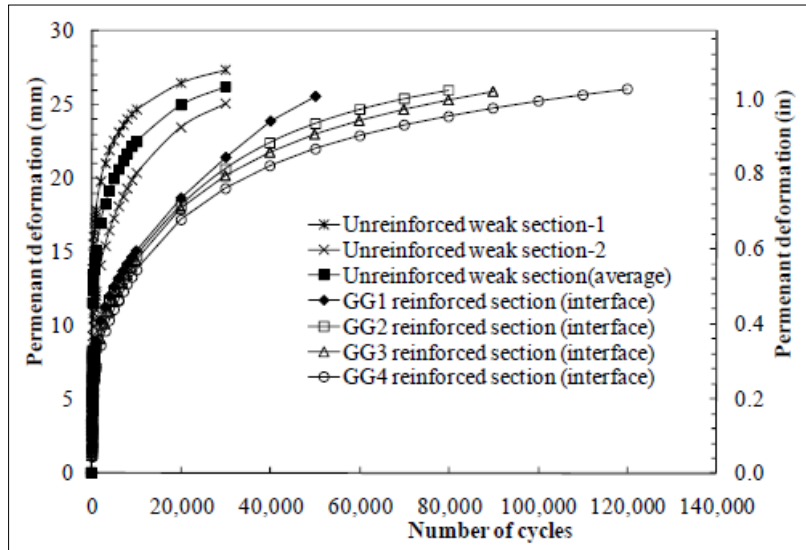


Figure 30. Measured permanent deformation at the base/subgrade interface for tests with different types of geogrids used in the study by Abu-Farsakh and Chen (2010)

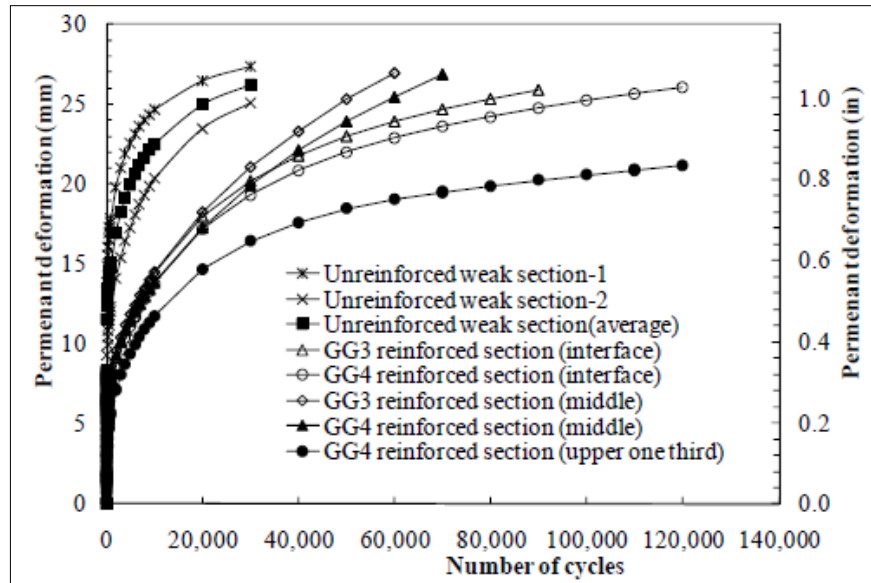


Figure 31. Surface permanent deformation for tests with GG3 and GG4 geogrids placed at different locations in the study by Abu-Farsakh and Chen (2010)

Based on the results of the cyclic plate load tests on pavement sections with and without geogrid reinforcement, Abu-Farsakh and Chen (2010) presented the following conclusions:

- The inclusion of geogrid for stabilization and base reinforcement can significantly reduce the rut depth and extend the service life of pavement sections built on weak subgrades. The TBR can be increased up to 15 at a rut depth of 0.75 inch for pavement constructed using a 12-inch-thick base course layer on top of a weak subgrade soil with  $CBR \leq 1$ .
- The improvement in performance of geogrid stabilized pavement is proportional to the geogrid tensile modulus. At a rut depth of 0.75 inch, the TBR increased from 5.5 for the biaxial geogrid GG1 to 6.1 for the biaxial geogrid GG2, of higher

tensile modulus. Meanwhile, the TBR increased from 6.4 for the triaxial geogrid GG3 to 7.4 for the triaxial geogrid GG4 with a higher tensile modulus.

- The triaxial geogrids with triangular aperture geometry performed better than biaxial geogrids with rectangular aperture geometry. At a rut depth of 0.75 inch, the TBR increased from 5.5 for the biaxial geogrid GG1 to 6.4 for the triaxial geogrid GG3. Meanwhile, the TBR increased from 6.1 for the biaxial geogrid GG2 to 7.4 for the triaxial geogrid GG4.

- The use of geogrid results in redistributing the applied load to a wider area, thus reducing the stress concentration and achieving an improved vertical stress distribution on top of the subgrade layer (Figure 32 shows the surface deformation after 30,000 cycles).

- Based on a new laboratory compaction technique for geogrid placed at the upper one third of the base layer, a better performance was observed in comparison to the tests when the geogrid was placed at the base-subgrade interface or at the middle of base layer. The new compaction technique consisted on placing the geogrid on top of loose limestone aggregate layer and then sandwiched by the confined limestone aggregate layer. Both the support and the confined limestone aggregate layers were compacted together in order to improve the interlocking between the geogrid and limestone aggregate.

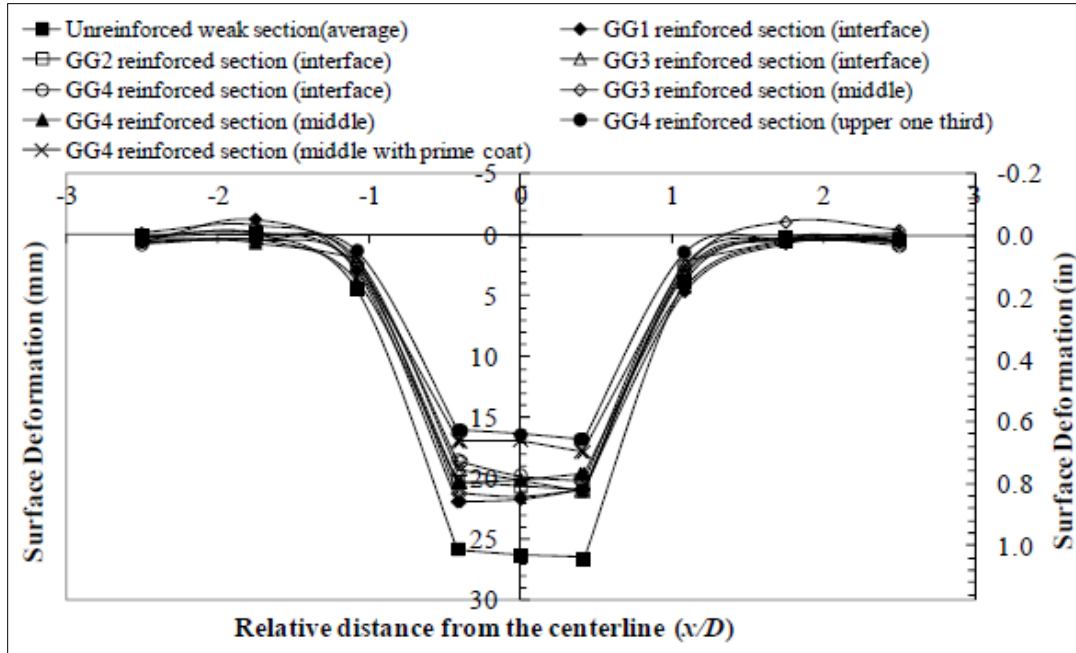


Figure 32. Summary of permanent surface deformation profiles for all cyclic plate load tests after 30,000 cycles in the study by Abu-Farsakh and Chen (2010)

In addition to their laboratory investigation, Abu-Farsakh and Chen (2010) performed two series of field tests, i.e. field cyclic plate load tests and rolling wheel load tests, in order to investigate the field performance of raw blended calcium sulfate (BCS), stabilized BCS, stabilized recycled asphalt pavement (RAP), stabilized soil as base/sub-base materials and to identify the differences in pavement response to cyclic plate and rolling wheel loads.

Abu-Farsakh and Chen (2010) constructed seven pavement test sections at the Louisiana Pavement Research Facility using typical highway construction equipment and procedures. The locations of the cyclic plate load test and rolling wheel load test for each section are shown in Figure 33. All test sections

consisted of a similar 2-inch-thick HMA top layer, an 8.5-inch-thick base layer, a 12-inch-thick sub-base layer and a similar subgrade layer. Base and sub-base layer materials varied between the different sections. A thin HMA layer was used due to the consideration that the purpose of testing was to investigate the performance of base/sub-base materials.

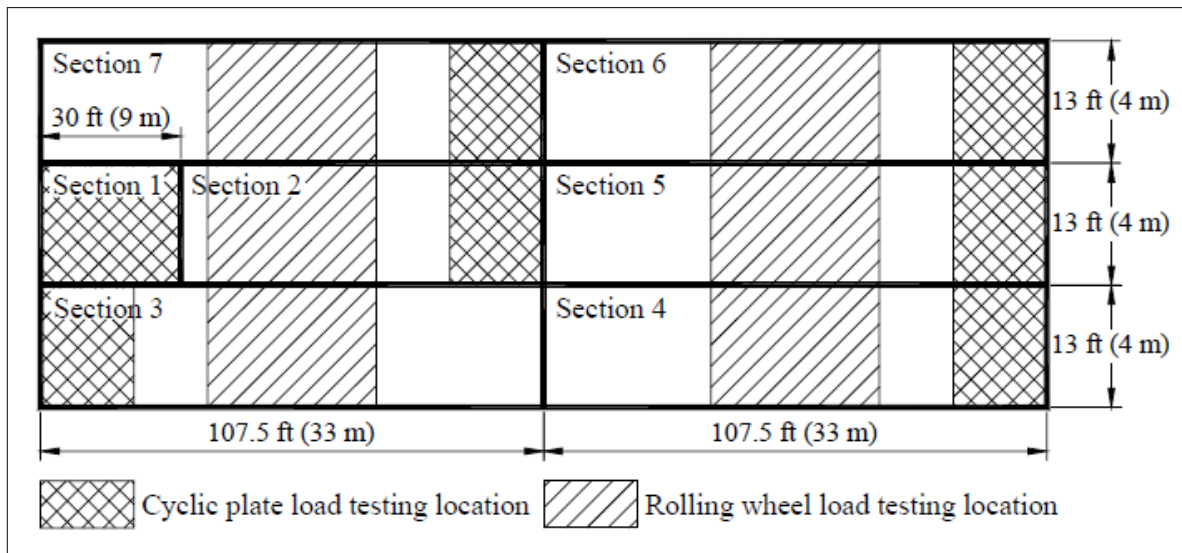


Figure 33. Layout of the field cyclic plate load and rolling wheel load test sections in the study by Abu-Farsakh and Chen (2010)

The cyclic plate loads tests were applied using a 22-kip MTS hydraulic actuator with a dynamic stroke of 6 inches. The cyclic load was applied through a steel rod that fit into a concave-shaped hole on the loading plate that sat on the surface of the HMA (hot mix asphalt) layer. The loading plate was a 1-inch-thick steel plate which was 12 inches in diameter. The maximum applied load in tests was 12 kips, which resulted in a loading pressure of 106 psi simulating dual wheels under an equivalent 18 kips single axle load. The load pulse had a linear

load increase from 0.5 kip to 12 kips in 0.3 second, followed by a 0.2-second period where the load was held constant at 12 kips followed by a linear load decrease to 0.5 kip over a 0.3-second period, then followed by a 0.5-second period of 0.5 kip (rest period), before the next loading cycle was applied. This load pulse resulted in a frequency of 0.77 Hz.

The rolling wheel load tests were conducted using an ALF (Accelerated Load Facility), which simulated half of a single axle with “X” ZE Michelin dual tires. The load was adjustable from 9,750 lb to 18,950 lb. The starting load was 9,750 lb. The load was increased to 12,050 lb after 175,000 cycles (241,039 ESALs), then to 14,350 lb. after 225,000 cycles (401,714 ESALs) and then to 16,650 lb after 325,000 cycles (1,048,019 ESALs). The tire pressure was set to 105 psi. The shape of the applied load was approximated as two 6-in.-apart uniformly loaded rectangular areas (9 x 10.7 inches). With a computer-controlled load trolley, the weight and movement of traffic was simulated in one direction at a speed of 10.5 mph.

As shown in Table 15, pavement test Sections 1 through 4 had the same sub-base material (i.e. lime treated soil, LTS) with various base course materials: raw BCS, Class C fly ash stabilized BCS, 120 grade ground granulated blast furnace slag (GGBFS) stabilized BCS and crushed limestone, respectively. Pavement test Sections 5 through 7 had a cement treated soil (CTS) sub-base material with base course materials of crushed limestone, foamed asphalt (FA) RAP and FA stabilized RAP plus soil cement blend, respectively. The subgrade consisted of

silty-clay embankment soil, having a liquid limit of 31 and a plastic index (PI) of 12. The soil contained 60.3% silt and 23.5% clay. The top 12 inches of the subgrade was treated with lime or cement to provide a sub-base layer of low plasticity and low water susceptibility.

Table 15. Base and sub-base materials for the pavement test section in the study by Abu-Farsakh and Chen (2010)

| Section  | Base                | Subbase  | Rolling wheel load |          | Cyclic plate load |          |
|----------|---------------------|--|--------------------|----------|-------------------|----------|
|          |                     |  | Test Start         | Test End | Test Start        | Test End |
| <b>1</b> | BCS+LTS             | Raw BCS  | N/A                | N/A      | 11/2008           | 12/2008  |
| <b>2</b> | BCS/Flyash +LTS     | Class C flyash (15% by volume) stabilized BCS  | 10/2005            | 10/2006  | 12/2008           | 01/2009  |
| <b>3</b> | BCS/Slag+LTS        | 120 grade GGBFS (10% by volume) stabilized BCS | 10/2005            | 10/2006  | 10/2008           | 11/2008  |
| <b>4</b> | LS+LTS              | Crushed limestone                              | 01/2007            | 04/2007  | 05/2008           | 06/2008  |
| <b>5</b> | LS+CTS              | Crushed limestone                              | 01/2007            | 08/2007  | 06/2008           | 07/2008  |
| <b>6</b> | 100%RAP/FA +CTS     | FA stabilized 100% RAP                         | 01/2007            | 07/2007  | 08/2008           | 09/2008  |
| <b>7</b> | 50%RAP50% SC/FA+CTS | FA stabilized 50%RAP and 50% soil cement blend | 10/2005            | 06/2006  | 01/2009           | 02/2009  |

Based on the field cyclic plate load and the rolling wheel load test results, Abu-Farsakh and Chen (2010) presented the following conclusions:

- The rut depths resulted from rolling wheel load tests (Figure 34), in all test sections, were much higher than those obtained from cyclic plate load tests (Figure 35). The differences were as much as 3 to 7 times between these two types of loading. This indicates that the rolling wheel load has a more damaging loading condition than the cyclic plate load. Three possible factors can attribute to the difference in pavement responses under these two types of loading conditions: principal stress rotation, friction induced tangential forces and lateral wander. The extension-compression-extension multiple stress path type test with principal stress rotation causes a much higher permanent deformation than the single compression stress path type test with no principal stress rotation. The lateral wander most likely decreases the stability of unbound and weak bound granular base materials by inducing constant particle movement.

- The resilient modulus ( $M_R$ ) of stabilized/treated soil increases rapidly during the early stages of curing time and continues to increase at a slower rate thereafter. The authors believed that this age effect partially contributed to the differences between the field rolling wheel load tests and cyclic plate load tests that were performed at least 10 months after rolling wheel load tests. To validate the field cyclic plate load tests, Section 4 (with crushed limestone as base and lime treated soil as sub-base) was compared with an additional laboratory cyclic plate load test constructed with the same specifications. Figure 36 shows a comparison of the rutting development curves between the field and laboratory cyclic plate load tests. Stiffer response was observed in the field cyclic plate load test. The authors pointed out that the field plate load test was conducted more

than three years after the pavement section had been constructed, while the laboratory plate load test was performed immediately after it was set up. Once again the curing time difference is an important factor to take under consideration when comparing field and laboratory cyclic plate load tests.

- Even though the rolling wheel tests proved to be more damaging than the cyclic plate load tests, the comparative performances of different test sections under cyclic plate load and rolling wheel tests were found to be consistent and similar to each other (Figure 34 and Figure 35). Therefore, the cyclic plate load test could be used as a good performance indicator test for evaluating the pavement structure and for pre-selection of pavement sections for recommendation of further full-scale field test sections.

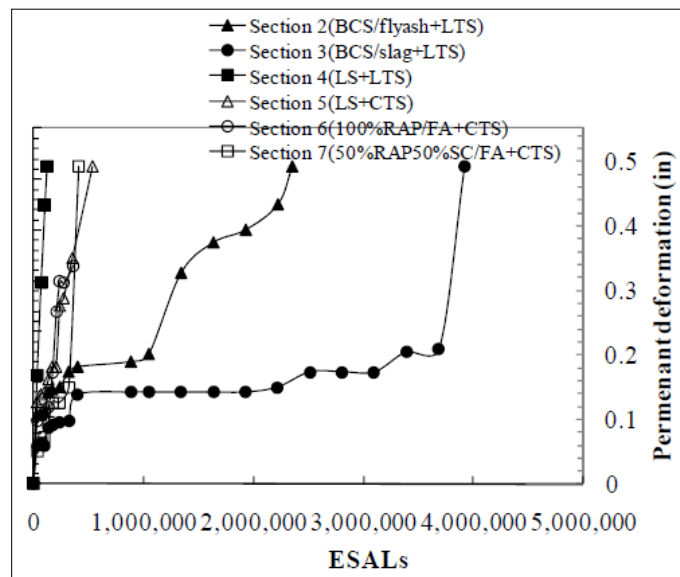


Figure 34. Summary of rut depths measured in rolling wheel load test sections in the study by Abu-Farsakh and Chen (2010)

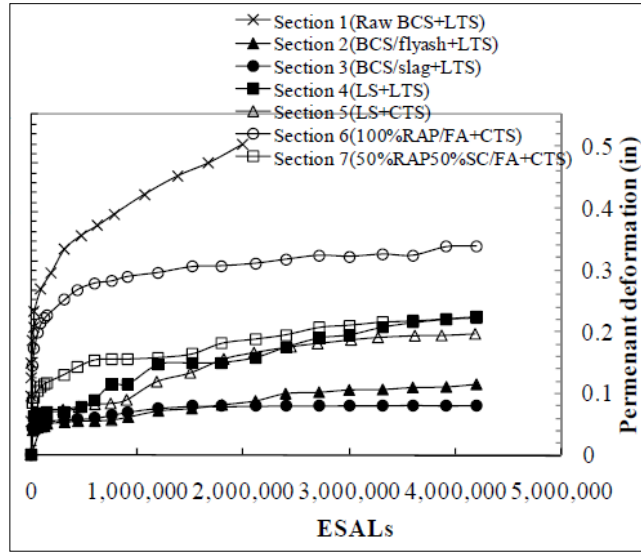


Figure 35. Summary of rut depths measured in cyclic plate load test sections in the study by Abu-Farsakh and Chen (2010)

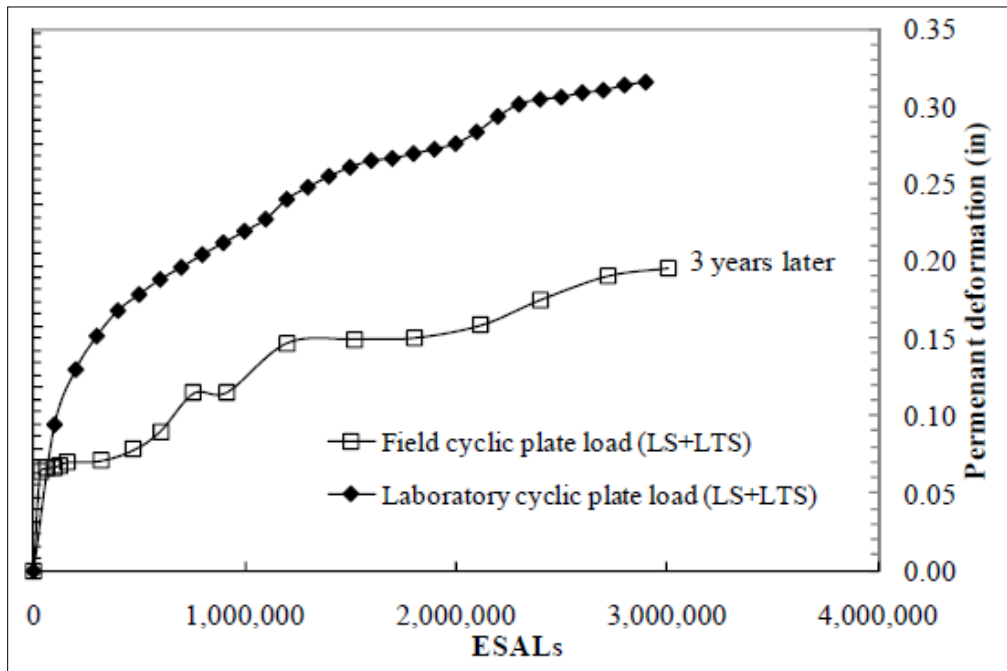


Figure 36. Comparison of field and laboratory cyclic plate load tests in the study by Abu-Farsakh and Chen (2010)

Oh (2011) studied the performance of geogrid-reinforced pavements over expansive clay. They carried out forensic investigations on a flexible pavement road called FM 1915 (from Farm to Market road) in Milam County, Texas. Oh carried out numerical simulations to verify the effectiveness of geogrids to reinforce flexible pavements. His field survey indicated that despite evidence of high swelling and shrinkage potential in expansive subgrade soils due to moisture change, roadway segments reinforced with geogrids performed better than the control segment as evidenced by fewer longitudinal cracks and lower values of roughness index.

The test section was constructed in 2000 as an effort by the Bryan District to rehabilitate the rural FM roadways using geogrid reinforcement. As shown in Figure 37, the construction was divided into three test sections. Geogrids were placed in Sections (S1 and S3) and Section S2 was used as control to quantify the effectiveness of the reinforcement. Historical performance data for the road indicated that it had undergone frequent maintenance activities to mitigate longitudinal cracking and edge failure associated with expansive soil movement due to moisture variation.

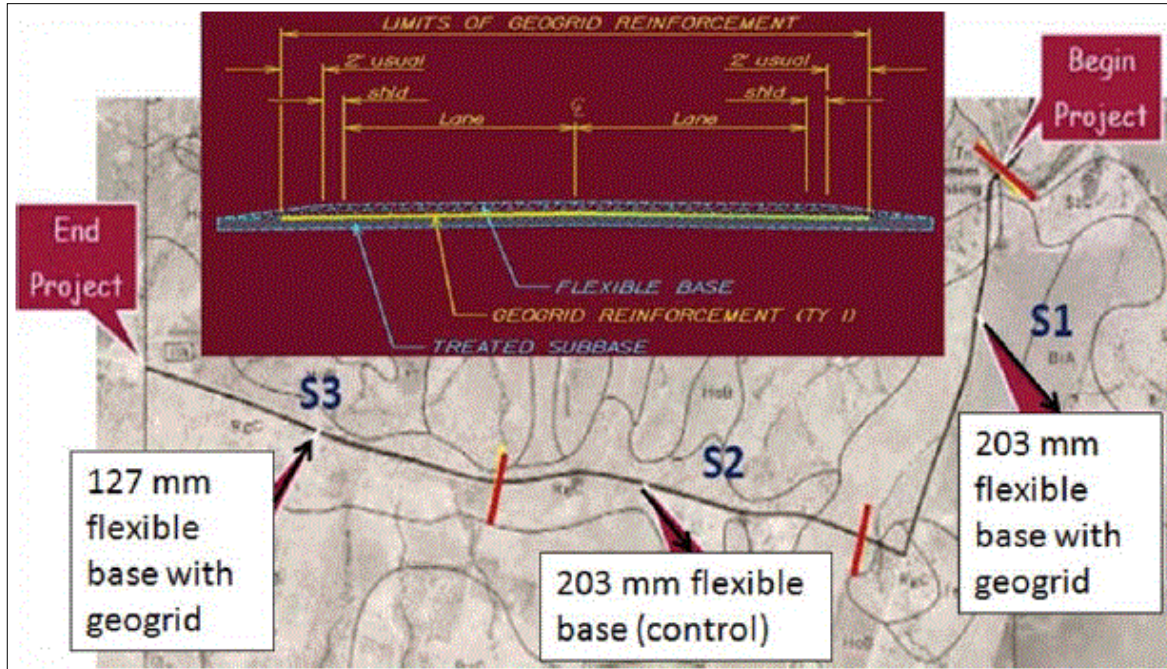


Figure 37. Test section layout in the study by Oh (2011)

Oh (2011) carried out a forensic investigation of the FM 1915 road that included the following procedures:

- Performed Falling Weight Deflectometer (FWD) and Ground Penetrating Radar (GPR) nondestructive tests to identify existing pavement condition, pavement layer profile and structural adequacy.
- Conducted a Dynamic Cone Penetrometer (DCP) tests to evaluate load bearing capacity of the subgrade.
- Sampled materials for the characterization of soil physical properties, shrinkage and swelling potential.

FWD tests were conducted to evaluate structural adequacy based on interpretation of deflection basin data. Figure 38 shows the variation of measured deflection from the outermost sensor with respect to the loading plate. The results indicated that “S1” generally yielded a structurally inadequate pavement support condition compared to those in “S2” and “S3”, even though the latter section was reinforced with geogrid. That was mainly attributed to the presence of an expansive clayey subgrade which was susceptible to volume change due to moisture variation.

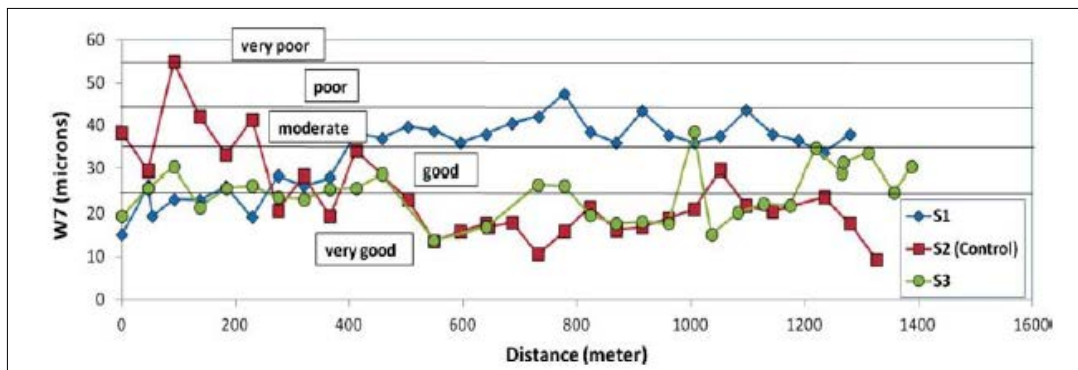


Figure 38. Falling Weigh Deflectometer results in the study by Oh (2011)

The GPR test was used to estimate pavement layer thickness using a video log system. Figure 39 shows snapshots taken at the material sampling location at the control section versus those in the geogrid-reinforced Section S3. The area adjacent to the sampling location in the control section had exhibited severe longitudinal cracking. The pavement profile in the control section appeared to be more irregular due to expansive soil movements as compared to that in the reinforced section.

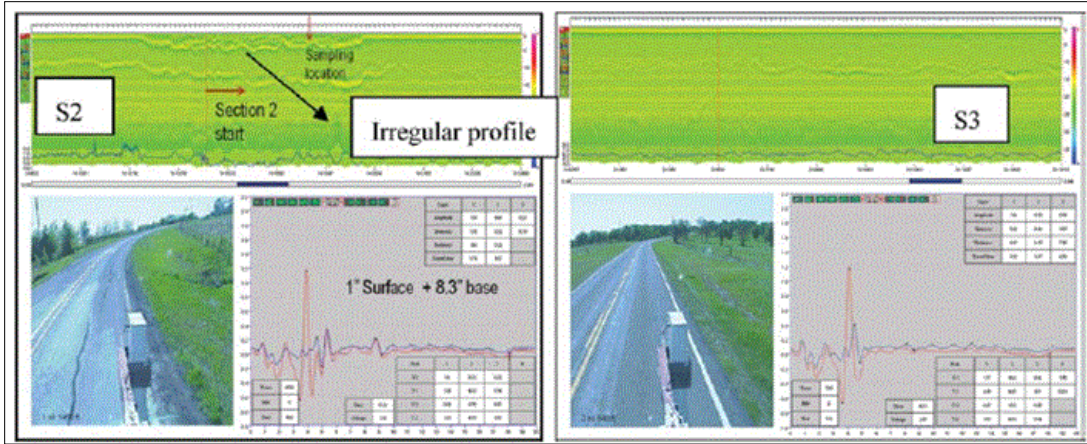


Figure 39. Ground Penetrating Radar data from snapshot at control Section 2 and reinforced Section 3 in the study by Oh (2011)

Oh (2011) carried out a field visual survey to observe severity of distresses as summarized in Table 16. The results indicated that the control section had more deteriorated areas by showing a larger number of observed distresses and a larger international roughness index (IRI) value. However, it should be noted that Section S1 reinforced with geogrid also revealed a considerable amount of longitudinal cracking along with irregular layer profile similar to S2. Overall, Section S3 seemed to perform the best with the least number of distresses observed.

Table 16. Severity of distresses observed in the field visual survey by Oh (2011)

| Section | Longitudinal crack in linear meter | No. of edge failure | Average IRI (m/km) |
|---------|------------------------------------|---------------------|--------------------|
| S1      | 186                                | 22                  | 3.0                |
| S2      | 210                                | 47                  | 3.4                |
| S3      | 130                                | 17                  | 2.7                |

The DCP test has been widely utilized to measure the soil strength and correlate DCP index with the California Bearing Ratio (CBR) and resilient modulus values. Layer resilient modulus values based on the DCP tests for Sections S1-S3 are listed in Table 17. Results showed that the layer resilient modulus values of base and sub-base layers in the geogrid-reinforced Sections (S1 and S3) were generally higher than those of the control section.

Table 17. Average resilient modulus from every layer of each test section in the study by Oh (2011)

| Section      | Layer    | Average Mr (MPa) |
|--------------|----------|------------------|
| S1           | Base     | 977              |
|              | Subbase  | 491              |
|              | Subgrade | 59               |
| S2 (Control) | Base     | 351              |
|              | Subbase  | 224              |
|              | Subgrade | 80               |
| S3           | Base     | 657              |
|              | Subbase  | 491              |
|              | Subgrade | 125              |

With respect to material characterization, Oh (2011) conducted a series of laboratory tests on subgrade soils sampled from the FM 1915 road. All tested soils were classified as high plasticity clay according to the test results shown in

Table 18. Particularly, the soil in the Section S1 exhibited very high values of PI and linear shrinkage, which might have been the primary cause of soil movement resulting in higher deflection and lower layer modulus obtained from the FWD and DCP tests. Furthermore, three-dimensional swell tests were conducted to gauge swelling potential that would cause the soil volume change due to moisture migration. The test results indicated that subgrade soils in Sections S1 and S2 were more susceptible to swelling than the soil in Section S3. This finding was consistent with the earlier results from the GPR, FWD and the field visual survey.

Table 18. Subgrade soil properties from each test section in the study by Oh (2011)

| Section                              | S1   | S2 (Control) | S3   |
|--------------------------------------|------|--------------|------|
| Plasticity Index (PI)                | 55.8 | 39.2         | 29.4 |
| Liquid Limit (LL)                    | 82.8 | 73.2         | 48.5 |
| Particles finer than #200 Sieves (%) | 63.4 | 76.8         | 47.3 |
| Linear Shrinkage (%)                 | 30   | 25           | 15   |
| Percent Swell (%)*                   | 27   | 31           | 15   |

Oh (2011) also carried out a series of numerical simulations using PLAXIS to verify the effectiveness of geogrid for base reinforcement. The unreinforced structure was modeled in axisymmetric condition subjected to a tire pressure of 80 psi over a circular area with a radius of 6 inches. Sublayer materials were simulated using the Mohr-Coulomb's model. The thicknesses and modulus values of each layer were determined from the field GPR and FWD data.

Table 19 shows the input parameters used in Oh's numerical simulation. The materials were analyzed for drained behavior without any pore water pressure changes because the test was performed in a zone where groundwater table was not encountered. The drained condition was argued to be well justified for north Texas. Figure 40 shows the reinforced pavement structure modeled with the same properties as the unreinforced model with the only difference that the geogrid layer was placed at the interface between base and sub-base layers. An interface strength reduction factor was employed to simulate the reduced friction angle along the interface among the base, geogrid and sub-base layer. This was set by assigning the interface reduction factor equal to 0.67, based on the previous studies (Kazemian et al. 2010). The axial stiffness of the geogrid was  $6.85 \times 10^6$  lb/ft based on the study by Subramaniam (2011).

Table 19. Input parameters for the numerical simulation in the study by Oh (2011)

| Material                   | Surface* | Base  | Subbase | Subgrade |
|----------------------------|----------|-------|---------|----------|
| Thickness (mm)             | 25.4     | 203.3 | 254     | -        |
| Layer Modulus (MPa)        | 1378     | 275.6 | 206.7   | 51.7     |
| Poisson's ratio            | 0.35     | 0.35  | 0.35    | 0.4      |
| Cohesion (kPa)             | -        | 2.2   | 2.0     | 1.9      |
| Friction Angle ( $\phi$ )  | -        | 50.0  | 35.0    | 25.0     |
| Dilatancy angle ( $\psi$ ) | -        | 13.0  | 10.0    | 0.0      |

\*Surface layer was modeled with linear elastic condition.

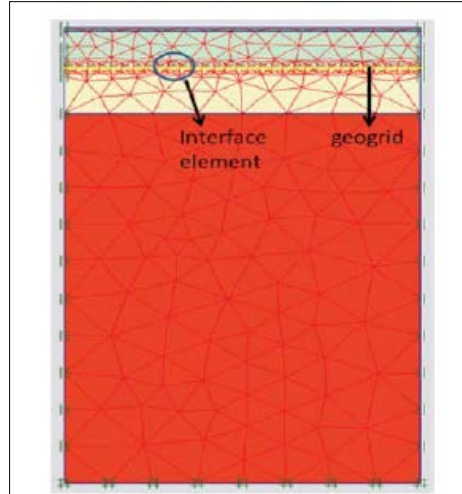


Figure 40. Generated mesh for geogrid reinforced pavement using Plaxis program in the study by Oh (2011)

To quantify the effectiveness of geogrid reinforcement, Oh (2011) compared the predicted values of the variables listed in Table 20. The results indicated that horizontal deformation was significantly reduced due to the presence of geogrid reinforcement. This was attributed to the lateral confinement of the interface layer.

Table 20. Summary of output of the numerical simulation in the study by Oh (2011)

| Variable                     | Unreinforced | Reinforced |
|------------------------------|--------------|------------|
| Horizontal displacement (mm) | 0.17         | 0.016      |
| Vertical displacement (mm)   | 3.65         | 2.62       |
| Horizontal strain, %         | 0.26%        | 0.02%      |
| Vertical strain, %           | 0.08%        | 0.06%      |
| Shear stress, kPa            | 152.1        | 190.8      |
| Shear strain, %              | 0.19%        | 0.22%      |

Findings of Oh's (2011) forensic investigation led to the following general observations and conclusions:

- Overall, the geogrid reinforcement contributed to an improvement in the layer resilient modulus and load bearing capacity of the comparatively thin flexible pavement over expansive clay soils.
- Nondestructive tests using FWD and GPR helped to identify the condition of the existing pavement and assess the effectiveness of geogrid-reinforcement in a timely fashion. DCP testing also proved to be a suitable method to determine the effectiveness of geogrid-reinforcement through a lower penetration rate as compared to an unreinforced case.
- If the subgrade soil only has a marginal potential for swelling and shrinkage geogrid reinforcement could be used to reduce the base thickness as was observed in Section S3. For the subgrade soil in Section S1 that showed a high swelling and shrinkage potential, it was recommended that other alternatives such as chemical stabilization or

placing two layers of geogrid be considered in order to magnify the effectiveness of the geogrid.

- Numerical simulations confirmed the capability of geogrid reinforcement to increase lateral confinement and reduce permanent deformation in a base-subgrade system. Acceptance of geogrid reinforcement would depend on the development of design methodology and successful full-scale applications.

Jersey et al. (2012) constructed a full-scale test section sponsored by Tensar International and performed by the U.S. Army Engineer Research and Development Center, Waterways Experiment Station in Vicksburg, MS. The objective of their study was to evaluate the benefits of a new triaxial geogrid product on the performance of thin flexible pavements. The evaluation was accomplished through the comparison of reinforced and unreinforced test sections. The performance of the test items was evaluated in terms of permanent surface deformation (rutting) under simulated truck traffic.

Jersey et al. (2012) constructed three test sections (8 ft by 50 ft test area) with different pavement profiles. The first test section (Item A) was reinforced with a triaxial geogrid that was installed at the base-subgrade interface. The other two test sections (Items B and C) were constructed without reinforcement. Items A and B were designed to compare the effect of the geogrid reinforcement directly in similar pavement sections. Items A and C were designed to evaluate the effect of the geogrid reinforcement compared with an extra inch of asphalt concrete.

Figure 41 describes the site view of the three test sections. The subgrade for each test item consisted of 28 inches of high-plasticity clay, which had a target subgrade California Bearing Ratio (CBR) of 3%, placed over a compacted silt soil with an in situ CBR of 8% to 10%. Once the subgrade was prepared, the geogrid product was installed in Item A. The subgrade was overlaid with an 8 inch-thick aggregate base course that consisted of crushed limestone. The limestone, classified as poorly graded silty gravel, was covered with a thin asphalt concrete surface course. Items A and B were each constructed with a 2-inch-thick asphalt concrete surface layer and Item C was constructed with 3 inches of the same material.

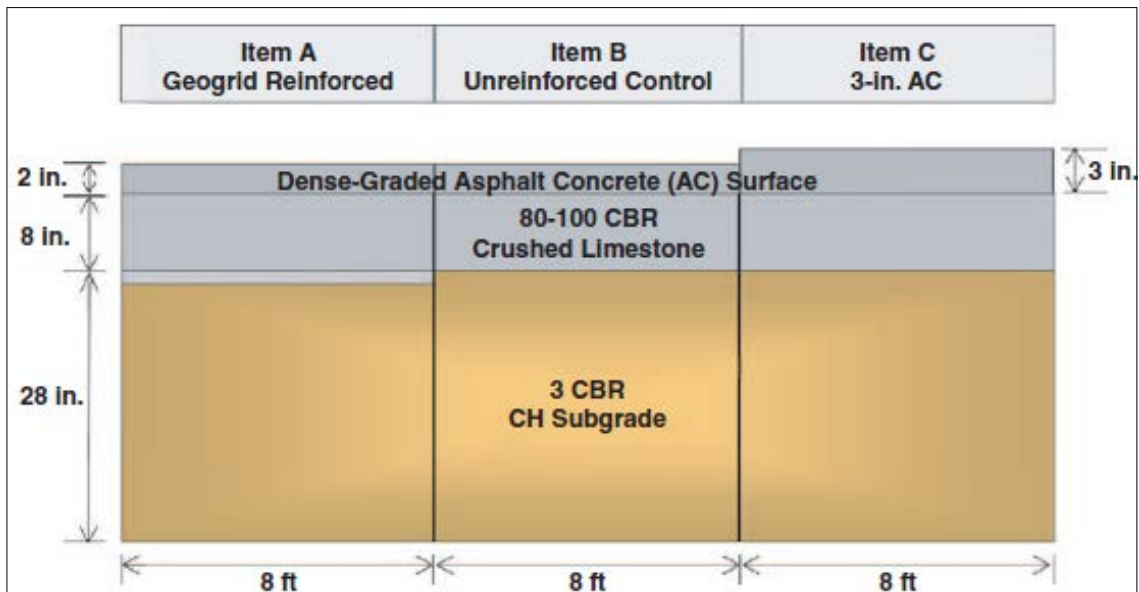


Figure 41. Profile of test section (Jersey et al. 2012) (CH = High-plasticity Clay; CBR = California Bearing Ratio)

Jersey et al. (2012) used a new triaxial geogrid product that consisted of a series of concentric triangles. It was composed of a black high-density polypropylene. The reported junction efficiency was 93%. The radial stiffness at 0.5% strain was reported as 20.6 kip/ft. Traffic testing of Item B (control item) was performed using a dual-wheel single axle with nominal load of 10,000 lb. The loaded contact pressure associated with the dual-wheel single-axle load was approximately 88 psi, with a recorded tire pressure of 120 psi. Traffic testing of the remaining test items was accomplished using a dual-wheel tandem axle loaded to a nominal load of 20,000 lb and recorded tire pressures of 120 psi. The dual-wheel tandem-axle loading applied two distinct load pulses, each with a loaded contact pressure of approximately 88 psi.

Rut depth was used as an indicator of the thin pavement structural performance. Subgrade failure was expected to rule performance of the test pavement. Table 21 compares the ESALs (Equivalent Single Axle Load) needed for the three test sections to reach a target rut deformation in a tabulated format. The unreinforced control item with the 2 inches of asphalt concrete surface (Item B) sustained the least amount of traffic, followed by the unreinforced item with the 3 inches of asphalt concrete surface (Item C) and the geogrid-reinforced item (Item A).

Table 21. ESALs at Various levels of surface deformation (Jersey et al. 2012)

| Test Item | Treatment        | 0.25 in. | 0.50 in. | 0.75 in. | 1.0 in.  |
|-----------|------------------|----------|----------|----------|----------|
| Item A    | GGA              | 19,300   | >100,000 | >100,000 | >100,000 |
| Item B    | 2-in. AC control | 1,800    | 8,100    | 9,500    | 13,000   |
| Item C    | 3-in. AC control | 4,220    | 16,300   | 24,500   | 27,870   |

After the test items had been subjected to traffic loading, post-test forensics were performed to characterize the pavement layers. Figure 42a shows minimal rutting in the base course of Item A and no distresses were observed in the subgrade, in comparison to Figure 42b and Figure 42c.

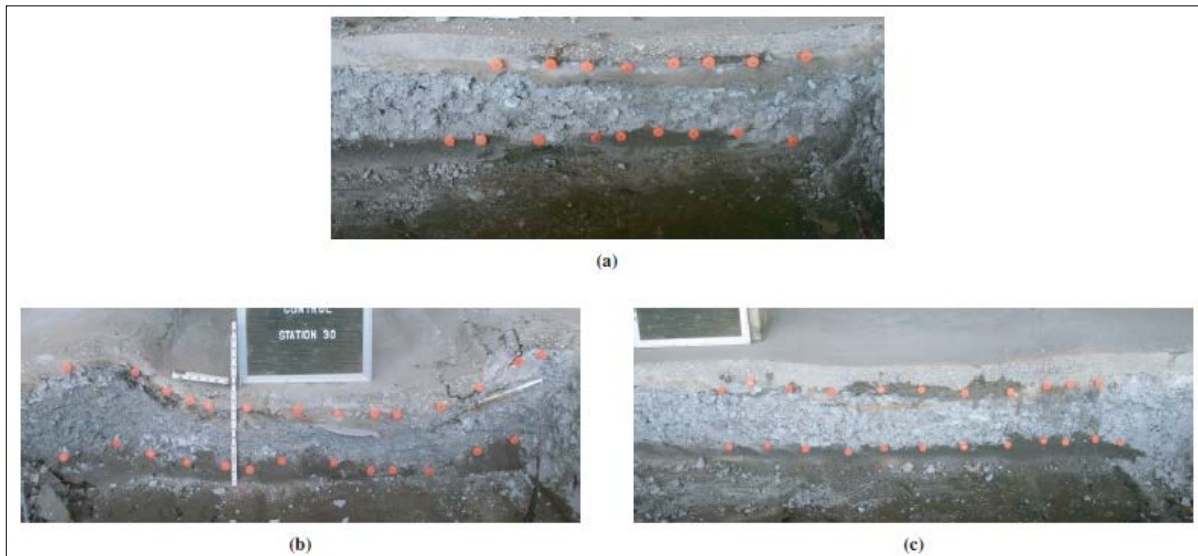


Figure 42. Pavement cross sections during post traffic forensic investigation (Jersey et al. 2012) (a) Item A, (b) Item B, (c) Item C

Jersey et al. (2012) used traffic benefit ratio as an index parameter, in order to show the benefit to pavement performance using a geosynthetic in the pavement

structure. Table 22 represents the improved performance of the geogrid as compared to the unreinforced control sections.

Table 22. Traffic Benefit Ratios at various rut depths (Jersey et al. 2012)

| Test Item | Treatment        | 0.25 in. | 0.50 in. | 0.75 in. | 1.0 in. |
|-----------|------------------|----------|----------|----------|---------|
| A         | GGA              | 11       | 12+      | 10+      | 7+      |
| B         | 2-in. AC control | 1        | 1        | 1        | 1       |
| C         | 3-in. AC control | 2        | 2        | 3        | 2       |

Calculations of effective structural coefficient for the base course of the three test items were made through the use of the AASHTO Mechanistic–Empirical pavement design guide (based on the as-built pavement thicknesses and the number of passes before failure). These coefficients are shown in Table 23. The effective structural number provided a better comparison when the difference in thickness of asphalt concrete in different test items was taken into account.

Table 23. Effect of geosynthetic on pavement performance (Jersey et al. 2012)

| Variable                         | Item A, Geogrid | Item B, Control | Item C, 3-in. AC |
|----------------------------------|-----------------|-----------------|------------------|
| Design base thickness (in.)      | 8               | 8               | 8                |
| Design structural number         | 2               | 2               | 2.44             |
| Design passes to failure         | 41,000          | 41,000          | 41,000           |
| As-built asphalt thickness (in.) | 1.81            | 1.66            | 2.61             |
| As-built base thickness (in.)    | 7.63            | 8.34            | 7.89             |
| Passes to failure                | >100,000        | 13,000          | 27,870           |
| Effective base coefficient       | >0.19           | 0.11            | 0.09             |
| Effective structural number      | >2.28           | 1.62            | 1.85             |

After the analysis of the test results, Jersey et al. (2012) drew several conclusions regarding the benefits of incorporating geosynthetics into thin asphalt pavements:

- The geogrid-reinforced pavement section significantly improved the resistance to rutting as compared to the unreinforced control test items.
- The geogrid-reinforced test item provided more resistance to rutting than did the 3-in. asphalt concrete–surfaced unreinforced control test item.
- The initial stiffness of the reinforced test item was not a good indicator of performance. However, a noticeable drop in pavement stiffness accompanied the onset of surface rutting.
- The computed traffic benefit ratios indicated that the geogrid used in this study would extend the service life of the pavement significantly.

Mishra and Tutumluer (2013) performed a study of the strength, stiffness and deformation behaviors of three aggregate types commonly used in Illinois for base course applications. For this purpose, they constructed a full-scale pavement test section subjected to accelerated loading at the University of Illinois Advanced Transportation and Research Engineering Laboratory (ATREL) facility. Performances of six different types of aggregates under loading were monitored through surface profile measurements as well as transverse scanning with ground-penetrating radar (GPR). The authors found that aggregate quality is an important characteristic that should be considered for thickness design of

aggregate layers. Moreover, their study highlighted the importance of using a geotextile separator layer to promote uniform distribution of stresses in the subgrade layer and prevent the intrusion of subgrade into the large-size aggregate layer.

Mishra and Tutumluer (2013) constructed six different full-scale unsurfaced pavement test cells over weak subgrades. The effects of different aggregate physical properties on the performance of the test sections were evaluated using their measured Immediate Bearing Values (IBV). IBV values are calculated from Dynamic Cone Penetrometer tests similar to the CBR values except that IBV testing counts the number of blows to achieve four inches of penetration immediately after compaction. In contrast, the CBR testing is performed 96 hours after compaction and counts the number of blows to achieve six inches of penetration.

The full-scale test sections were constructed using aggregate materials with significantly different qualities. The following material types were selected: Material 1: Uncrushed gravel with high amounts of nonplastic fines, Material 2: Crushed limestone with high amounts of plastic fines, Material 3: Crushed dolomite with high amounts of nonplastic fines, Material 4: Crushed limestone with low amounts of nonplastic fines. These four materials were selected to compare and evaluate the following effects: (1) aggregate angularity effect, which was studied through a comparison of materials 1 with 2 and/or 3; (2) the effect of fines content was studied by comparing materials 3 and 4; (3) the effect of

plasticity of fines was studied by comparing materials 2 and 3; and finally, (4) the effect of moisture on aggregate behavior was evaluated by testing each of the four materials under two different aggregate moisture conditions (optimum and wet).

Figure 43 shows the layout of the six cells along the three longitudinal test areas. Cells 1 through 4 were constructed with the four aggregate materials described earlier (Materials 1 through 4, respectively) over a weak subgrade with IBV = 3%. Identical subgrade conditions and aggregate layer thicknesses in different test cells ensured that differences in their field performance were directly linked to differences in their aggregate quality. Cell 5 was constructed using Material 2 (same as Cell 2) but over a stronger subgrade with IBV = 6%. The main purpose was to evaluate the effect of subgrade strength on working platform performance and mechanisms contributing to rut accumulation. Cell 6 was constructed over a subgrade with IBV = 1% by first placing a 12 in.-thick layer of large-size aggregates, which was subsequently capped by a 6 in.-thick layer of dense-graded aggregate (Material 2). Geotextile was placed at the subgrade/ aggregate interface along the south wheel path. The purpose was to evaluate the effectiveness of geotextile reinforcement alongside large-size aggregate materials.

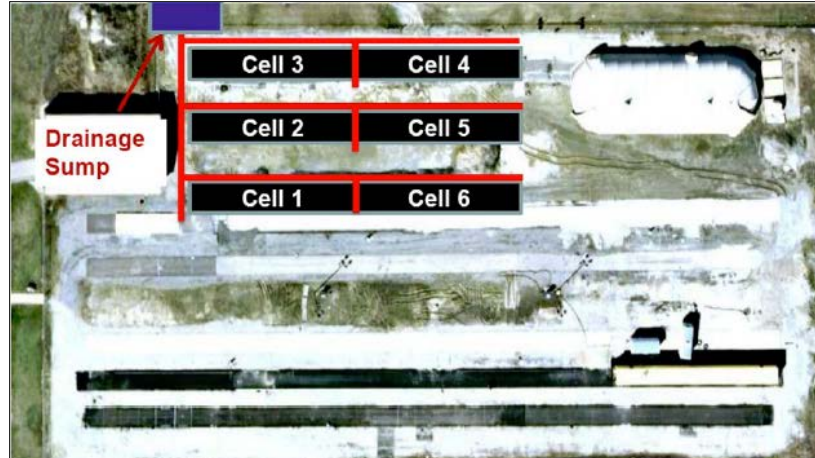


Figure 43. Test section layout in the study by Mishra and Tutumluer (2013)

Figure 44 shows the plan and cross-sectional views of a representative test cell constructed over a subgrade with  $IBV = 3\%$  (Cells 1 through 4). Each test cell constructed was 130 ft long and 18 ft wide. It was comprised of three test sections with different aggregate layer thicknesses equal to 14, 12 and 8 inches. Each cell had a 22.5 ft long transition section for placement of the ATLAS tracks. Each section was 15 ft long and was separated from adjacent sections by 10-ft long transition zones. As was mentioned earlier, Cell 5 was constructed over a subgrade with  $IBV = 6\%$ . Therefore, the aggregate layer thicknesses for the three sections were 10, 8 and 6 inches. The three sections for Cell 6 had the same thicknesses, but they were constructed with different aggregate materials, as described later in this section.

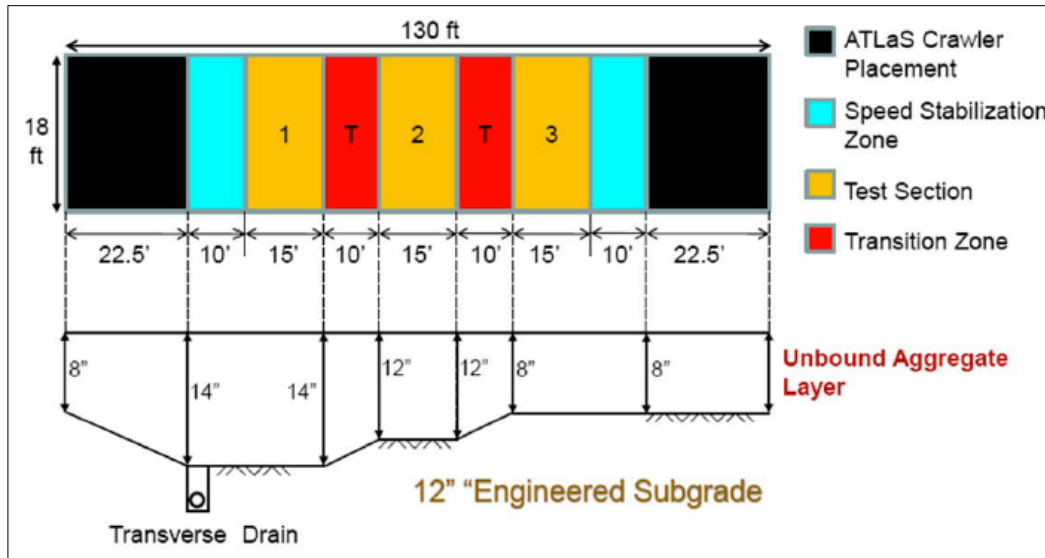


Figure 44. Plan (top) and cross-sectional views of the full-scale pavement test sections in the study by Mishra and Tutumluer (2013)

Mishra and Tutumluer (2013) loaded the test sections using an Accelerated Transportation Loading Assembly System (ATLAS) to simulate traffic of heavy trucks. Rut accumulation in the pavement sections under loading was monitored through surface profile measurements, as well as GPR scanning. Then, the test sections were loaded to failure by applying a 10 kip wheel load through a single tire at a pressure of 110 psi. Transverse trench sections were excavated across the wheel paths to obtain visual confirmation of the rut accumulation in aggregate and subgrade layers. Effects of different aggregate physical properties on the performance of construction the test sections were then evaluated through analyses of different mechanisms contributing to failure.

Mishra and Tutumluer (2013) monitored the development of rutting with load application for each test section through surface profile measurements using a

digital caliper. Rut depths were calculated through subtraction of the original constructed pavement profile (corresponding to zero load application) from the deformed profiles at different stages of loading. Trafficking of the test sections was continued up to a total rut depth (i.e. maximum difference between the peak and trough after deformation) of approximately 4 inches because this was the maximum vertical movement of the ATLAS system.

Mishra and Tutumluer (2013) constructed Cells 1 through 5 to evaluate the effect of moisture conditions on different types of aggregates. These cells were loaded to failure under near-optimum aggregate moisture conditions on the north wheel path and artificially flooded and loaded along the south wheel path. Flooding of the test sections was achieved using perforated water sprinklers until excessive water was observed seeping through the boundaries of the aggregate sections. Figure 45 shows an example of a cell performance after failure.

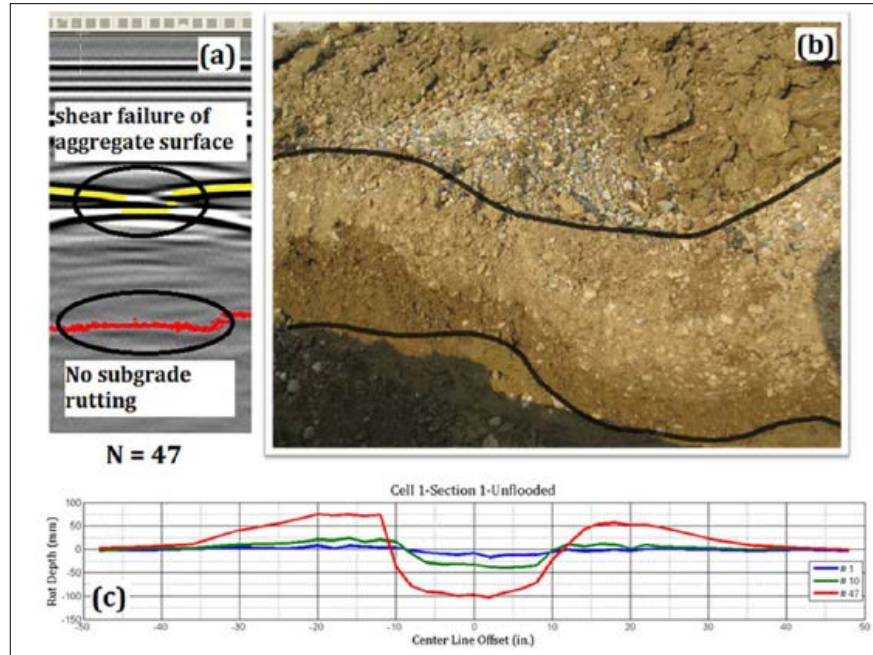


Figure 45. Example of a cell performance after failure in the study by Mishra and Tutumluer (2013) (a) Ground-Penetrating Radar (GPR) scan (b) excavated trench (c) surface rut profile.

Cell 6 was constructed by placing a 12 in-thick aggregate layer over a subgrade with IBV = 1% capped by 6 inches of a CA-6 layer (IDOT Coarse Aggregate gradation number 6, which is a dense graded aggregate). However, this cell was not tested under flooded conditions. Instead, the south wheel path of this cell was reinforced with a woven geotextile at the interface of the subgrade and aggregate layers. The three sections in Cell 6 were comprised of large-size aggregate materials obtained from the following three different sources: (1) D6 rockfill primary crusher run (largest in size); (2) intermediate size D3 aggregate; and (3) rip rap gradation #1 (the smallest size among the three large-size aggregate materials). Therefore, comparison of rut accumulations along the two wheel

paths for Cell 6 would highlight the effectiveness of geotextile reinforcement in pavements with different types of large-size aggregate materials constructed over very weak subgrades.

Mishra and Tutumluer (2013) observed that all geotextile reinforced sections greatly improved their wheel path trafficking performances. The number of load passes needed for the same rut depths increased for almost up to threefold. For example, Cell 6, Section 2 sustained 159 load applications before accumulating approximately 4 inches of rutting compared with 63 load applications in the unreinforced case because of the load distribution in the subgrade was more uniform (Figure 46). Unlike the unreinforced wheel path, no sudden increase in the rut depth was noticed with increased number of load applications.

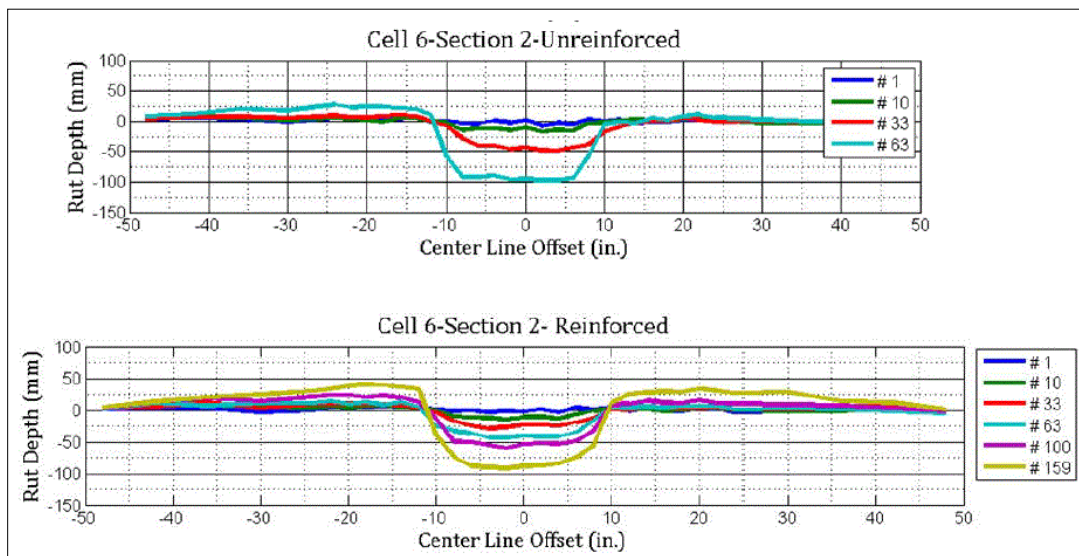


Figure 46. Rut deformation in Cell 6, Section 2 resulting from unidirectional ATLAS loading in the study by Mishra and Tutumluer (2013)

Mishra and Tutumluer (2013) concluded that the performance of three different large-size aggregate materials under unreinforced and geotextile reinforced conditions clearly highlighted the effectiveness of the woven geotextile in uniform dissipation of stresses as well as in separation and mitigation of subgrade intrusion into the large-size aggregate layer.

Wu (2013) studied the structural performance of a thin asphalt pavement section under accelerated pavement testing. The test was conducted at the Louisiana Accelerated Pavement Research Facility (LAPRF). The Accelerated Pavement Test (APT) was applied to three thin asphalt pavement sections with different chemically stabilized base and sub base materials, but having similar layer thicknesses. The objective of the study was to evaluate the structural performance of the test sections using nondestructive test results obtained by sensorial instruments which measured pavement response. Furthermore, the Mechanistic-Empirical Pavement Design Guide (MEPDG) software was implemented to predict rutting development on the tested sections. However it was concluded that this software overestimated the rut depths developed in the test sections. In addition, the study proposed a rutting prediction model which related the flexible pavement rutting to the in-situ surface deflection characteristics.

In order to evaluate the structural performance of thin asphalt pavements containing different chemically stabilized base and sub base materials, the scope of Wu's study included the Accelerated Pavement Test (APT), in situ pavement

instrumentation, non-destructive testing (NDT), surface distress survey and surface rutting prediction.

The three full-scale flexible pavement test sections in Wu's study were constructed over a silty-soil subgrade. Each section had 2 inches of hot mix asphalt (HMA) top layer, an 8.5-inch base and a 12-inch sub-base layer. The instrumentation plan consisted of two earth pressure cells embedded at two different depths in each test section directly under the center line (i.e. bottom of the base course and top of the subgrade layer - Figure 47). In addition, one Multi-Depth Deflectometer (MDD) was installed at each test section. MDDs were installed through a surface drilling operation after construction, 4.5 ft away from the pressure cells. Each MDD consisted of six potentiometers (labeled MDD1 through MDD6) for measuring load-induced plastic and elastic deformations at each of the selected depths. Figure 47 shows the pavement structure and the in-situ instrumentation layout of the test sections in Wu's (2003) study.

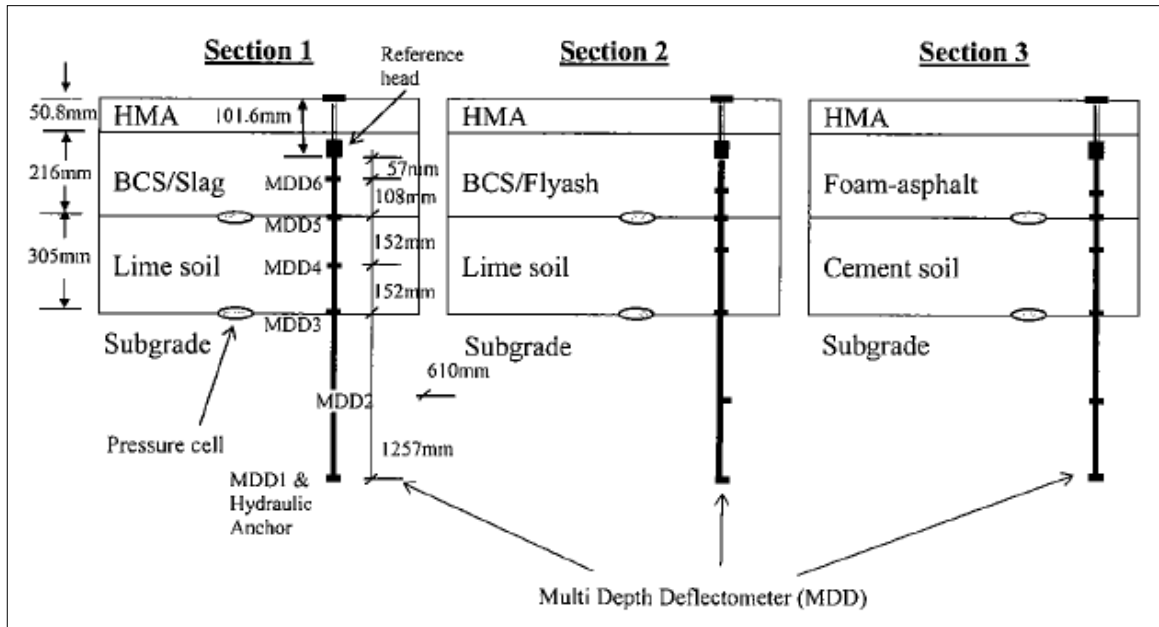


Figure 47. Pavement structure layout of the test lanes in the study by Wu (2013)

The APT loading was carried out using dual tires at the LAPRF Accelerated Loading Facility (ALF). The starting load was 9,750 lb (43.4 kN). After 175,000 repetitions, the load was increased to 12,050 lb (53.6 kN). After 225,000 repetitions, excessive rutting was found in Section 3. It is worth noting that 225,000 ALF repetitions is equivalent to 400,000 ESALs which is within the range of medium traffic volume (AASHTO 1993).

Collection of data from the pressure cells and MDDs was performed approximately at every 8,500 ALT load repetitions. NDT test including Dynaflect (Dynamic Pavement Deflection), Falling Weight Deflectometer (FWD) and rutting and cracking survey were performed at the end of each 25,000 load repetitions.

Wu (2013) presented pressure cell results in a tabulated format (Table 24). The table shows the average vertical stress measured from 0 to 175,000 and from 175,000 to 225,000 load passes in the columns “43.4 kN (9,750 lb) and 53.6 kN (12,050 lb)”, respectively. The Coefficient of Variation (COV) indicated the variation of pavement response due to the effects of seasonal variation and trafficking-induced material deterioration. Wu found that in general, stiffer base had better load spreading capability. This is demonstrated in Table 24. The results implied that the stiff material in Section 1 could provide a large load-spreading angle as compared to those of the other two base materials. In addition, Wu (2013) found higher percentages of stress increase on the top of the subgrade (last two columns in Table 24). This implied that a heavier truck would have a deeper influence zone and could cause more damage to the subgrade than a lighter truck.

Table 24. Vertical compressive stress results in the study by Wu (2013)

| Test Section No. | Type | Vertical Compressive Stress (kPa) |                  |                    |                  | % Change due to load increase of 24% |                  |
|------------------|------|-----------------------------------|------------------|--------------------|------------------|--------------------------------------|------------------|
|                  |      | Under 43.4 kN                     |                  | Under 53.6 kN      |                  | @bottom of base                      | @top of subgrade |
|                  |      | @bottom of base                   | @top of subgrade | @bottom of base    | @top of subgrade |                                      |                  |
| 1                | Avg  | 5.9                               | 3.5              | 6.0                | 4.3              | 1.2                                  | 24.8             |
|                  | Std  | 0.8                               | 0.5              | 0.5                | 0.2              |                                      |                  |
|                  | COV  | 13%                               | 14%              | 0.9%               | 0.5%             |                                      |                  |
| 2                | Avg  | 34.5                              | 12               | Data not available | 17.0             | Data not available                   | 42.2             |
|                  | Std  | 3.5                               | 1.2              |                    | 1.1              |                                      |                  |
|                  | COV  | 10%                               | 10%              |                    | 0.6%             |                                      |                  |
| 3                | Avg  | 70.4                              | 2.6              | 85.2               | 5.3              | 21.0                                 | 100.4            |
|                  | Std  | 8.6                               | 0.5              | 1.6                | 0.4              |                                      |                  |
|                  | COV  | 12%                               | 19%              | 0.2%               | 0.8              |                                      |                  |

Wu (2013) implemented MDD potentiometers to measure both elastic and plastic deformations of the test section profiles. Figure 48 shows elastic

deflection profiles obtained in Wu's study. These results indicate that Section 1 developed the smallest elastic deformation at all depths, followed by Sections 2 and 3. However, plastic deformations were used to calculate the permanent deformations that were developed within each pavement structural layer. Figure 49 shows permanent deformations in the three pavement layers in Section 3 as measured using the MDD. The data indicate a large amount of permanent deformation in the asphalt layer after 200,000 ESALs.

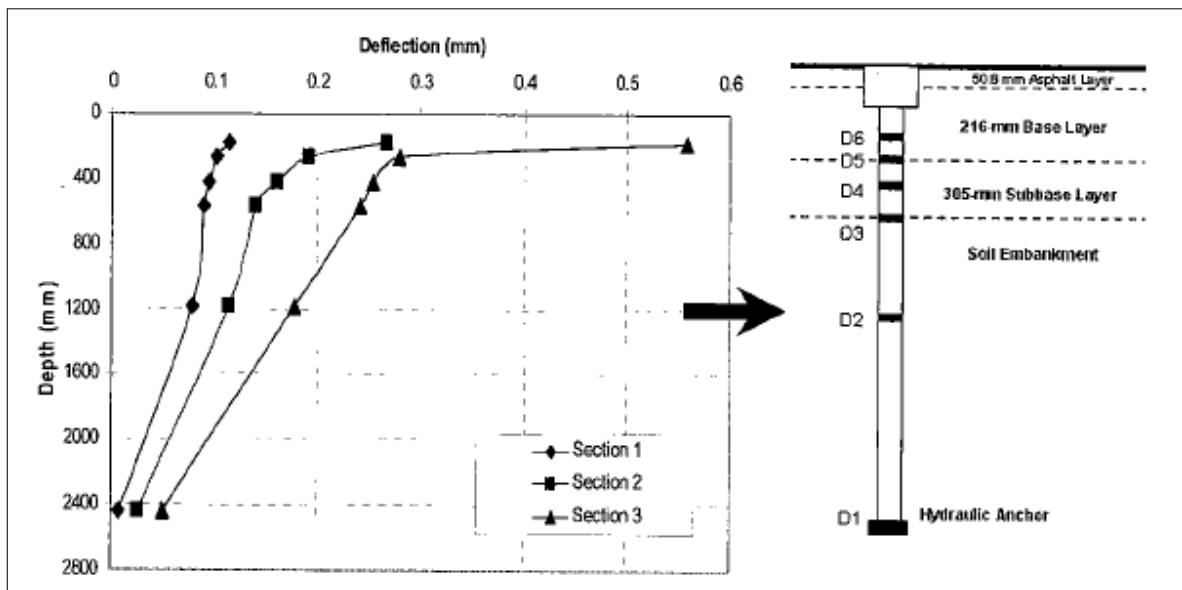


Figure 48. Elastic deformation profiles obtained from MDD in the study by Wu (2013)

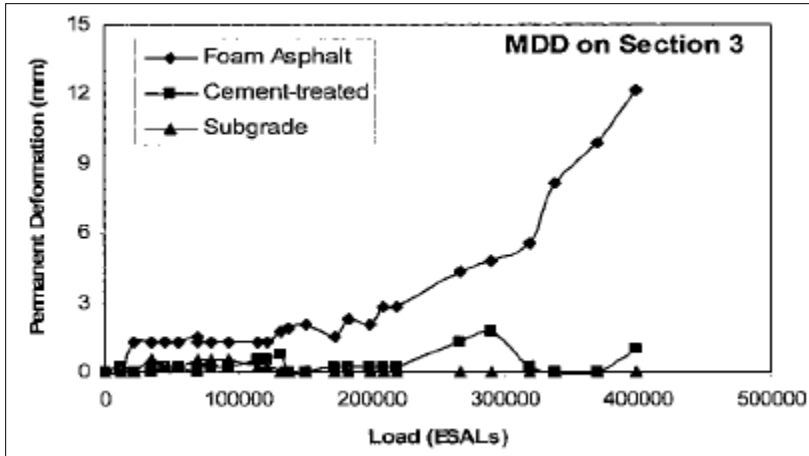


Figure 49. Plastic deformations from MDD in Section 3 in the study by Wu (2013)

Figure 50 shows Wu's Dynaflect test results, which include the structural number (SN) values measured for the three test sections under different loading passes (ESALs values). The initial increase in structural number (before 50,000 ESALs) was due to the compaction of pavement layers under wheel loading and the curing of the chemically stabilized base and treated sub-base layers. The SN values for all three test sections generally decreased with load repetitions and deterioration of pavement structures.

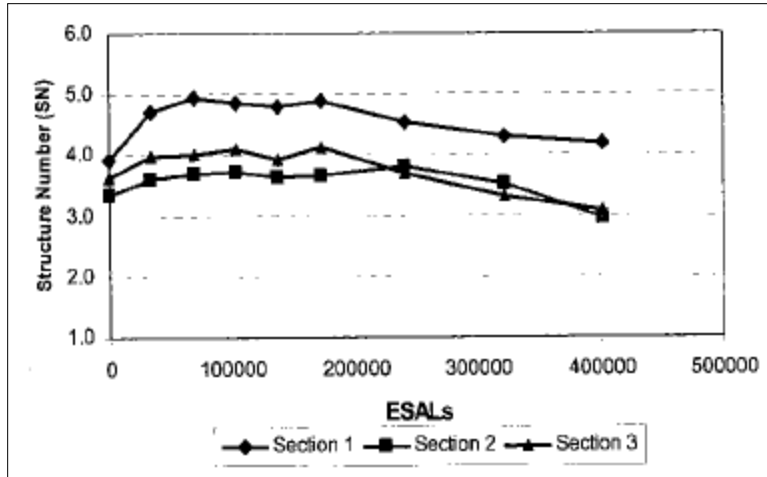


Figure 50. Dynaflect pavement structure number results in the study by Wu (2013)

Wu (2013) reported the following observations and conclusions:

- Field performance measurements indicate that the BCS/Slag base material performed significantly better than the BCS with the alternative materials, i.e. BCS/Fly ash and BCS/foam asphalt. This was evident by all measured results in a consistent way: the section with the BCS/Slag (i.e. Section 1) exhibited smaller MDD permanent deformations, vertical compressive stresses, FWD center deflections and surface rutting, while maintaining larger structural numbers throughout the tests.
- The cement-treated sub-base possessed higher load-induced structural capacity than the lime-treated sub-base as demonstrate by its higher resilient modulus, greater load-carrying capability and smaller permanent deformations.

- It was observed that a heavier load caused a proportionally larger percentage of increase in vertical stresses on top of the subgrade than on top of the sub-base.

Table 25 summarizes the sensors and methods that have been reported in the past studies to measure roadway performance in the field.

Table 25. Summary of instrumentation plans used in previous field test sections

| Authors                               | Black and Holtz (1999) | Al-Qadi and Appea (2003) | Chehab et al. (2007)  | Henry <i>et al.</i> (2008)                                      |
|---------------------------------------|------------------------|--------------------------|---|---|
| Instruments                           |                        |                          |   |   |
| Thermocouples                         | -                      | -                        | -   | Copper-constantan, Type T in all pavement layers                |
| Temperature Sensors                   | -                      | -                        | PQI model 301 Density gauge   | -   |
| Moisture Sensors                      | -                      | -                        | PQI model 301 Density gauge   | ECH2O model EC-20 at base course and subgrade                   |
| Strain Gauges                         | -                      | -                        | -   | FLA-5-23, 10 per test section                                   |
| Earth Pressure Cells                  | -                      | -                        | Three pressure cells, transversal, longitudinal and vertical directions | -   |
| Electromagnetic Induction (εmu) Coils | -                      | -                        | -   | Triaxial strain gauges, three every 6 in. height (11 locations) |
| Data Acquisition Systems (DAS)        | -                      | -                        | -   | -Environmet - Traffic -Rutting - Static and dynamic response    |

| Authors             | Black and Holtz (1999)  | Al-Qadi and Appea (2003)                  | Chehab et al. (2007)                         | Henry <i>et al.</i> (2008)  |
|---------------------|---|---|--|-----------------------------|
| Instruments         |   |   |  |                             |
| Forensic Evaluation | Permisitivity and wide width tests on geotextiles, measurement of migration of fines and sieve analysis | Exploring excavation                      | Observation of subgrade and geogrid response | -                           |
| In-Situ Tests       | FWD, Nuclear Gauge, Pocket Penetrometer, Torvane Tests  | Falling Weigh Deflectometer (FWD)         | -  | -                           |
| Rutting Measurement | -   | Straight Edge method (ASTM E 1703)        | Profilometer on pavement surface             | -                           |
| Traffic Measurement | -   | Traffic counter and Piezoelectric sensors | -  | Accelerated traffic loading |

Table 25. Summary of instrumentation plans used in previous field test sections (Cont'd).

| Authors                                   | Al-Qadi <i>et al.</i> (2008) | Warren et al. (2008) | Cuelho and Perkins (2009)                            | Tingle and Jersey (2009)   | Abu-Farsakh and Chen (2010)   |
|---|------------------------------|----------------------|--|--|---|
| Instruments                               |                              |                      |  |  |   |
| Thermocouples                             | 82 in total                  | -                    | -  | -  | -   |
| Temperature Sensors                       | -                            | -                    | -  | Two Campbell Scientific time domain reflectometry moisture and temperature at subgrade and aggregate | -   |
| Moisture Sensors                          | -                            | -                    | -  |  | -   |
| Time Domain Reflectometers (TDR)          | Two per section              | -                    | -  | -  | -   |
| Pore Water Pressure Sensors               | -                            | -                    | One per section, 6 inches below the subgrade surface | One per section  | Three Model 4500AL vibrating wire piezometer at the top of the subgrade |
| Piezometers                               | Two per section              | -                    | -  | -  | -   |
| Linear Variable Differential Transformers | Four to eighth per section   | -                    | Three per section                                    | Three per section  | -Eight at the HMA surface (DCTH)  |

| Authors                               | Al-Qadi <i>et al.</i> (2008)                | Warren <i>et al.</i> (2008)                                   | Cuelho and Perkins (2009)                           | Tingle and Jersey (2009)   | Abu-Farsakh and Chen (2010)   |
|---------------------------------------|---|---|---|--|---|
| Instruments                           |   |   |   |  |   |
| (LVDT's)                              |   |   |   |  | -Strain soil gauge (RDP model D5/400W)  |
| Strain Gauges                         | One or two asphalt strain gauge pre section | EP-08-230DS-120 for geogrids, EP-08-19CDZ-350 for geotextiles | -   | 8 foil strain gauges per section   | 16 Model EP-08-250BG-120  |
| Earth Pressure Cells                  | Two per section                             | -   | -   | Eight 229-mm Geokon, one per test section, in the wheelpath approximately 2 in below the base-subgrade                   | Four beneath the subgrade surface (three Kulite and one 3500-1 Geokon   |
| Electromagnetic Induction (emu) Coils | -   | -   | -   | -  | -   |
| Depth Deflectometers (DDs)            | -   | -   | -   | Single DD, 1-2 per section   | -   |
| Data Acquisition Systems (DAS)        | One DAS (environmental and dynamic data)    | -   | 3 Data acquisition computers (20 measurements each) | - OPTIM system to measure the Static and dynamic responses<br>-Campbell Scientific data logger for environmental sensors | -Stain guages amplifier<br>- Digital signal conditioning module<br>- FlexTest GT test controller(MTS systems) |
| Solar Panels and batteries            | -   | -   | one per each DAS                                    | -  | -   |
| Forensic Evaluation                   | -   | -   | -   | -  | -   |
| In-Situ Tests                         | -   | -   | -   | FWD  | -   |
| Rutting Measurement                   | Straight Steel Edge method                  | -   | Elevation rut method using a digital level          | Folding rule and a 3.05-m straightedge   | -   |
| Traffic Measurement                   | Accelerated traffic loading                 | -   | -   | -  | Cyclic Plate Load Tests   |

Table 25. Summary of instrumentation plans used in previous field test sections (Cont'd).

| Authors                          | Oh (2011)  | Jersey et al. (2012)   | Mishra and Tutumluer (2013)   | Wu (2013)   |
|----------------------------------|--|--|---|---|
| Instruments                      |  |  |   |   |
| Earth Pressure Cells             | -  | -  | -   | One at the bottom of the base course and one at the top of the subgrade layers  |
| Depth Deflectometers (DDs)       | -  | -  | -   | Multiple DD, one at each test section   |
| Exhumation of pavement materials | Sieve analysis, shrinkage and swelling potential                             | -  | Visual inspection of pavement layer boundaries after excavation of transverse trenches across the wheel paths | -   |
| In-situ tests                    | FWD, Dynamic cone penetrometer (DCP) on subgrade after exhumation of geogrid | In-field CBR, DCP, nuclear density, and oven-dried moisture tests were performed at the top of the base course and subgrade layers | Ground Penetrating Radar (GPR), Dynamic cone penetrometer (DCP)   | FWD and Dynaflect to determine structural number and subgrade resilient modulus |
| Rutting Measurement              | Ground Penetrating Radar (GPR)   | Failure criterion for these pavements was a 1-in. surface rut measured at the center of the wheel path                             | Surface profile measurements and (GPR) scanning   | -   |
| Traffic Measurement              | -  | Accelerated traffic loading  | Accelerated transportation Assembly System (ATLAS)  | Accelerated Pavement Test   |

### **3. Field Test Section**

#### ***3.1 Field Project Selection***

A target test section for this study is a full-depth road project that involves an aggregate base unpaved road or a road with flexible pavement. The selected construction project should allow monitoring and measuring any signs of distress in the road test section within the period of the project (i.e. 1.5 - 2 years). This constraint required to focus our attention on the following factors:

1. Category of road: Secondary or service/haul road
2. Location: Proximity to the University of Oklahoma main campus (i.e. preferably in Central Oklahoma) to facilitate the monitoring and measurement of the test section
3. AADT (Annual Average Daily Traffic): High (>3,000)
4. Percentage of truck traffic: High (>10%)
5. Type of pavement: Aggregate base unpaved road or with flexible pavement

##### *3.1.1 Choice of Road Category*

The project should be selected from among secondary or service roads so that its level of design and service life will allow it to exhibit detectable signs of distress. Moreover, the consequence of distress on a haul road will not be too severe so that it would still be operational and not require major repairs at the

end of the observation period. Additionally, selecting a secondary or service/haul road for this study will help minimize the impact of any distress in the road on the general public/stakeholders utilizing the road.

### 3.1.2 Location

A roadway test section in Central Oklahoma will allow the research team to carry out frequent monitoring and measuring of its performance when subjected to field traffic. Figure 51 shows a combined color map of Oklahoma counties and the eight ODOT divisions. The circle in the middle of the map indicates the geographical location where the search for a suitable site was focused. The map was adopted from the Oklahoma Department of Transportation website, Planning and Research Division, Data Collection Branch.

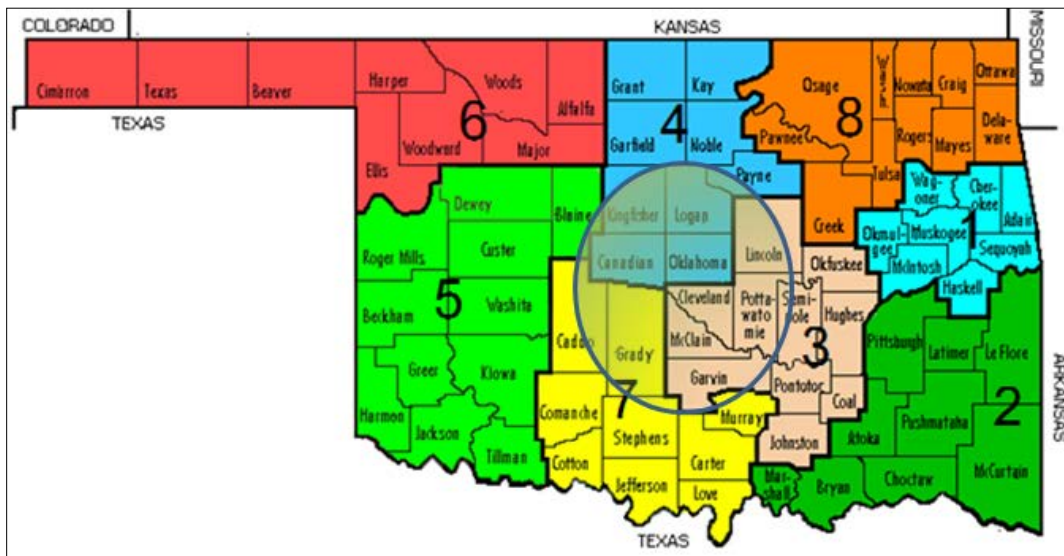


Figure 51. Map of Oklahoma counties and ODOT divisions (adopted and revised; Source: <http://www.okladot.state.ok.us/aadtcnt/>)

### 3.1.3 Annual Average Daily Traffic (AADT)

The most current AADT data from the Oklahoma roadway system was obtained from the Oklahoma Traffic Count Information System website (<http://www.okladot.state.ok.us/aadtcnt/>).

AADT data of all seventy seven (77) counties in Oklahoma was collected for the period between 1995 and 2011. After further analysis of the county roads AADT data, it was estimated that an AADT value within the range between 3,000 and 10,000 would provide a sufficient traffic load for our field test section and yet, it would not correspond to a heavily trafficked highway where the required quality of design and construction would not allow the formation of measurable distress in the pavement within the time frame of this project.

Table 26 shows count sites with AADT values higher than 3,000 and the corresponding candidate roads in Central Oklahoma.

Table 26. Candidate roads in Central Oklahoma for this study based on their AADT data

| ODOT Divisions | County    | City          | Count Site Number | Location      | Year | AADT |
|----------------|-----------|---------------|-------------------|---------------|------|------|
| 3              | Cleveland | Oklahoma City | 116               | SE 149th St   | 2010 | 3312 |
|                |           |               | 505               |               |      | 3428 |
|                |           | McCloud       | 443               | 192nd Ave NE  |      | 4113 |
|                |           |               | 537               |               |      | 4563 |
|                |           | Norman        | 502               | S Western Ave |      | 3381 |
|                |           |               | 504               | E Franklin Rd |      | 3796 |
|                |           |               | 506               | 60th Ave NW   |      | 3285 |
|                |           |               | 435               | Alameda St    |      | 3644 |
|                |           |               |                   |               |      | 4284 |
|                |           |               | 542               | E Robinson St |      | 3812 |
|                |           |               | 549               | Alameda DR    |      | 3063 |

| ODOT Divisions | County        | City              | Count Site Number | Location         | Year | AADT  |
|----------------|---------------|-------------------|-------------------|------------------|------|-------|
|                |               | Nobel             | 514               | E Maguire Rd     |      | 3194  |
|                | McClain       | Blanchard         | 524               | 2nd St           | 2007 | 3884  |
|                |               |                   | 526               | N Council Ave    |      | 4645  |
|                | Pottawatomie  | Shawnee           | 407               | N Kickapoo St    | 2007 | 4166  |
|                | Garvin        | N/A               | N/A               | N/A              | N/A  | N/A   |
|                | Lincoln       | N/A               | N/A               | N/A              | N/A  | N/A   |
| 4              | Oklahoma      | Edmond            | 410               | N MacArthur Blvd | 2006 | 5975  |
|                |               |                   | 536               | N Rockwell Ave   |      | 3167  |
|                |               |                   | 537               | N May Ave        |      | 6986  |
|                |               |                   | 548               | NE 136th St      |      | 5216  |
|                |               |                   | 550               | N Sooner Rd      |      | 3147  |
|                |               |                   | 504               | NW 248th St      |      | 7723  |
|                |               |                   | 515               | N MacArthur Blvd |      | 8228  |
|                |               | 534 (411-511-512) | NW 178th St       | 2010             | 3145 |       |
|                |               | 538               | NW 164th St       |                  | 5979 |       |
|                |               | Harrah            | 522               | N Luther Rd      | 2006 | 3377  |
|                | 524           |                   | SE 29th St        | 2010             | 3717 |       |
|                | 525           |                   | S Harrah Rd       |                  | 7437 |       |
|                | Oklahoma City | 514               | N Council Rd      | 2006             | 3010 |       |
|                |               | 551               | NE 108th St       |                  | 3332 |       |
|                | Jones         | 573               | E Britton Rd      | 2006             | 5192 |       |
|                |               | 577               | E Main St         |                  | 5253 |       |
|                | Canadian      | Yukon             | 443               | N Czech Hall Rd  | 2011 | 4803  |
|                |               | Piedmont          | 508               | Piedmont Rd N    |      | 3795  |
|                |               |                   | 509               | NW 178th St      |      | 3004  |
|                |               | Oklahoma City     | 531               | NW 10th St       |      | 10943 |
|                | Mustang       | 550               | S Morgan Rd       | 16673            |      |       |
|                | Logan         | Guthrie           | 531               | S Broadway St    | 2011 | 6880  |
| 551            |               |                   | S Sooner Rd       | 4076             |      |       |
| 560            |               | 5246              |                   |                  |      |       |
| Edmond         |               | 562               | 3964              |                  |      |       |
| 564            | S Santa Fe    | 3557              |                   |                  |      |       |
| 7              | Grady         | Tuttle            | 503               | N2970 Rd         | 2010 | 3189  |

### 3.1.4 Percentage of Truck Traffic

The search for a suitable roadway project was focused on roads that would be subjected to sufficient traffic load (especially heavy trucks) so that they will

experience detectable and measurable distress for a comparative study of different geosynthetic-reinforced vs. unreinforced test sections.

The Percentage of Truck Traffic (PTT) data on the secondary roads in Oklahoma are not available. Therefore, the search for a suitable test site was focused on roadways near industrial parks with the expectation that they are naturally subjected to a fairly significant truck traffic load. We found a directory of industrial parks across Oklahoma on the Oklahoma Department of Commerce website ([www.okcommerce.gov](http://www.okcommerce.gov)) and shortlisted nine locations that were comparatively close to the OU campus. Table 27 includes a list of candidate roads that were selected for query from the corresponding ODOT field offices for any possible construction or repair projects in the near future.

Table 27. Location of industrial parks within a 35-mile radius from Norman

| Industrial Park Name                       | City         | County       | Acres | Location                              |
|--|--------------|--------------|-------|---------------------------------------|
| Chickasha Regional Airport Industrial Park | Chickasha    | Grady        | 340   | Airport Road, OK 73018                |
| Methvin Industrial Park                    |              |              | 18    | Highway 62 West & 81, OK              |
| Canadian Valley Industrial Park            | El Reno      | Canadian     | 160   | E. Jensen Rd., El Reno, OK 73036      |
| El Reno Industrial Park                    |              |              | 50    | Industrial Park Rd, El Reno, OK 73036 |
| El Reno Industrial Park II                 |              |              | 73.5  | Industrial Park Rd, El Reno, OK 73036 |
| Tinker Business and Industrial Park        | Midwest City | Oklahoma     | 70    | Liberty Parkway, Oklahoma City, OK    |
| Shawnee Industrial Park                    | Shawnee      | Pottawatomie | 20    | N Harrison St, Shawnee, OK 74804      |

| Industrial Park Name      | City | County | Acres | Location                           |
|---------------------------|------|--------|-------|------------------------------------|
| American Way              |      |        | 40    | Acme road, Shawnee, OK<br>74804    |
| Wolverine Industrial Park |      |        | 160   | Wolverine Rd, Shawnee, OK<br>74804 |

### *3.1.5 Pavement Type*

An ideal field project for this study would involve an unpaved road or a road with flexible pavement. A flexible surface is more amenable to measuring its rutting and visual identification of distress on the road surface as compared to a rigid (concrete) pavement alternative.

### *3.1.6 Proposed Location of the Field Test Section*

In parallel with our search for a suitable county road or city street for a test section, a proposal was submitted to Dolese Bros. Co. for the possible use of an access road in one of their quarries or sand plants as an alternative option. Discussions with Dolese Engineers indicated that their quarries in Central Oklahoma have been in operation for an extended period of time. Therefore, the subgrade soil beneath the access roads in these quarries is fairly dense and compacted. As a result, base reinforcement would not provide a noticeable improvement in their performance, not to mention providing the opportunity to distinguish between different reinforcement products in different test segments.

Consequently, an access road in one of Dolese's sand plants was identified as a more suitable option for a roadway test section.

Figure 52 and Figure 53 show the test section proposed by the Dolese Bros. Co. Engineering Department, located on one side of the existing entrance road to the Prairie Park Sand Plant in Oklahoma City. This site would provide the following main advantages for this research study:

1. The traffic load will be more accurately estimated as compared to a secondary or county road because the number of trucks and their weights can be assessed more accurately as compared to the traffic which is of a more random nature on the latter types of roads.
2. The road will be loaded more closely to its design load (due to the trafficking of heavy trucks loaded with sand) and the traffic load will be more uniform (as compared to the traffic expected on a county road), both of which help with a more accurate interpretation of the test data (i.e. the road performance) and validation of numerical models toward the development of mechanistic-empirical methodologies by minimizing the variability in the traffic load.
3. The heavy traffic load will help impart a measurable amount of rutting and distress in the road within the time frame of the project (e.g. 1.5-2 years following construction) to achieve the main objective of the project, which is to be able to examine comparative performance of test segments reinforced/stabilized with different roadway reinforcement products.

These advantages make the proposed site an ideal outdoor test section in that it will be constructed using the typical construction practice and equipment in the field and yet, it will allow a desirable degree of control over the test parameters similar to what is typically aimed at within an indoor laboratory environment.

The site shown in Figure 52 and Figure 53 has been communicated to ODOT for their review and possible approval. Figure 53 shows the cross-section of the unpaved road design proposed by Dolese Bros. Co. Engineering Department.

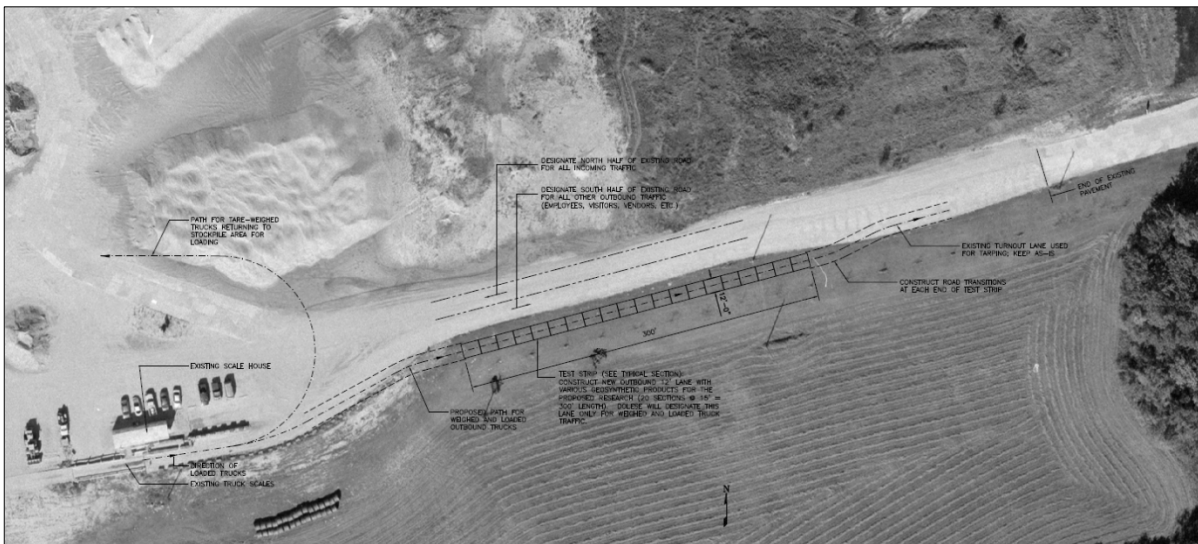


Figure 52. Proposed location of a test section located on the Dolese Bros. Co. Prairie Park Sand Plant in Oklahoma City (Hall 2013)

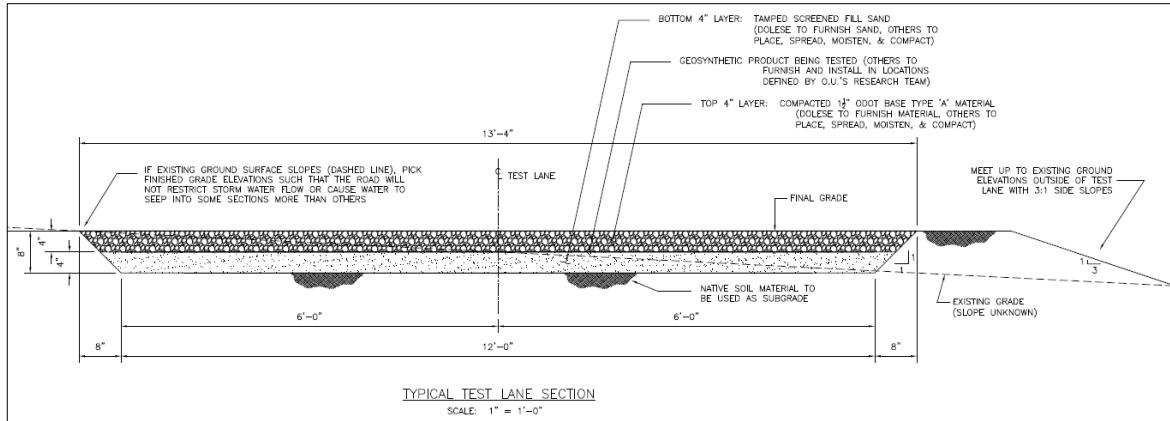


Figure 53. Cross-section of the unpaved road design proposed by Dolese Bros. Co. Engineering Department

Additionally, Dolese Bros. Co. Engineering Department proposed the following benefits and conditions in case ODOT representatives approve the construction of the test section in their Prairie Park Sand Plant:

- Dolese will provide the test site as shown in Figure 52 and may be able to provide useful data to the research team over time including the weight of trucks trafficking the test road.
- Dolese is also willing to furnish/donate approximately 90 tons of ODOT Type-A aggregate and 70 tons of screened fill sand to be used in the test strip.
- Others will be responsible for overall construction, including performing construction, surveying and excavating native soil to desired depth and placing of the road
- Dolese may be able to provide the use of a front-end loader during construction. However, its availability depends on the plant business.

- Dolese's requirements for those conducting work on the property consist of both MSHA training and records (if the work will take longer than 5 days) because the property is an MSHA-registered mine site.

## **3.2. Selection of Geosynthetic Samples**

### *3.2.1 Pavement Type*

The project team carried out a survey on a wide range of commonly available geosynthetics on the market in order to identify candidate products for their inclusion in the field test section. Candidate geogrids were initially screened from a previous study (Hatami et al. 2012) which involved laboratory pullout and plate load tests on eight geogrids from four different companies. However, it is a fact that the geosynthetics industry is constantly evolving. Some manufacturer companies are phasing out several of their geogrid products, resulting in extruded geogrids and new high-performance geotextiles dominating the base reinforcement application (Odgers 2013). Geosynthetic companies are developing new technologies and products such as triangular-aperture geogrids and cellular confinement systems for load support (i.e. triaxial geogrids and geocells). For these reasons, we updated the list of candidate geosynthetic products for base reinforcement that we had come up with in our previous study (Hatami et al. 2012). Various industry websites and publications including the Geosynthetics Specifier's Guide (IFAI 2013) were examined to include any new products that are currently used for base aggregate reinforcement.

The selection of the most suitable geosynthetic products for a specific roadway project is determined based on a number of factors including the strength of the subgrade material, traffic volume, geosynthetic structural coefficient and the thickness and the structural and drainage coefficients of different pavement layers (AASHTO 1993, Berg et. al 2000). The pavement design depends on the resilient modulus of the subgrade as well as the traffic volume and the serviceability factors of the road. We contacted six different geosynthetic manufacturing companies to obtain information on their geosynthetic products used for base course reinforcement applications. The information gathered included the geosynthetics tensile strength, design methodology, fabrication category, polymer material type and price, as shown in Table 28. The final selection of geogrids for field testing will be made from these products once sufficient information on the subgrade condition and the traffic volume of the test section is available.

Table 28. Summary of tentative geosynthetics intended for use in the field test section

| Test Section | Geogrid Series | Manufacturer | Geosynthetics Models | Strength at 5 % (lb/ft)          |        | Category                       | Method of design (unpaved road)               | Price |
|--------------|----------------|--------------|----------------------|----------------------------------|--------|--------------------------------|---|-------|
|              |                |              |                      | MD                               | XD     |                                |   |       |
| 1            | TriAx TX       | Tensar       | TX140                | Radial Stiffness at 0.5 % strain | 15,430 | Extruded Geogrid Polypropylene | Giroud and Han (2004a,b) SpectraPave Software | -     |
|              |                |              | TX160                |                                  | 20,580 |                                |   | -     |
|              |                |              | TX5                  |                                  | -      |                                |   | -     |
|              |                |              | TX7                  |                                  | -      |                                |   | -     |
| 2            | Biaxial BX     | Tensar       | BX Type1             | 580                              | 920    | Extruded Geogrid Polypropylene | Giroud and Han (2004a,b)                      | -     |
|              |                |              | BX Type 2            | 810                              | 1,340  |                                |   | -     |
|              |                |              | BX 1300              | 720                              | 1,200  |                                |   | -     |
|              |                |              | BX1500               | 1,200                            | 1,370  |                                |   | -     |

| Test Section | Geogrid Series  | Manufacturer | Geosynthetics Models | Strength at 5 % (lb/ft) |       | Category                       | Method of design (unpaved road)   | Price     |
|--------------|-----------------|--------------|----------------------|-------------------------|-------|--------------------------------|---|-----------|
|              |                 |              |                      | MD                      | XD    |                                |   |           |
| 3            | StrataBase SB   | Strata       | SB11                 | 580                     | 920   | Extruded Geogrid Polypropylene | Giroud and Han (2004a,b)  | -         |
|              |                 |              | SB12                 | 810                     | 1,340 |                                |   | -         |
|              |                 |              | SB30                 | 1370                    | 1,370 |                                |   | -         |
| 4            | MacGrid EG      | Maccaferri   | EG11                 | 580                     | 920   | Extruded Geogrid Polypropylene | Giroud and Han (2004a,b)  | \$0.85/SY |
|              |                 |              | EG12                 | 810                     | 1,340 |                                |   | \$1.40/SY |
| 5            | STF             | Synteen      | P11                  | 580                     | 920   | Extruded Geogrid Polypropylene | Giroud and Han (2004a,b)  | -         |
|              |                 |              | P12                  | 810                     | 1,340 |                                |   | -         |
| 6            | Mirafi RSi      | TenCate      | RS280i               | -                       | -     | Geotextile                     | Giroud and Han (2004a,b)<br>Tencate flexible Pavement Design software   | \$2.15/SY |
|              |                 |              | RS380i               | 120*                    | 197*  |                                |   | \$3.15/SY |
|              |                 |              | RS580i               | 132*                    | 385*  |                                |   | \$4.00/SY |
| 7            | Geotex HF       | Propex       | 2x2 HF               | 90                      | 117   | Geotextile                     | FHWA Geosynthetic Design & Construction Guidelines, No. FHWA NHI-07-092 | -         |
|              |                 |              | 3x3 HF               | 125                     | 145   |                                |   | -         |
|              |                 |              | 4x4 HF               | 209                     | 225   |                                |   | -         |
| 8            | Control Section | -            | -                    | -                       | -     | -                              | -   | -         |

\* Obtained at OU geosynthetics laboratory

### 3.2.2 Reinforced Base Design Methods and Software Available in Practice

A number of industrial flexible pavement design software programs and design methods were examined in order to study how manufacturers of geosynthetic products select suitable reinforcement products for a specific site. These design methods were compared with the national guidelines for aggregate base course reinforcement.

Geosynthetic manufacturer companies were contacted in order to obtain their base course design software. Tensar International Corporation and TenCate

Geosynthetics made their design programs available to our research team. On the other hand, we were told that the pavement design software developed by companies such as Maccaferri, Strata, Tenax and Hanes Geo is primarily for internal use within these companies. Nevertheless, we were furnished with the design software from some of these companies for educational purposes.

Inspection of the design methodologies followed by Tensar, Tencate, Tenax and Hanes Geo indicated that all of these companies follow the AASHTO (1993) standard for flexible pavements (Figure 54). Input parameters for the design equation to determine the total pavement thickness for a given road include subgrade stiffness parameters, structural coefficients for different layers, serviceability parameters, predicted ESALs based on the type of road and some additional statistical parameters.

$$\log_{10}(W_{18}) = Z_R \times S_o + 9.36 \times \log_{10}(SN+1) - 0.20 + \frac{\log_{10}\left(\frac{\Delta PSI}{4.2-1.5}\right)}{0.40 + \frac{1094}{(SN+1)^{5.19}}} + 2.32 \times \log_{10}(M_R) - 8.07$$

$W_{18}$  = predicted number of 80 kN (18,000 lb.) ESALs  
 $Z_R$  = standard normal deviate  
 $S_o$  = combined standard error of the traffic prediction and performance prediction  
 $S_N$  = Structural Number (an index that is indicative of the total pavement thickness required)  
 $= a_1 D_1 + a_2 D_2 m_2 + a_3 D_3 m_3 + \dots$   
 $a_i$  =  $i^{\text{th}}$  layer coefficient  
 $D_i$  =  $i^{\text{th}}$  layer thickness (inches)  
 $m_i$  =  $i^{\text{th}}$  layer drainage coefficient  
 $DPSI$  = difference between the initial design serviceability index,  $p_o$ , and the design terminal serviceability index,  $p_t$   
 $M_R$  = subgrade resilient modulus (in psi)

Figure 54. Design equation for flexible pavements (AASHTO 1993)

For reinforced aggregate base design, the equation for the pavement Structural Number (SN) is modified using a Geosynthetic Structural Coefficient (GSC) (Figure 55). The GSC represents the improvement in load-carrying capabilities of the aggregate due to reinforcement. This coefficient is based on empirical pavement tests in which otherwise identical pavement structures with and without geosynthetic reinforcement are compared. In addition, these values depend on the values of subgrade CBR, ESALs and allowable rut depth.

$$SN = (a * d)_{hma} + GSC (a * d * m)_{base} + (a * d * m)_{subbase}$$

a = structural-layer coefficients  
 d = layer thickness (inches)  
 m = layer drainage coefficient  
 GCS = Geosynthetic Structural Coefficient

Figure 55. Structural Number equation for geosynthetic reinforced pavement (AASHTO 1993)

*Tensor Design Software:* Example designs were investigated using the software *Spectrapave 4 Pro* by Tensor. Paved road base course reinforcement design was performed using input soil parameters and coefficients for selected subgrade soils in central Oklahoma. Figure 56 shows the input parameters for unreinforced and reinforced pavement sections in separate tables together with the analysis results in the form of two diagrams which show the calculated thicknesses of the pavement layers for a given ESALs value. As mentioned previously, in order to calculate the required thickness of the reinforced and unreinforced layers of the pavements, the software is designed to recall the equations shown in Figure 54 and Figure 55. Tensor's TX5 geogrid was used for this trial investigation. It is important to mention that TX5 and TX7 geogrids are the only products currently available to use in this software. Information about the design methodology used in this software was obtained from a Tensor design report (Tensor 2012).



Figure 56. Tensor design software SpectraPave4 PRO trial results for this study

*TenCate Design Software:* MiraSpec Design Solutions Software from TenCate was evaluated for flexible pavement design. Given that there are some small differences between the programs used by different companies and in order to compare geosynthetic performance, the same input parameters used in Tensor's program were used in TenCate's program. The input parameters as well as the final thicknesses for the reinforced and unreinforced pavement designs are presented in Figure 57. TenCate's RS3801 geotextile was used for this trial. Presently, the only geosynthetic products available for design using TenCate's software are RS380i and RS580i geotextiles. Information about the design methodology implemented in this software was obtained from a TenCate report (TenCate 2010).

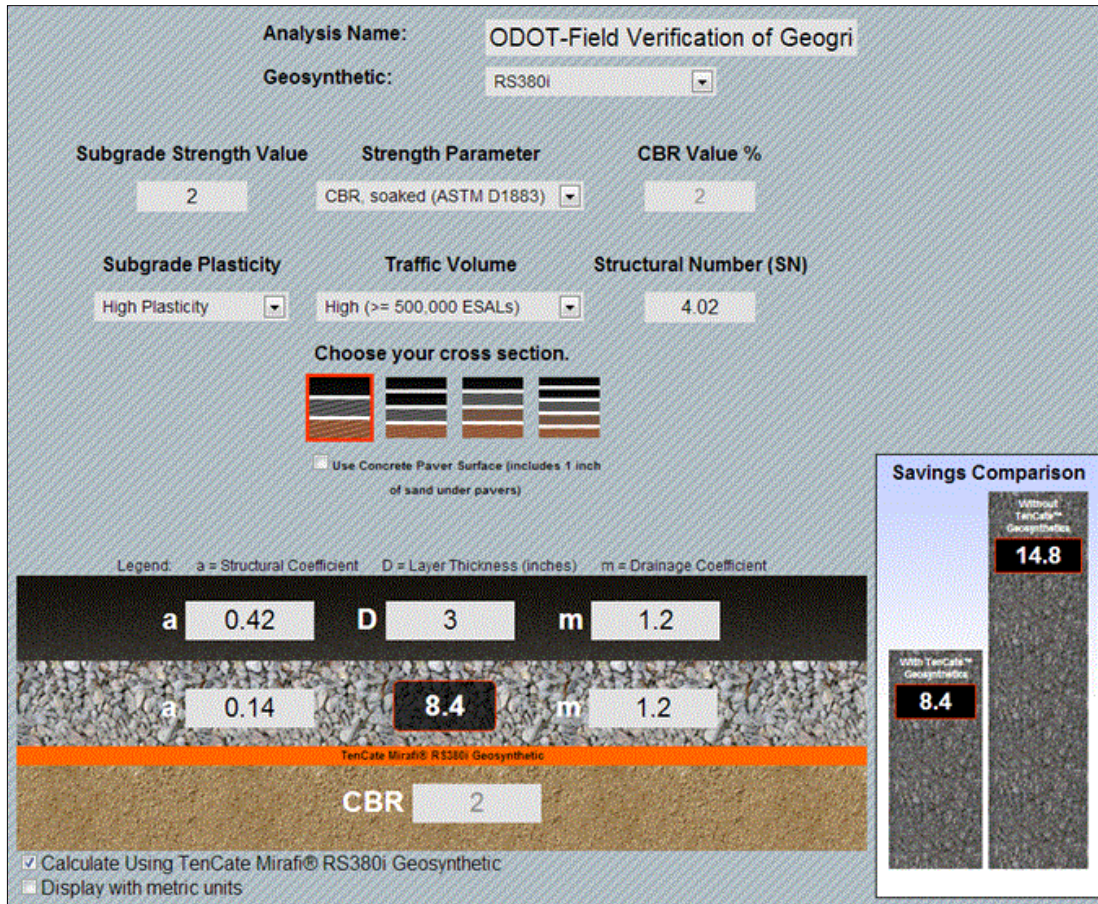


Figure 57. TenCate design software MiraSpec Design Solutions trial results for this study

As a third approach, Hanes Geo Components methodology was studied in order to develop reinforced and unreinforced pavement designs and compare them with those from previous computer programs. For this purpose the geosynthetic structural coefficient value (GSC) of the Hanes Geo B120 geogrid was obtained from their design methodology report (Hanes Geo 2008). Hand calculations were subsequently performed using the 1993 AASHTO equation (Figure 54) and the same input parameters and coefficients as those used in earlier examples.

The results from the Tensar and TenCate software and the Hages Geo design methodology calculations are compared in Table 29. In all of the design examples above, the objective was to reach optimum serviceability (i.e. terminal serviceability of 2.5 (Abaza and Abu-Eisheh 2003) for ESALs higher than 500,000, with a hot mix asphalt thickness of 3 inches, for the same given values of layer and drainage coefficients. For this trial investigation, results show that Tensar's TX5 geogrid requires a slightly smaller aggregate thickness as compared to TenCate's RS380i and Hanes Geo's B120 geosynthetic products. The comparison between the required thicknesses of aggregate layers using different design approaches and corresponding geosynthetic products demonstrates the comparative effectiveness of the specific geosynthetic product as a reinforcing element in aggregate base layers. However, the differences between the products examined in these example calculations could be considered as negligible. Therefore, these products could be considered as practically equivalent for the given design requirements. However, all of them consistently result in a significant reduction (i.e. 38.5% - 43.2%) in the quantity of base aggregate in the project.

Table 29. Predicted aggregate thickness results in this study using selected methods available in the geosynthetic industry

| Geogrid                   | Agg Base Thickness unreinforced (in) | Agg Base Thickness reinforced (in) | % Reduction in Thickness |
|---------------------------|--------------------------------------|------------------------------------|--------------------------|
| Tensar TX 5               | 13                                   | 7.5                                | 42.3                     |
| TenCate RS380i            | 14.8                                 | 8.4                                | 43.2                     |
| Hanes Geo Terra Grid B120 | 13                                   | 8                                  | 38.5                     |

### **3.3. Test Section Layout**

The layout of test section was designed to carry out a comparative study of the field performance of selected base reinforcement geosynthetic products. The length of each test segment (i.e. using a given geosynthetic product) was chosen as 30 feet long by 12 feet wide (i.e. width of a roadway lane) based on a review of previous field studies (Table 30). Even though shorter test segments have been used in the past, it was decided that a 30 ft-long segment would provide sufficient anchorage length for the reinforcement under the truck traffic load and to confidently attribute any distress patterns in any given segment of the pavement to the performance of the reinforcement product used within that segment. The full-scale test section shown in Figure 58 is divided into eight individual test segments, which include selected geogrids from a recent study by the authors (Hatami et al. 2012) as well as newer geosynthetic products.

Table 30. Summary of test section dimensions in previous field studies

|                              | Authors                   | Length of Segments (ft) | Width (ft) | Number of segments | Total Length of Test Section (ft) |
|------------------------------|---------------------------|-------------------------|------------|--------------------|-----------------------------------|
| Actual Road (field)          | Black and Holtz (1999)    | 25                      | 12         | 6                  | 75                                |
|                              | Tingle and Jersey (2009)  | 25-30                   | 12         | 8                  | 234                               |
|                              | Oh (2011)                 | 4200-4600               | 24         | 3                  | 13300                             |
|                              | Cuelho and Perkins (2009) | 49.21                   | 13         | 12                 | 640                               |
| Accelerated Loading Facility | Al-Qadi et al. (2008)     | 20-25                   | 11.5       | 9                  | 190                               |
|                              | Jersey et al. (2012)      | 50                      | 8          | 3                  | 50                                |
|                              | Henry et al. (2008)       | 26                      | 3          | 8                  | 110                               |
|                              | Chehab et al. (2007)      | 4.7                     | 1.8        | 4                  | 4.7                               |
|                              | Current Study (Proposed)  | 30                      | 12         | 8                  | 300                               |

With respect to the location of the individual geosynthetic products in different test segments, stronger geosynthetics are planned to be installed at the beginning of the test section in the traffic direction. This arrangement can help to prevent any adverse effects of excessive rutting or failure of weaker sections on the performance of the subsequent segments further down the test section. Therefore, the sequence of products in the test section was decided based on the results of laboratory tests on the individual products in the authors' recent study (Hatami et al. 2012) in addition to the information available on the individual

products from the corresponding vendors. Hence, the current ODOT Type 1 geogrid was considered for placement in Segment 1, followed by an integrally-drawn triaxial geogrid in Segment 2 and three new extruded biaxial geogrids in Segments 3 through 5. Two geotextile reinforcement products were considered for Segments 6 and 7. Finally, an unreinforced control segment was considered as Segment 8 (Figure 58).

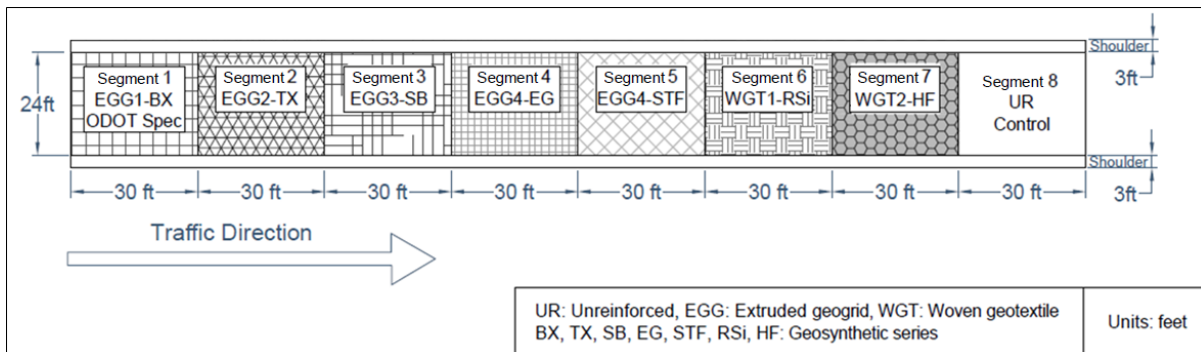


Figure 58. Proposed layout of the field road test section for this study (scale: 1:600)

### 3.4. Instrumentation Plan

The instrumentation plan to measure the geogrid and pavement structure performance subjected to traffic and environmental loads was developed based on the authors' experience in the recent ODOT- and OkTC-funded projects (i.e. Hatami et al. 2013, Hatami et al. 2012), a survey of related literature on laboratory and full-scale studies and communications with instrumentation suppliers for product specifications. Table 31 includes a description of the instruments planned for the test section together with their quoted prices.

Table 31. Description of the instruments planned for the proposed test section in this study

| Instrument                            | Model and Manufacturer or Supplier | Capabilities   | Price                       | Accessories                                 |
|---------------------------------------|------------------------------------|--|-----------------------------|---|
| Electrical resistance strain gauge    | FLA-5-23, Texas Measurements Inc.  | 5% strain limit, Operational temperature (-4°F to 176 °F)                            | \$61.75, 10 gauges          | 2 or 3 lead wire                            |
| Earth Pressure Cells                  | Model 3515, Geokon, Inc.           | Measures dynamic pressure changes up to 870 psi                                      | \$875.00                    | PVC cable                                   |
| Tensiometers                          | MPS-2, Decagon Devices Inc.        | Measure soil water potential (pF 1.71 to pF 3.71) and temperature (-40 °F to 120 °F) | \$155.00                    | 5m Cable and Em50 series logger (5-channel) |
| Electromagnetic Induction (emu) Coils | not available on the market        | Measures dynamic and permanent strains in the soil                                   | Not available in the market | Electronic calibration, copper wires        |
| Data Logger                           | Em50, Decagon Devices Inc.         | Power, read and log data from five sensors   | \$458.00                    | -   |
| Data Acquisition Systems (DAS)        | DI-785, DATAQ Instruments          | Measures temperature, voltage, current, strains, displacements and frequency         | \$3,995.00                  | Computer                                    |

Figure 59 and Figure 60 depict schematic plan view and cross sectional layouts of the instrumentation intended for each test segment of the entire field test section, respectively. The location and width of the wheel path were initially estimated considering the axle lengths of two different categories of vehicles: (1) a tandem-axle (6 wheel) mid-size truck (82 inches) and (2) a small sedan (60 inches). However, if the Dolese site is approved for this project (Section 3.2), the wheel path may have to be adjusted to some extent based on the anticipated type of trucks utilizing the test road. The diagonal arrangement of strain gauges on the

geogrids across the width of the wheel path allows us to obtain a representative distribution of strains across the width of the wheel path in each test section.

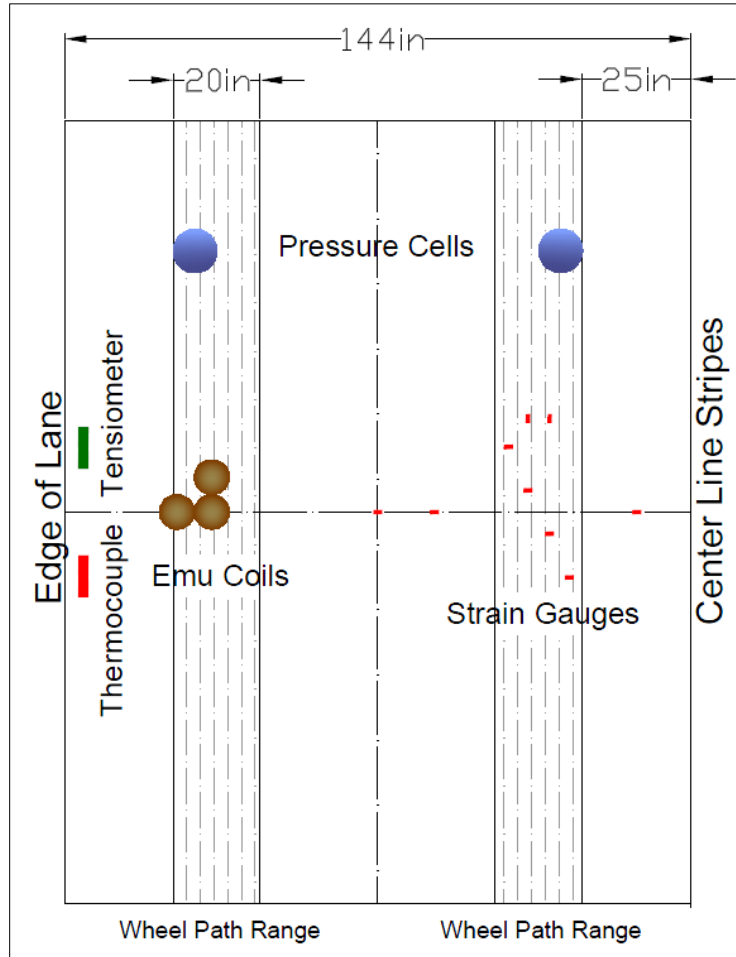


Figure 59. Plan view of a tentative instrumentation plan for different test sections in this project (Scale 1:60)

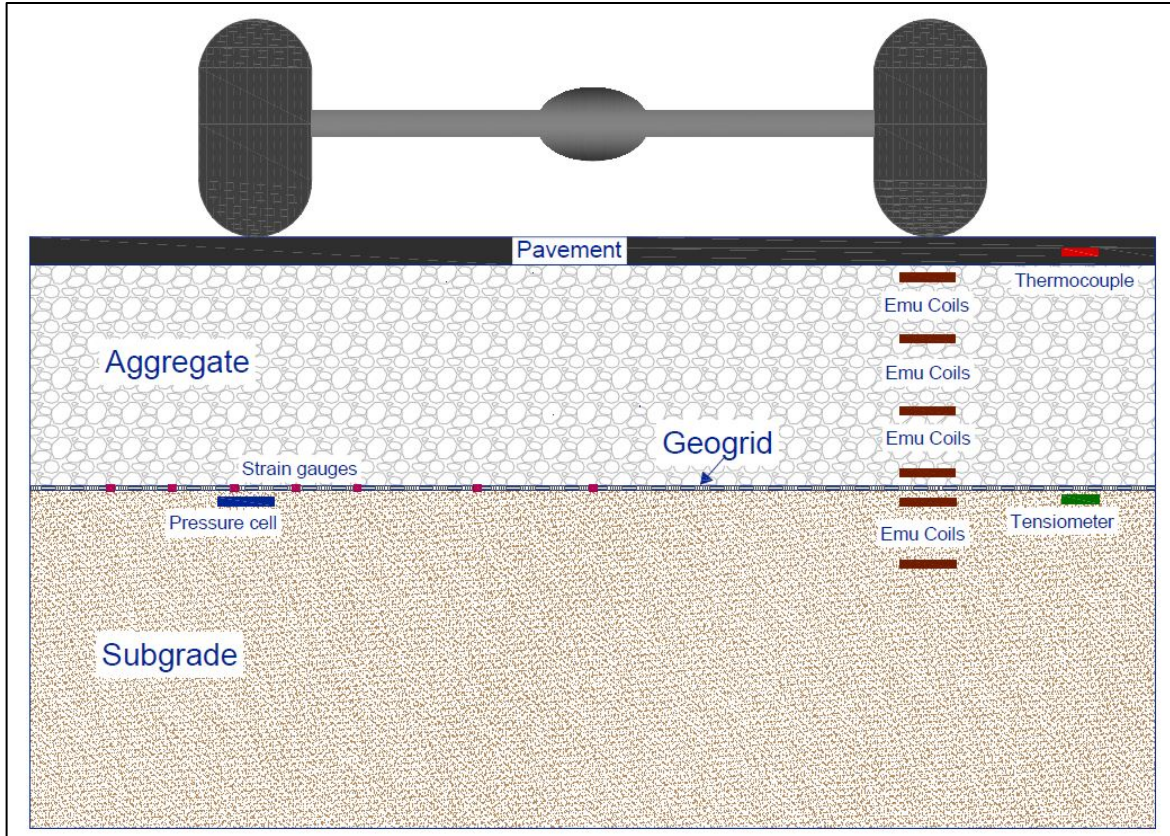


Figure 60. Typical instrumentation plan intended for each segment of the field test section (Not to scale)

## **4. Material Characterization**

### ***4.1 Testing Plan***

Once the field test section proposed for this study (Figure 52) is approved by ODOT, a series of laboratory and field tests will be carried out to characterize and determine the properties of the subgrade soil and aggregates used in the test section. The laboratory tests will include the Atterberg limits (ASTM D4318), sieve analysis (ASTM C136), CBR (ASTM D1883) and L.A. abrasion (ASTM C131) tests. The in-situ test will include the Vane shear (ASTM D2573), Dynamic cone penetrometer (ASTM D6951M), Densometer (ASTM D2167) and Falling weight deflectometer (ASTM D4695). Tests such as the FWD and (possibly) the DCP will be performed in collaboration with the ODOT personnel to collect and monitor pavement properties after construction and throughout the duration of the project.

### ***4.2 Laboratory Testing on Aggregates***

#### ***4.2.1 Los Angeles (LA) Abrasion Test***

We carried out a Los Angeles abrasion test on our ODOT Type-A aggregate following ASTM C131-06 standard in order to determine the aggregate durability since this material was used in previous cyclic plate load tests (Figure 61). The grading used for the LA abrasion test was Type B, which would best represent the ODOT Type-A particle size distribution with respect to the percentages

retained on the 1/2- and 3/8-inch sieves. The percentage of aggregate weight loss after the completion of the test was 28% which was well below the maximum allowable loss of 50% according to ODOT requirements for base aggregates. As a result, the ODOT Type-A aggregate used in our tests readily satisfied ODOT durability requirements.



Figure 61. Los Angeles abrasion machine after the test of ODOT Type-A aggregate at Ray Broce Materials Laboratory

## 5. Laboratory Testing of Geosynthetics

We carried out a series of tensile strength tests on Mirafi® RS580i geotextile product manufactured by TenCate Geosynthetics. ASTM D4595 standard was followed to determine the geotextile ultimate tensile strength as well as strength at 2% and 5% strain. Eight-inch-wide specimens were tested using a Baldwin hydraulic universal testing machine at the Fears laboratory (Figure 62). Additional three-inch-wide specimens were tested using a more accurate but lower capacity (i.e. 10 kN) tensile testing machine model United "Smart-1" STM in the geosynthetics laboratory (Figure 63). The deformations of the specimens tested on the Baldwin machine were recorded using a camcorder. These images were processed digitally after the test to determine the history of specimen strains as a function of the applied load, which was measured directly using the Baldwin machine. Similarly, deformations of specimens tested on the United testing machine were recorded and processed using digital imagery (Wang 2009) but the applied force was obtained directly from the test equipment.

Table 32 and Table 33 show the test results for the specimens tested in the machine and cross-machine directions, respectively. Figure 64 and Figure 65 show the load-strain data for five three-inch-wide specimens in the machine and cross-machine directions, respectively. It was noticed that the RS580i ultimate strength in cross-machine direction (XD) was attained more rapidly (i.e. specimens exhibited a more brittle response) as compared to the comparable ultimate strength in the machine direction. When a fiber started to rupture in XD,

the specimen would fail shortly after whereas in the MD, the specimen would maintain its strength long after an initial rupture.



Figure 62. A 3-inch-wide specimen of the Mirafi RS580i geotextile at the end of a tensile strength test using the new universal testing machine (model United "Smart-1" STM) at the OU Geosynthetics laboratory



Figure 63. 8-inch-wide specimen of the Mirafi RS580i geotextile subjected to a tensile strength test using the Baldwin hydraulic universal testing machine at the Fears engineering laboratory

Table 32. Mirafi RS580i geotextile tensile strength test results in machine direction

| Parameter Measured           | Geotextile width | MD1     | MD2     | MD3       | MD4     | MD5     | Mean ( $\mu$ ) | Standard Deviation ( $\sigma$ ) | Coefficient of Variation COV (%) | MARV value from manufacturer |
|------------------------------|------------------|---------|---------|-----------|---------|---------|----------------|---------------------------------|----------------------------------|------------------------------|
| Strength at 2% strain(lb/ft) | RS580i 3_in.     | 499.89  | 480.55  | 521.17    | 534.40  | 537.29  | 514.66         | 21.57                           | 4.19                             | 480                          |
|                              | RS580i 8_in.     | 489.60  | 614.23  | 631.55    | -       | -       | 578.46         | 8.66                            | 1.50                             | 480                          |
| Strength at 5% strain(lb/ft) | RS580i 3_in.     | 1407.73 | 1409.59 | [1226.25] | 1437.06 | 1385.58 | 1409.99        | 18.26                           | 1.30                             | 1440                         |
|                              | RS580i 8_in.     | 1364.93 | 1553.71 | 1644.00   | -       | -       | 1520.88        | 116.27                          | 7.65                             | 1440                         |
| Ultimate Strength (lb/ft)    | RS580i 3_in.     | 5123.12 | 5213.03 | 4938.44   | 4791.99 | 4927.55 | 4998.83        | 150.23                          | 3.01                             | 4800                         |
|                              | RS580i 8_in.     | 5265.64 | 4763.66 | 4885.44   | -       | -       | 4971.58        | 213.79                          | 4.30                             | 4800                         |

Table 33. Mirafi RS580i geotextile tensile strength test results in cross-machine direction

| Parameter Measured            | Geotextile width | XD1      | XD2     | XD3     | XD4     | XD5      | Mean ( $\mu$ ) | Standard Deviation ( $\sigma$ ) | Coefficient of Variation COV (%) | MARV value from manufacturer |
|-------------------------------|------------------|----------|---------|---------|---------|----------|----------------|---------------------------------|----------------------------------|------------------------------|
| Strength at 2% strain (lb/ft) | RS580i 3_in.     | 1907.38  | 1808.00 | 2014.98 | 1788.58 | [1625.4] | 1879.73        | 129.82                          | 7.10                             | 1800                         |
|                               | RS580i 8_in.     | 1762.49  | 2207.11 | 1656.14 | -       | -        | 1875.25        | 238.64                          | 12.73                            | 1800                         |
| Strength at 5% strain (lb/ft) | RS580i 3_in.     | 4852.68  | 4461.95 | 4617.64 | 4539.22 | 4193.60  | 4533.02        | 214.31                          | 4.73                             | 4380                         |
|                               | RS580i 8_in.     | [3585.3] | 4237.40 | 3995.28 | -       | -        | 4116.34        | 121.06                          | 2.94                             | 4380                         |
| Ultimate Strength (lb/ft)     | RS580i 3_in.     | 5483.23  | 5101.77 | 5314.39 | 4931.39 | 5215.16  | 5209.19        | 187.04                          | 3.59                             | 4800                         |
|                               | RS580i 8_in.     | [3720]   | 4359.87 | 4800.00 | -       | -        | 4579.93        | 220.07                          | 4.80                             | 4800                         |

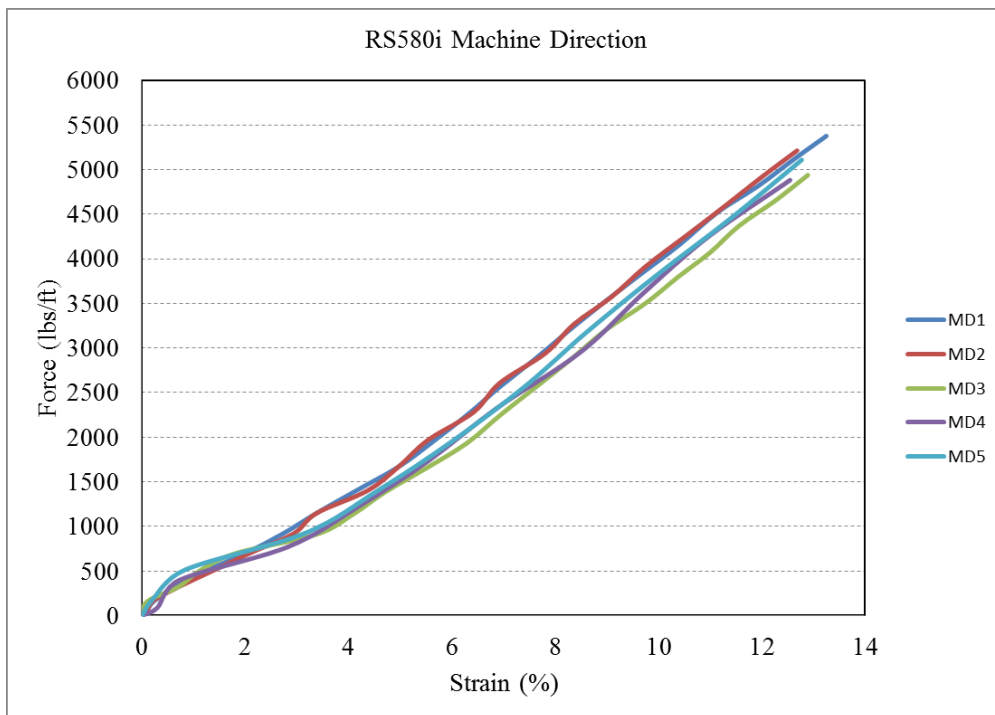


Figure 64. Tensile test results for the Mirafi RS580i geotextile (3 inch-wide specimens) in machine direction

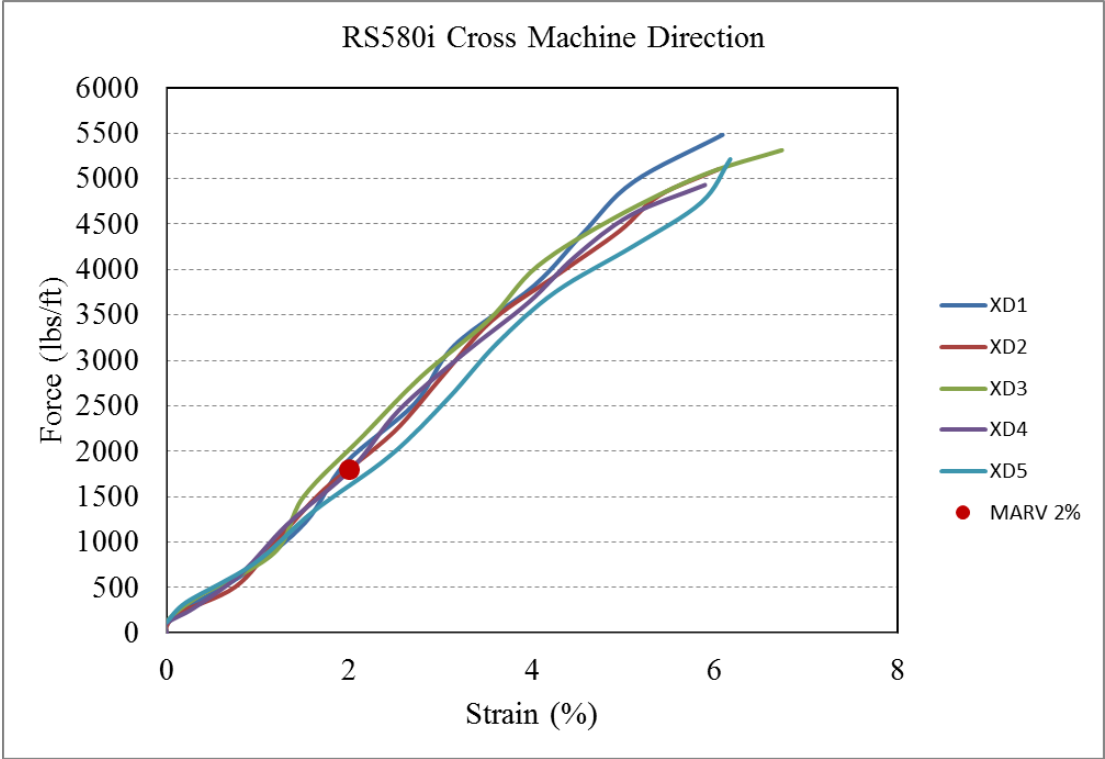


Figure 65. Tensile test results for the Mirafi RS580i geotextile (3-inch-wide specimens) in cross-machine direction

Figure 66 and Figure 67 show comparisons of the mean tensile strength results for the 3-inch-wide and 8-inch-wide specimens in machine and cross-machine directions, respectively.

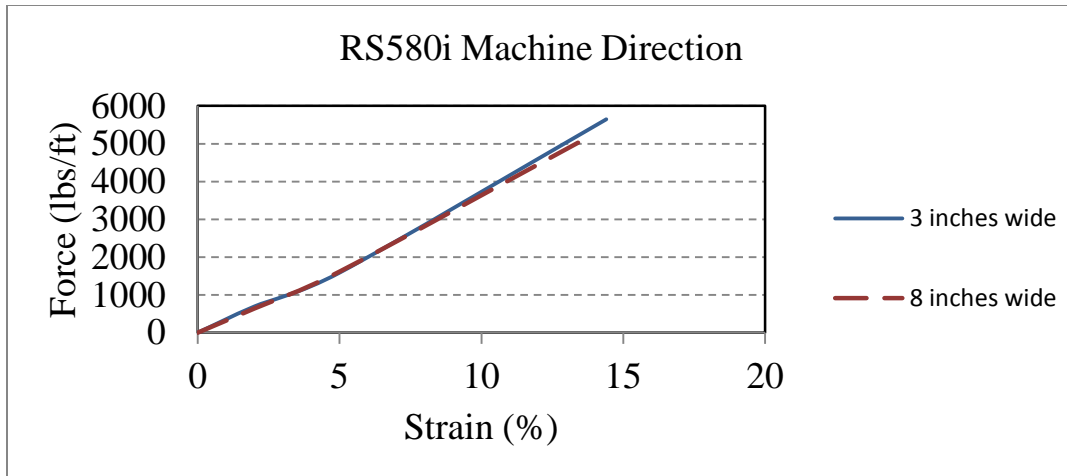


Figure 66. Comparison of geotextile RS580i tensile strength test results in machine direction

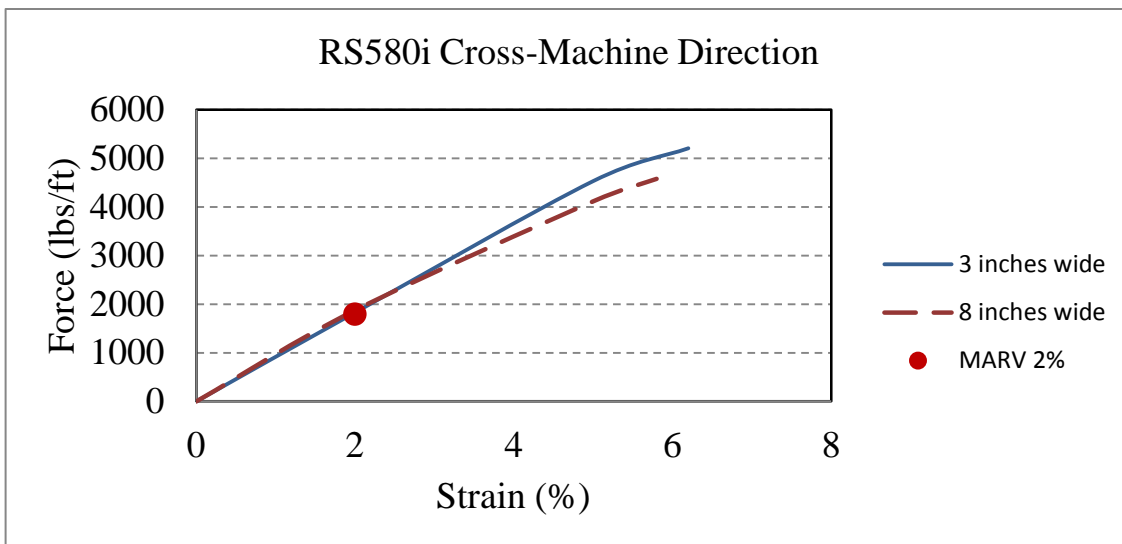


Figure 67. Comparison of geotextile RS580i tensile strength test results in cross-machine direction

The strength at 2%-strain, 5%-strain and ultimate tensile strength properties of the Mirafi RS580i geotextile in machine and cross-machine direction were reported by TenCate Geosynthetics (2013). The Minimum Average Roll Value

(MARV) for strength at 2% strain was reported equal to 1800 lb/ft as per the ASTM D4595 standard. Results shown in Figure 67 indicate that the mean 2%-strain tensile strength in cross-machine direction in our tests on 3-inch-wide specimens was 1879.73 lb/ft, which is comparable to (and slightly exceeds) the MARV value reported by the manufacture. This result was corroborated by the tests on 8-inch-wide specimens which yielded a mean value of 1875.25 lb/ft for the 2%-strain tensile strength.

Table 34 and Table 35 show similar results for the Mirafi® RS380i product. Figure 68 and Figure 69 show the corresponding load-strain data for five three-inch-wide specimens in machine and cross-machine directions, respectively.

Table 34. Mirafi RS380i geotextile tensile strength test results in machine direction (MD)

| Parameter Measured           | Geotextile width | MD1     | MD2     | MD3     | MD4     | MD5      | Mean ( $\mu$ ) | Standard Deviation ( $\sigma$ ) | Coefficient of Variation COV (%) | MARV value from manufacturer |
|------------------------------|------------------|---------|---------|---------|---------|----------|----------------|---------------------------------|----------------------------------|------------------------------|
| Strength at 2% strain(lb/ft) | RS380i 3_in.     | 532.08  | 641.98  | 657.87  | 603.05  | 646.29   | 616.25         | 51.50                           | 8.36                             | 600                          |
| Strength at 5% strain(lb/ft) | RS380i 3_in.     | 1783.64 | 1940.05 | 2156.76 | 2040.17 | 1931.65  | 1970.45        | 124.02                          | 6.29                             | 1800                         |
| Ultimate Strength (lb/ft)    | RS380i 3_in.     | 4366.83 | 4252.49 | 4522.04 | 4321.14 | [4054.8] | 4365.63        | 99.05                           | 2.27                             | 4500                         |

Table 35. Mirafi RS380i geotextile tensile strength test results in cross-machine direction (XD)

| Parameter Measured           | Geotextile width | XD1     | XD2     | XD3       | XD4     | XD5     | Mean ( $\mu$ ) | Standard Deviation ( $\sigma$ ) | Coefficient of Variation COV (%) | MARV value from manufacturer |
|------------------------------|------------------|---------|---------|-----------|---------|---------|----------------|---------------------------------|----------------------------------|------------------------------|
| Strength at 2% strain(lb/ft) | RS380i 3_in.     | 1061.97 | 1083.33 | [830.50]  | 1026.34 | 1111.23 | 1070.72        | 31.01                           | 2.90                             | 1020                         |
| Strength at 5% strain(lb/ft) | RS380i 3_in.     | 2251.46 | 2436.23 | [2118.75] | 2344.18 | 2408.19 | 2360.02        | 71.00                           | 3.01                             | 2256                         |
| Ultimate Strength (lb/ft)    | RS380i 3_in.     | 4111.30 | 4131.50 | 4319.39   | 4418.66 | 3968.99 | 4189.97        | 159.68                          | 3.81                             | 3600                         |

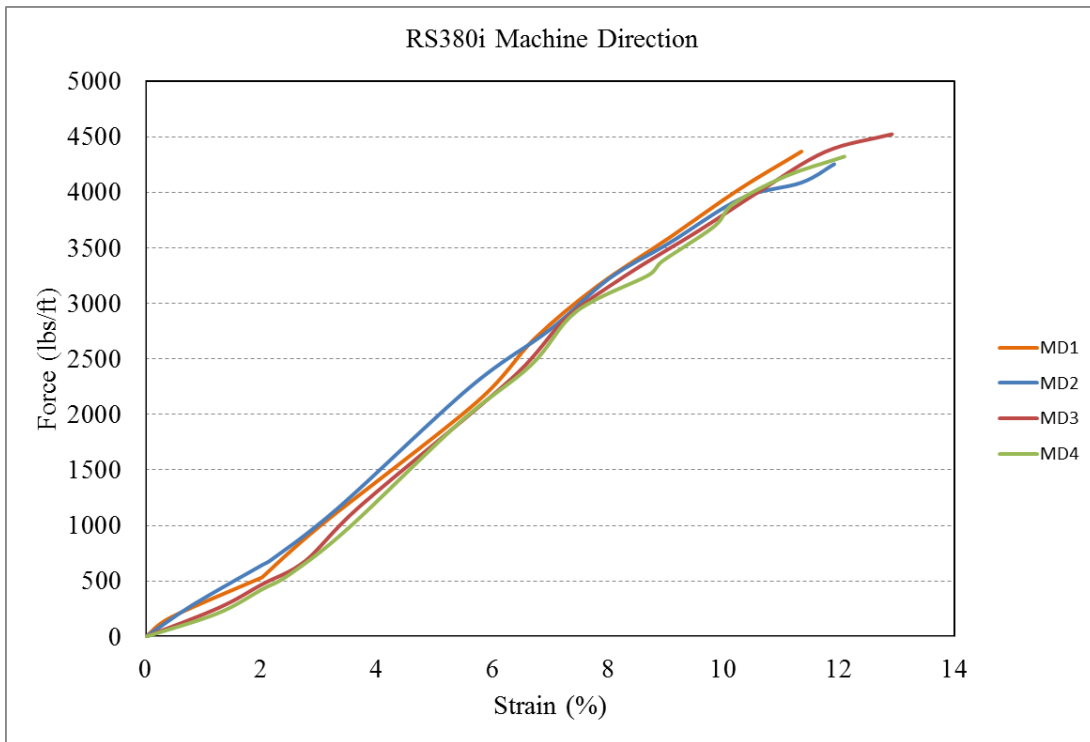


Figure 68. Tensile test results on Mirafi RS380i geotextile (3 inch-wide specimens) in machine direction

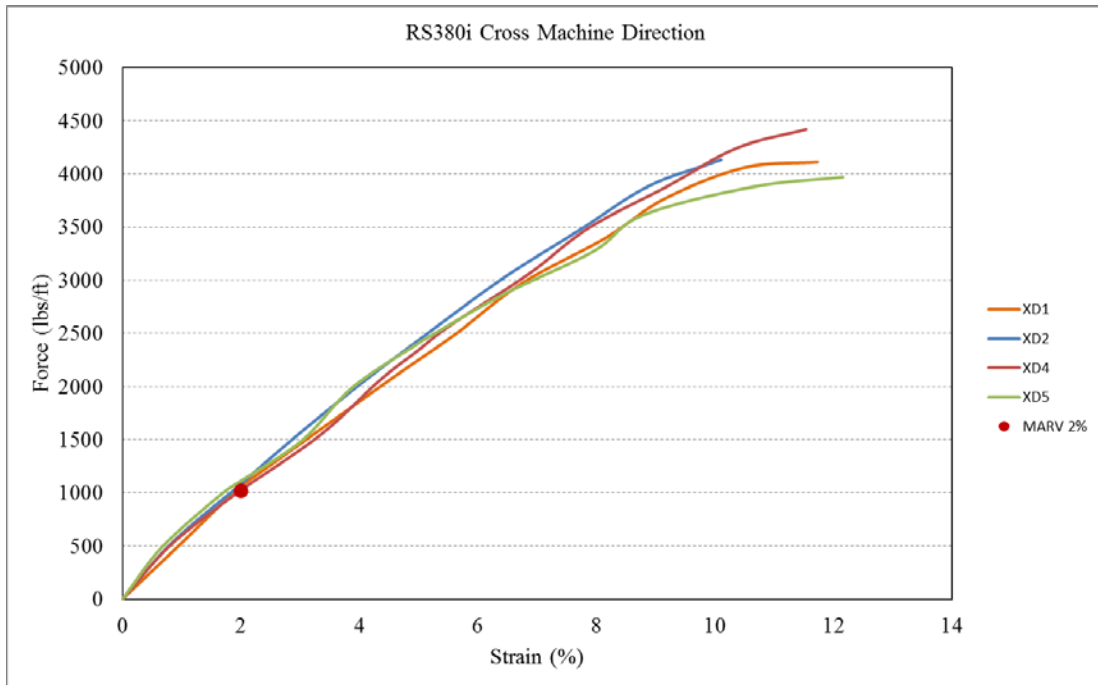


Figure 69. Tensile test results on Mirafi RS380i geotextile (3-inch-wide specimens) in cross-machine direction

The strength at 2%-strain, 5%-strain and ultimate tensile strength properties of the Mirafi RS380i geotextile in machine and cross-machine direction were reported by TenCate Geosynthetics (2013). The Minimum Average Roll Value (MARV) for strength at 2%-strain was reported equal to 1020 lb/ft as per the ASTM D4595 standard. Results shown in Table 35 indicate that the average 2%-strain tensile strength in cross-machine direction in our tests on 3-inch-wide specimens was 1070.72 lb/ft, which is comparable to (and slightly exceeds) the MARV value reported by the manufacturer. Table 36 and Table 37 compare the tensile strength properties of Mirafi RS580i and RS380i in machine (MD) and cross-machine directions (XD), respectively.

Table 36. Comparison of Mirafi RS580i and RS380i tensile strength properties (MD)

| Parameter Measured           | Geotextile width | Mean ( $\mu$ ) | Standard Deviation ( $\sigma$ ) | Co-efficient of Variation COV (%) | MARV value from manufacturer |
|------------------------------|------------------|----------------|---------------------------------|-----------------------------------|------------------------------|
| Strength at 2% strain(lb/ft) | RS580i           | 514.66         | 21.57                           | 4.19                              | 480                          |
|                              | RS380i           | 616.25         | 51.50                           | 8.36                              | 600                          |
| Strength at 5% strain(lb/ft) | RS580i           | 1409.99        | 18.26                           | 1.30                              | 1440                         |
|                              | RS380i           | 1970.45        | 124.02                          | 6.29                              | 1800                         |
| Ultimate Strength (lb/ft)    | RS580i           | 4998.83        | 150.23                          | 3.01                              | 4800                         |
|                              | RS380i           | 4365.63        | 99.05                           | 2.27                              | 4500                         |

Table 37. Comparison of Mirafi RS580i and RS380i tensile strength properties (XD)

| Parameter Measured           | Geotextile width | Mean ( $\mu$ ) | Standard Deviation ( $\sigma$ ) | Co-efficient of Variation COV (%) | MARV value from manufacturer |
|------------------------------|------------------|----------------|---------------------------------|-----------------------------------|------------------------------|
| Strength at 2% strain(lb/ft) | RS580i           | 1879.73        | 90.15                           | 4.80                              | 1800                         |
|                              | RS380i           | 1070.72        | 31.01                           | 2.90                              | 1020                         |
| Strength at 5% strain(lb/ft) | RS580i           | 4617.87        | 146.32                          | 3.17                              | 4380                         |
|                              | RS380i           | 2360.02        | 71.00                           | 3.01                              | 2256                         |
| Ultimate Strength (lb/ft)    | RS580i           | 5278.64        | 140.04                          | 2.65                              | 4800                         |
|                              | RS380i           | 4189.97        | 159.68                          | 3.81                              | 3600                         |

## **6. In Aggregate Laboratory Tests of Geosynthetics for Base Reinforcement**

### **6.1 Pullout Test**

A pullout test was carried out on Tensar TX 160 geogrid (Figure 70) to establish a reference for future tests by comparing the test results from the new rounds of tests with those reported by Hatami et al. (2012). The same pullout test procedure reported by Hatami et al. (2012) was followed to carry out this new test under 69 psf overburden pressure. A 31-inch-long by 14-inch-wide geogrid sample was cut and placed in the test box (embedment length = 22 inches) in the cross machine direction. The horizontal displacement and tensile load in the specimen were measured using four wire potentiometers attached to the geogrid and a hydraulic actuator that pulled the geogrid out of the test box (Hatami et al. 2012). Figure 71 shows the pullout response results for the TX 160 specimen.



Figure 70. A pullout test in progress on Tensar TX 160 geogrid at the OU Geosynthetics laboratory

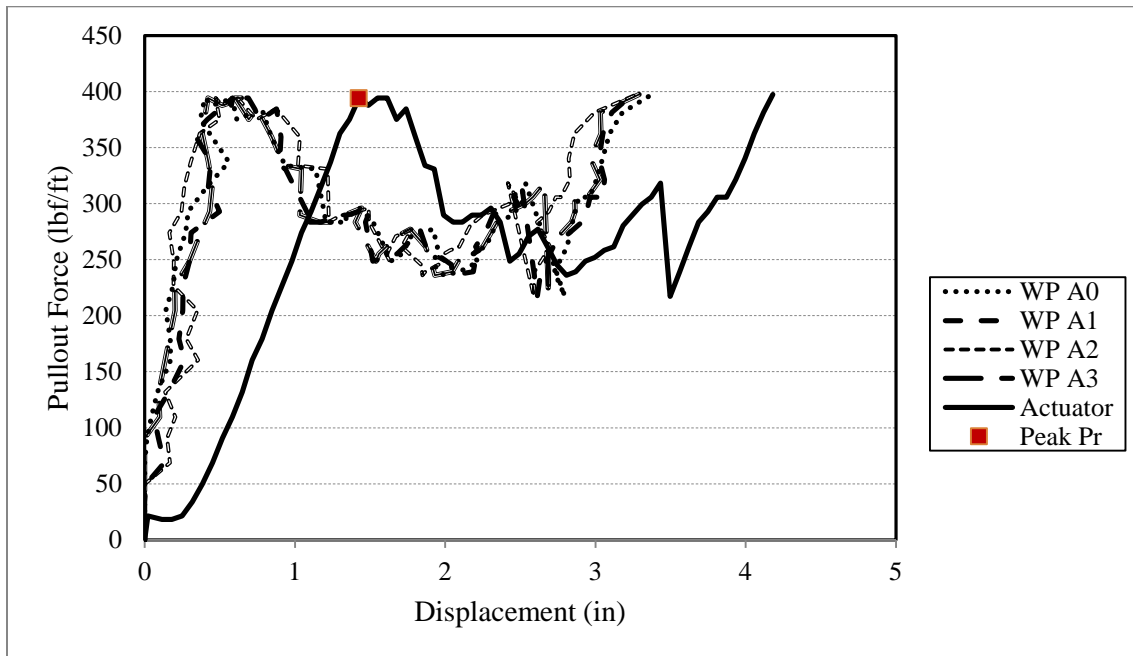


Figure 71. Pullout response results for TX 160 geogrid in ODOT Type-A aggregate subjected to 69 psf overburden pressure

The ultimate pullout resistance calculated in this test was 394 lb/ft, which was comparable to the 388 lb/ft value reported by Hatami et al. (2012) for the ultimate pullout resistance of the same geogrid in the same conditions (i.e. ODOT Type-A aggregate, the same overburden pressure and the same sample length). This close agreement provided further confidence in the setup and the execution of the pullout tests as needed for the current project in the future.

## ***6.2 Large-Scale Cyclic Plate Load Tests***

Two cyclic plate load tests were carried out on Mirafi SR580i and SR380i geotextiles (Figure 72) to compare the reinforcement performance of these two geotextiles with the performance of different geogrids reported by Hatami et al. (2012) under the same conditions. The same cyclic plate load test procedures reported by Hatami et al. (2012) was followed.



Figure 72. Cyclic plate load test on Mirafi SR580i geotextile at Donald G. Fears Structural Engineering Laboratory

The tests were carried out inside a test box [with inside dimensions 63-inches (L) x 66-inches (W) x 42-inches (H)] using an actuator connected to a hydraulic pump (Figure 72). One inch thick Styrofoam blocks were located on the inside walls of the box to minimize the influence of an otherwise rigid front boundary on the test results. The test box was filled with uniformly graded loose sand as the

subgrade and ODOT Type-A aggregate as the base layer. The geotextile was placed between the two layers. The sand was compacted to a density that corresponded to a CBR value of 4 [Dry unit weight of 103.3 lb/ft<sup>3</sup> and relative density of 95.7%, Hatami et. al. (2012)].

The aggregate unit weight and moisture content were 135 lb/ft<sup>3</sup> and 0.02%, respectively. Maximum dry unit weight of ODOT Type-A aggregate from modified proctor tests (AASHTO T 180-01) had been found equal to 146.5 lb/ft<sup>3</sup> (Kazmee 2010). Figure 73 shows the layout of the cyclic plate load tests performed in this study including the thickness of the sand and aggregate layers as well as the location of different instruments. As shown in Figure 73, sand with CBR=4 and Styrofoam layers were used to simulate a weak subgrade/substrate for the aggregate layer in the test setup.

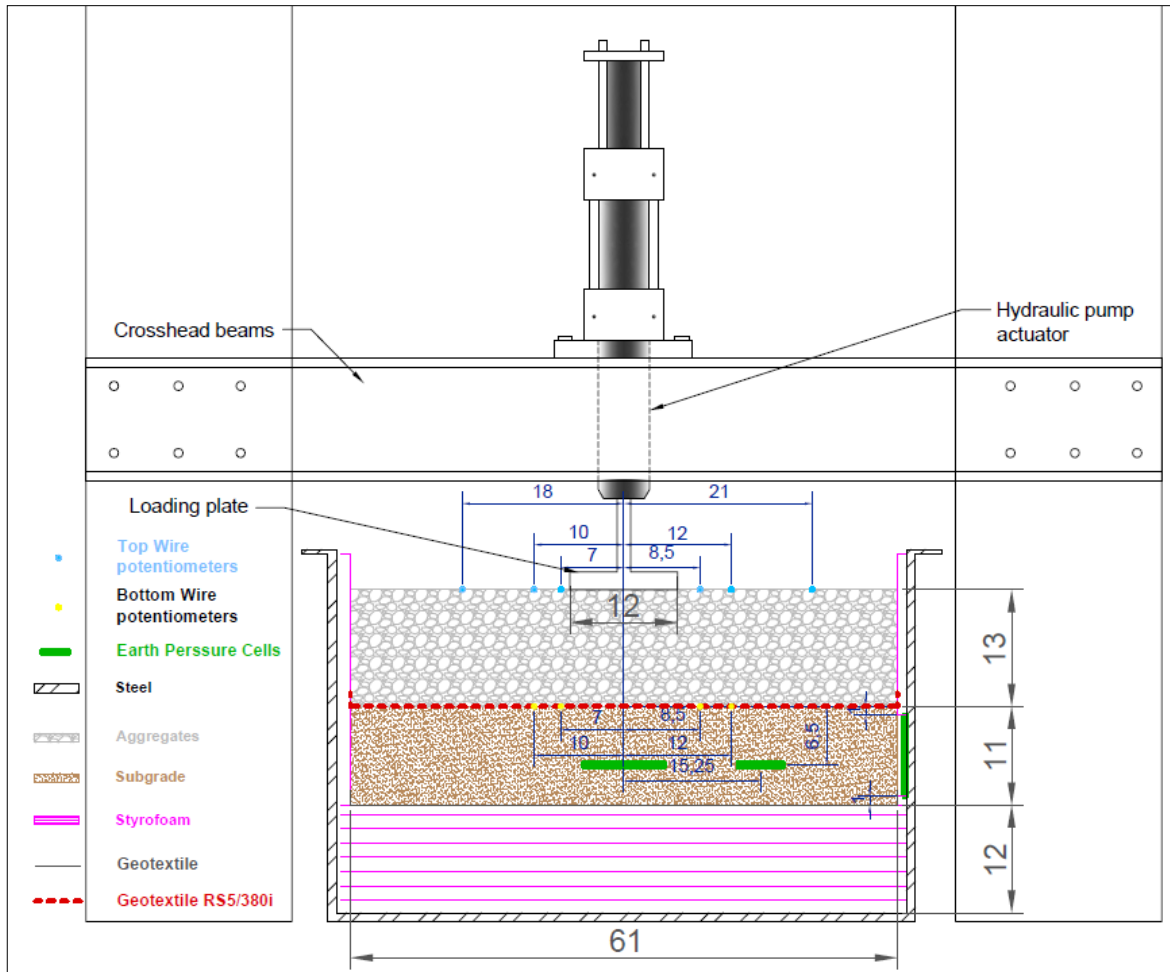


Figure 73. Layout of the cyclic plate load tests performed on Mirafi RS580i and RS380i geotextiles (units: inches)

The instrumentation plan for the cyclic plate load tests included three earth pressure cells (EPC) from Geokon Inc., Models 4810-2, 4800-1-2 and 4800-1x-170, located 6.5 inches below the top of the subgrade. After the subgrade layer was instrumented, a 63-inch (L) x 66-inch (W) geotextile specimen (i.e. RS580i or RS380i, as applicable) was installed over the subgrade surface. The geotextile sample was instrumented with four brass wire potentiometers (17-inches long)

covered with flexible rubber tubes (i.e. extensometers) to measure the deformation profile at the bottom of the aggregate layer due to cyclic loading. The boundaries of the geotextiles were folded upwards 1-inch in every side of the geotextile to ensure separation between the base course and the subgrade layers. A one-inch-thick ODOT Type-A aggregate layer was carefully placed on the geotextile specimen as an initial cover for the instrumented geotextile. Afterwards, three 4-inch-thick base course layers were placed and compacted to the desired unit weight, attaining a total base course thickness of 13 inches. After the last layer of aggregate was compacted, ten vertical wire potentiometers (WP) were mounted on the bottom side of the reaction beam. Four WPs were connected to the brass wires (extensometers connected to the geotextile) and the other six WPs were connected to circular telltale plates to measure the surface deflection of the aggregate layer. Figure 74 shows the layout of the EPCs and the locations of the settlement telltales in a plan view of the test box.

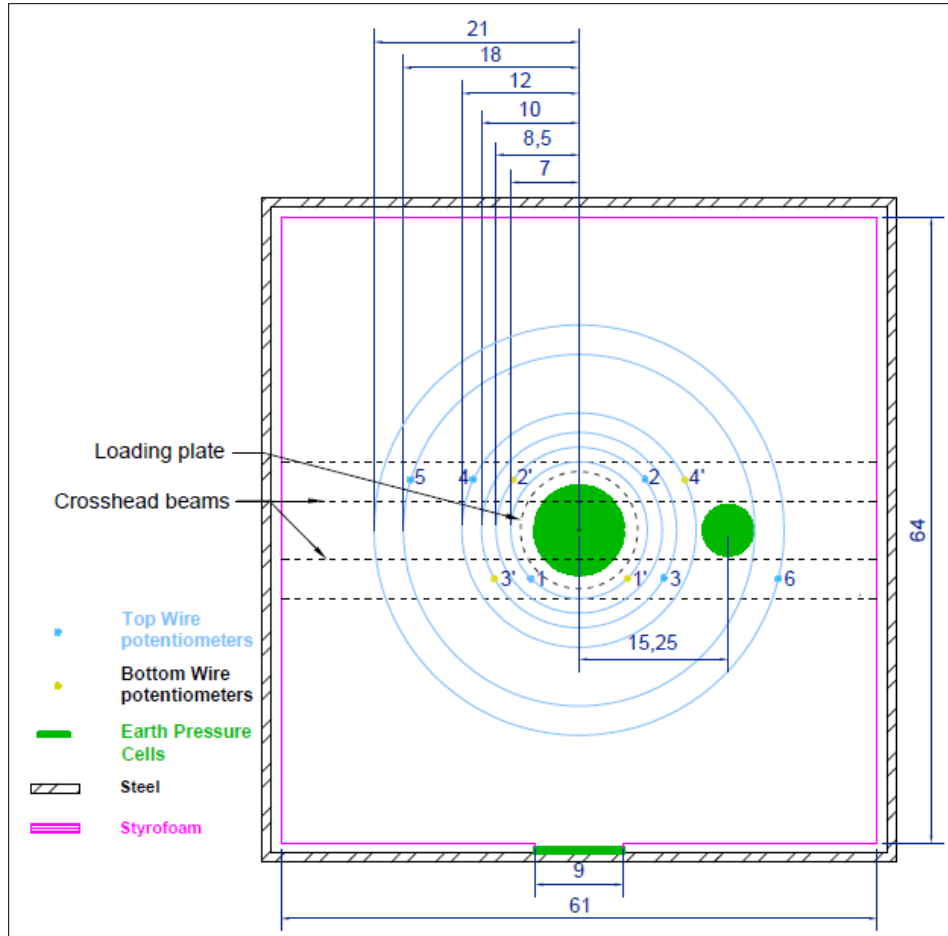


Figure 74. Instrumentation layout for the cyclic plate load tests (units: inches)

The magnitudes of the cyclic load applied to the circular plate and its settlement were recorded during the tests using the dynamic controller system software. Time-history responses of the ten WPs were recorded using the program LabVIEW 2010 on the Data Acquisition System (DAQ). A separate data acquisition system was used to collect the EPC data. That system consisted of a Geokon Model 8032 MICRO-1000 Data logger connected to a DAQ running a Multi-logger software program.

The maximum load applied by the actuator was 9 kips, which represents a loading pressure of 80 psi of dual wheels under an equivalent 18-kip single-axle load. The loading cycle started with a monotonic increase from the initial seating load of 0.5 kips to a final magnitude of 9 kips in 10 equal increments. Then, a 1 Hz force-controlled periodic load was applied, which consisted on a 0.1-sec loading period followed by a 0.9-sec resting period. The loading period varied between 0.5 kips and 9 kips for 1,000 load cycles (Figure 75).

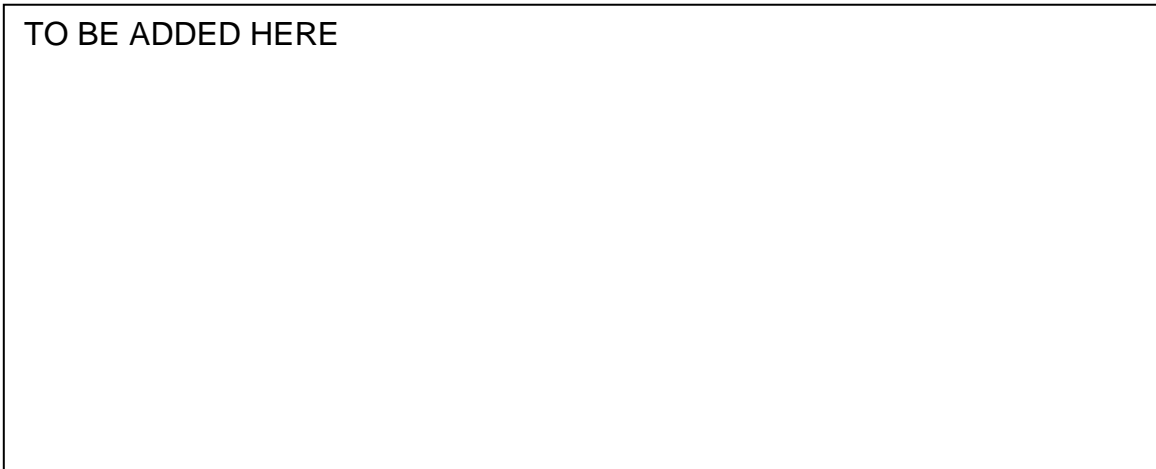


Figure 75. Load pulse applied in the cyclic plate load tests

Figure 76 and Figure 77 show the measured static and dynamic settlements of the plate load for the tests with Mirafi RS580i and RS380i geotextiles, respectively. It can be observed that the model with RS580i geotextile experienced a larger static settlement than the test with RS380i. However, the total settlements at the end of the test were very similar, indicating that the model with the stiffer RS580i geotextile experienced a larger dynamic settlement. The implication to design of this observation is in the calculation of Settlement

Reduction Factor (SRF) and Traffic Benefit Ratio (TBR) for each geosynthetic product (as presented later in this report) since these parameters are calculated using dynamic settlement.

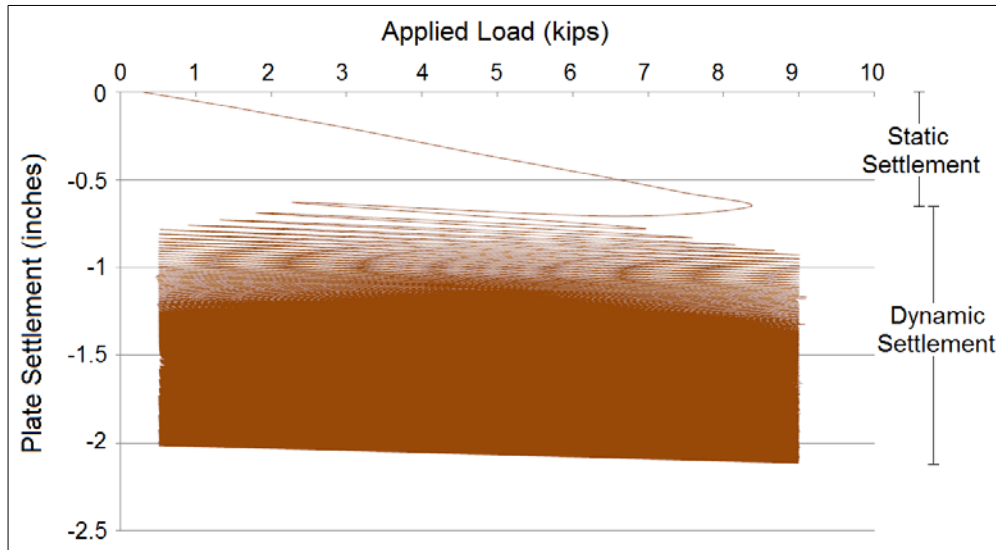


Figure 76. Plate load settlement response during cyclic plate load test on the model with Mirafi RS580i geotextile

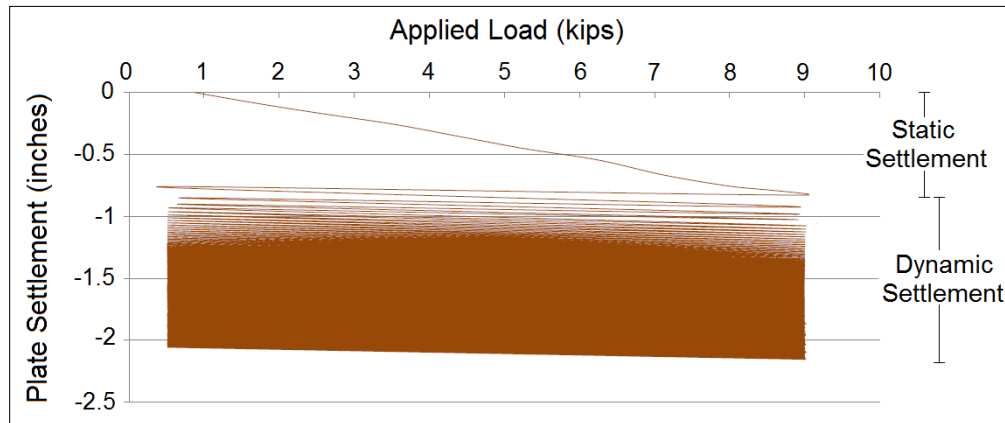


Figure 77. Plate load settlement response during cyclic plate load test on the model with Mirafi RS380i geotextile

Figure 78 and Figure 79 show cumulative total settlements after every 100 loading cycles for the cyclic plate load test on the model with Mirafi RS580i geotextile reinforcement. The figures show the cumulative total deflections obtained from wire potentiometers located at the top of the aggregate and the sand layer, respectively. Figure 80 and Figure 81 show the corresponding deflection results for the tests on the model with Mirafi RS380i geotextile reinforcement.

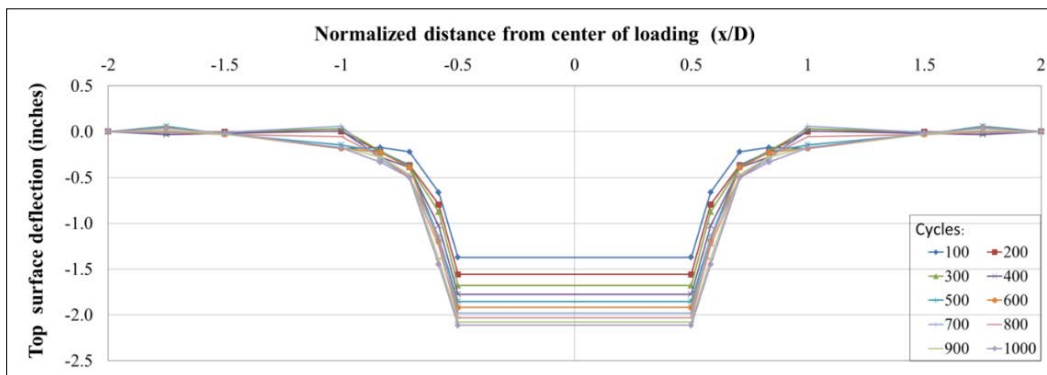


Figure 78. Total cumulative deflection at the top surface during cyclic plate load test using Mirafi RS580i geotextile

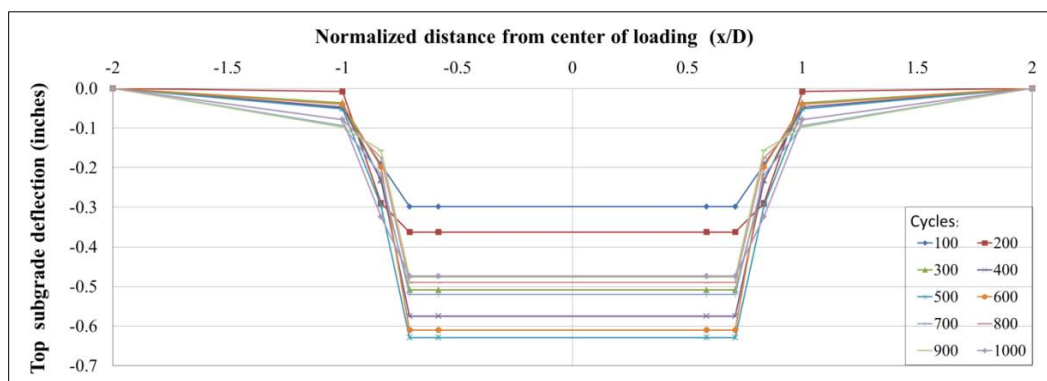


Figure 79. Total cumulative deflection at the top of subgrade during cyclic plate load test using Mirafi RS580i geotextile

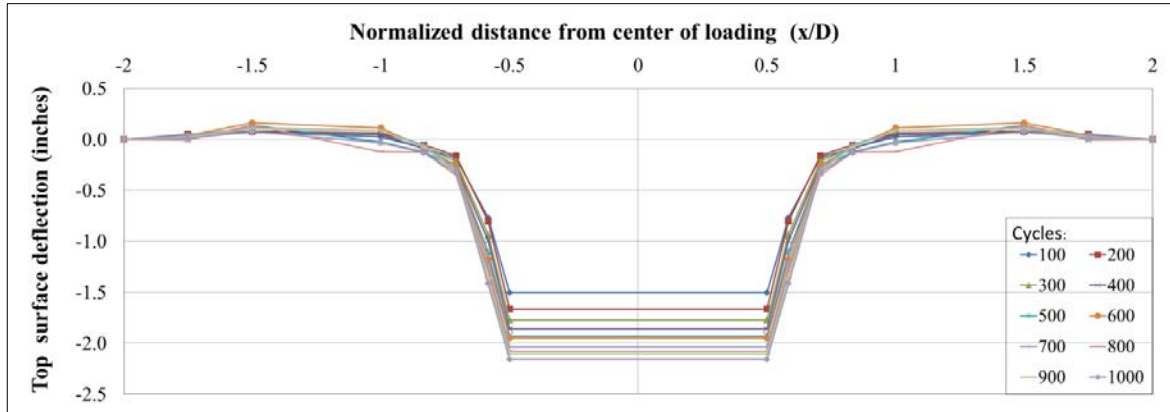


Figure 80. Total cumulative deflection at the top surface during cyclic plate load test using Mirafi RS380i geotextile

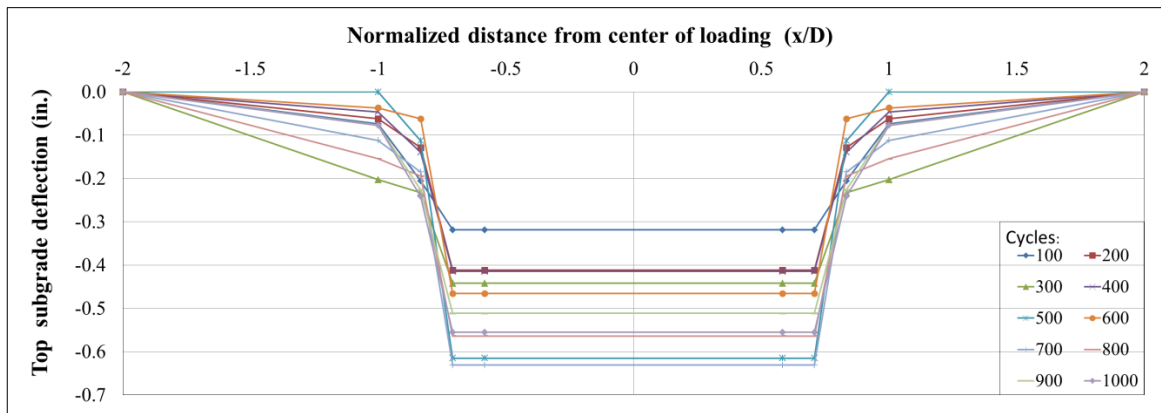


Figure 81. Total cumulative deflection at the top of subgrade during cyclic plate load test using Mirafi RS380i geotextile

Figure 82 shows a comparison of the aggregate surface deflections in cyclic plate load tests using Mirafi RS580i and Mirafi RS380i geotextiles. The results show that the maximum permanent deformation obtained after 1000 cycles in the test involving the RS380i geotextile with significantly lower tensile strength and modulus in the cross-machine direction was slightly larger than that in the test with the RS580i product (2.16 inches vs. 2.11 inches). Similarly, Figure 83 shows

a comparison of deflections at the top of the subgrade (sand) layer for these two cases. Similarly, this figure shows that the permanent deformation at the top of the subgrade after 1000 cycles in the test with RS380i geotextile is slightly larger than in the test with the RS580i product (0.63 inches vs. 0.61 inches). However, the observed differences noted above are too small to indicate a meaningful difference in the performances of the reinforcement products examined in the plate load tests.

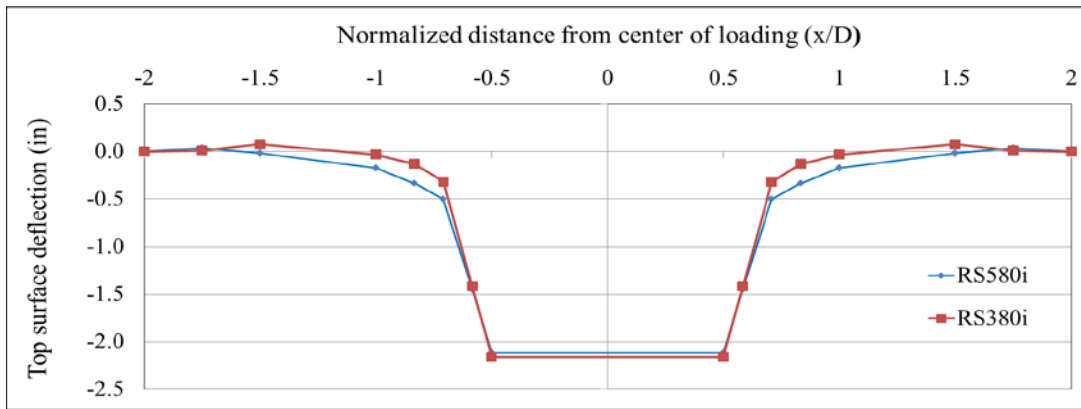


Figure 82. Comparison of top surface deflections between different cyclic plate load tests

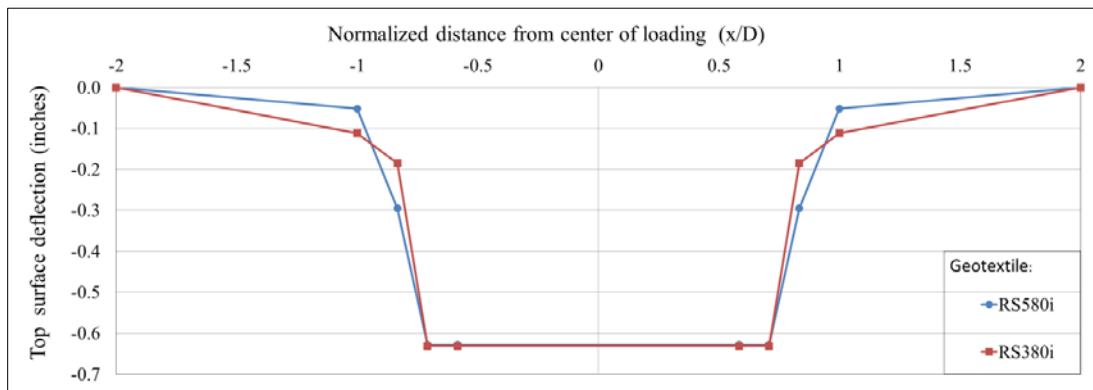


Figure 83. Comparison of subgrade deflections at the top between different cyclic plate load tests

The earth pressure results in the subgrade obtained during the cyclic plate load tests show that the subgrade under Mirafi RS580i geotextile was subjected to slightly lower pressure than the subgrade under Mirafi RS380i product (Table 38).

Taken together, results of the cyclic plate load tests in this study suggest that the mechanical properties of the geotextiles tested are not sufficiently different to influence the cyclic loading response of the reinforced models at the scale that they have been tested in the laboratory. Therefore, comparative testing at the field scale and using an actual subgrade soil would be necessary to detect any significant difference between the performances of these products in field applications.

Table 38. Maximum earth pressure measured at three different locations during cyclic plate load tests

| Geotextile tested | EPC (psi)  |                  |          |
|-------------------|------------|------------------|----------|
|                   | (1) Center | (2) Intermediate | (3) Wall |
| RS580i            | 31.59      | 4.43             | 1.92     |
| RS380i            | 33.73      | 4.34             | 1.84     |

The results of these geotextile-reinforced sections were compared with the results of nine earlier geogrid-reinforced sections and one unreinforced section reported by Hatami et al. (2012). The parameters compared among the twelve cyclic plate load tests included the settlement of the loading plate in addition to values of the Settlement Reduction Factor (SRF) and the Traffic Benefit Ratio (TBR) calculated for each case. The measured plate settlements show the

magnitude of permanent deformation of the unpaved sections at their surface after 1000 cycles of the 9-kip load. Figure 84 compares measured dynamic settlements in different test cases. Static settlement is the permanent deformation of the aggregate surface at the end of the 9-kip load, which was gradually reached in increments of 0.9 kip per second as shown in Figure 75. On the other hand, dynamic settlement shown in Figure 75 through Figure 77 is the total deformation at the end of the test produced by a cyclic loading repetition between 0.5 and 9 kips in excess of the initial static value.

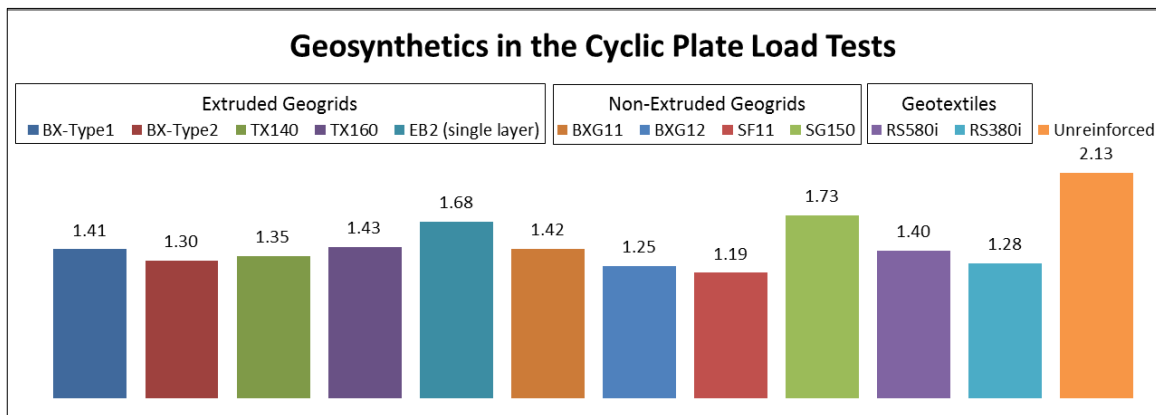


Figure 84. Dynamic settlement of the loading plate as measured in different cyclic plate load tests (inches)

The Settlement Reduction Factor (SRF) is defined as the ratio of the settlement of an unreinforced aggregate base test model ( $S_{UR}$ ) to that of an otherwise identical reinforced model ( $S_R$ ) for a given applied load (Christopher et al. 2010). As was noted earlier, the dynamic portion of the settlement was used to calculate the SRF values shown in Figure 85 and Figure 77. Figure 85 compares the SRF

values for all laboratory models tested in the authors' current and recent studies in which a geosynthetic reinforcement layer was placed at the base/substrate interface.

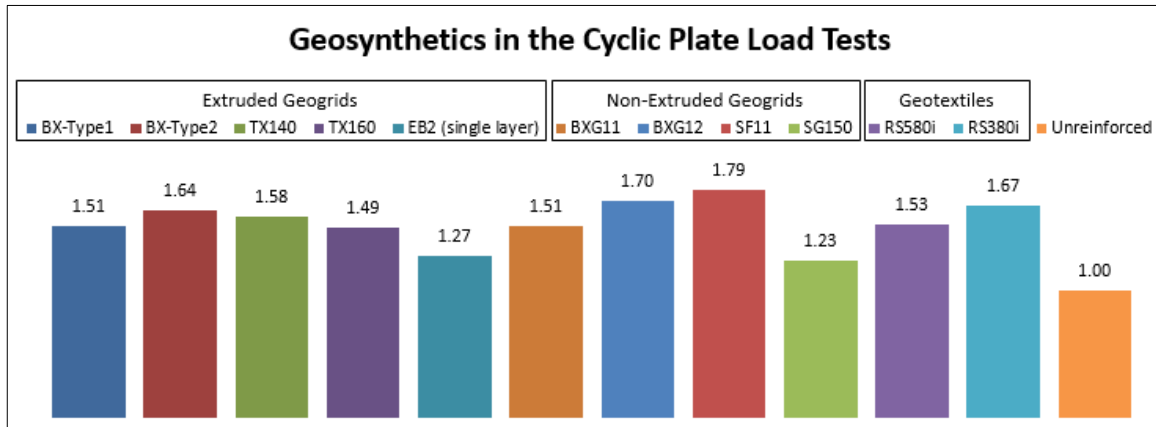


Figure 85. Dynamic Settlement Reduction Factors (SRF) from different cyclic plate load tests

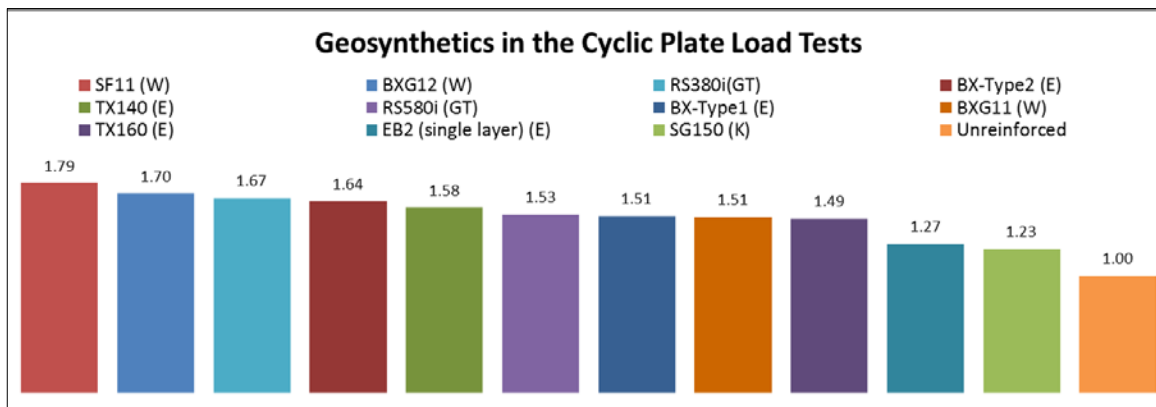


Figure 86. Dynamic settlement performance of different test models sorted according to their SRF values (W: woven geogrid, E: extruded geogrid, K: knitted geogrid, GT: geotextile)

The traffic benefit ratio (TBR) is defined as the number of load cycles carried by a reinforced section at a specific rut depth (1 inch of dynamic settlement for this study) divided by that of an equivalent unreinforced section (Christopher et al. 2010). The TBR values for different laboratory models were calculated to

evaluate the comparative benefit and performance of different geosynthetic products for base reinforcement. The TBR results for unreinforced and geosynthetic-reinforced pavement sections are summarized in Figure 87.

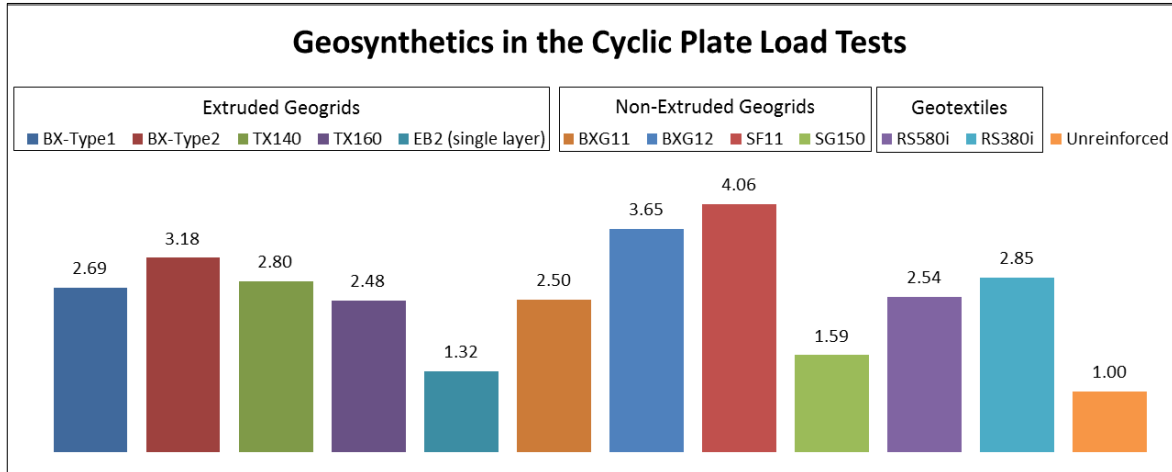


Figure 87. Traffic Benefit Ratio (TBR) on different cyclic plate load tests

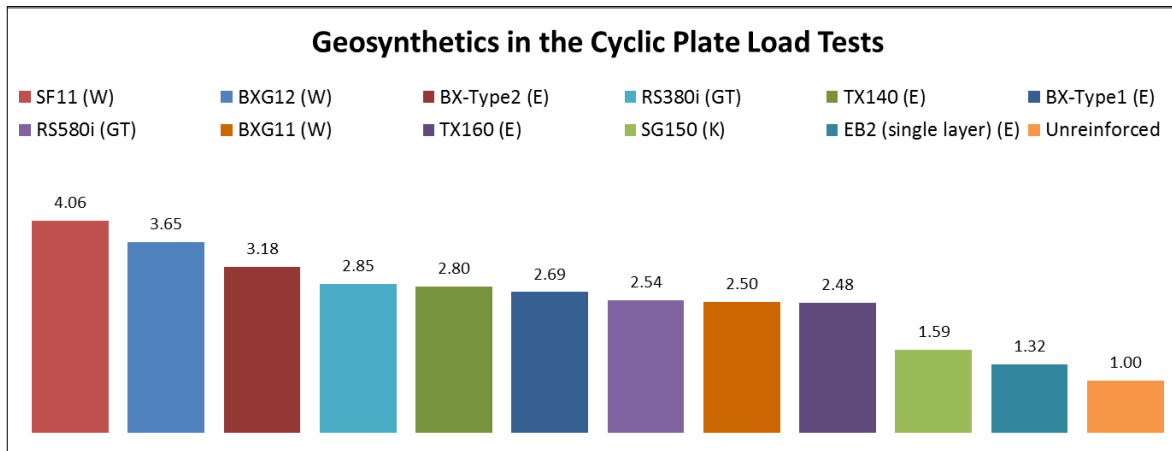


Figure 88. Traffic Benefit Ratio from high to low (W: woven geogrid, E: extruded geogrid, K: knitted geogrid, GT: geotextile)

A comparison of different geogrids and geotextiles in-aggregate performance based on the results of the cyclic plate load tests leads to the following observations:

- The measured permanent deformations of the aggregate surface (i.e. between 1.3 and 1.5 inches) for the two geotextiles examined (i.e. RS380i and RS580i) are comparable to those obtained for models constructed with the triaxial geogrids (TX140 and TX160) and the ODOT Type-1 and Type-2 geogrids (BX1200 and BX1100, respectively). This conclusion is also supported by the corresponding products SRF and TRB values, which were calculated using dynamic settlement. Nevertheless, the woven geogrids BXG12 and SF11 showed the best performance in terms of their SRF and TBR ratios.
- In comparing the observed performance of different geosynthetic products in Figures X and Y, it is important to note that the cyclic plate load tests reinforced with geogrid products included a geotextile separator between the sand substrate and the aggregate layer. However, in models reinforced with geotextiles, these products were used as both the reinforcement and the separator between the sand and the aggregate layers.
- A comparison of the TBR and SRF values for the models using the RS350i and RS580i geotextiles indicates that larger tensile strength and stiffness properties of the latter product resulted in slightly better performance in the corresponding model under cyclic plate loading.

However, the extent of this difference in actual field performance needs to be quantified using the field test data in the continuation of this study (Section 2.2).

## 7. Overall Summary of Work Performed

- A comprehensive literature survey was carried out on the related field and laboratory studies to investigate the performance of geosynthetic reinforcement products for base reinforcement and subgrade stabilization applications.
- In order to select a suitable site for a roadway test section, a detailed survey was carried out on the network of roads and highways in several counties in Central Oklahoma. A list of possible roads was prepared based on their corresponding AADT and truck traffic data.
- A candidate test section was eventually identified in collaboration with a local company (Dolese Brothers, Co.) which provides the following major advantages:
  1. It is heavily trafficked by loaded trucks returning from a sand plant. Therefore, the test section will be subjected to traffic load that would more closely resemble the actual design condition.
  2. The traffic data (including representative weights of the trucks using the road) can be evaluated/estimated readily with reasonable accuracy.
  3. Since the test section will be subjected to frequent truck load which is fairly uniform (i.e. loaded trucks), it provides uniformity and an ideal loading condition (as much as practically and

realistically possible) to study the performance of the test section in the field.

4. It provides a “best of both worlds” condition in the sense that, frequent and heavy load applied on the test section facilitates and expedites the occurrence and development of signs of distress and rutting during the period of time that is available to this study (e.g. 1.5 - 2 years). At the same time, due to the nature of the road (which is a haul/access road in a sand plant), the occurrence of this distress and rutting does not hinder the performance and serviceability of the road as opposed to e.g., a city street or a major highway.
5. The construction of the test section will not face planning challenges such as traffic control and requirements for coordination and approvals from different authorities as would be the case for city streets and major highways.
6. The test section with the advantages noted above provides an ideal “outdoor laboratory model” which is constructed as an actual field project (i.e. by a local contractor using field equipment and techniques) and hence represents a field roadway. At the same time, it provides us with a significant degree of uniformity with respect to the traffic load, subgrade condition, base course aggregate and climatic conditions. These advantages help to increase the reliability and facilitate the

interpretation of the test results. Furthermore, these controlled test conditions and reliable results will be desirable for the development and validation of analytical and numerical models which are essential for the development of mechanistic-empirical design methodologies that would be compatible with current design methods (e.g. AASHTO 2002).

- A layout and instrumentation plan was prepared for the full-scale test section
- Geosynthetic reinforcement products to be used in the study were shortlisted based on a survey of their material properties from the suppliers and in-house laboratory tests and considering the latest developments in the industry
- Thirty two (32) tensile strength tests were carried out on two new base course reinforcement geotextiles (i.e. Mirafi RS380i and RS580i) in both machine (MD) and cross-machine (XD) directions to compare their performance against those of geogrids examined in an earlier study by the authors.
- A Los Angeles Abrasion test was performed to examine the durability of the ODOT Type-A aggregate for this study.

- A verification pullout test was carried out on the TX1600 geogrid product in ODOT Type-A aggregate which showed a close agreement with the data obtained in an earlier study by the authors.
- Two (2) large-scale cyclic plate load tests were carried out on geotextile reinforced base-substrate systems. The test results were analyzed and compared against the data obtained from similar tests on a selection of geogrid products for base reinforcement in an earlier study by the authors.

## References

- Abaza, K. A. and Abu-Eisheh, S. A. (2003) An Optimum Design Approach for Flexible Pavements, *International Journal of Pavement Engineering*, 4:1, 1-11, DOI: 10.1080/1029843031000087464
- Abu-Farsakh and Chen (2010). "Evaluation of the Base/Subgrade Soil under Repeated Loading: Phase II– In-Box and ALF Cyclic Plate Load Tests", Louisiana Transportation Research Center, Final Report – Phase II, June 2010.
- American Association of State Highway and Transportation Officials (1993). "AASHTO Guide for Design of Pavement Structures", Washington, D.C.
- American Association of State Highway and Transportation Officials (2008), "AASHTO Manual of Practice", Mechanistic–Empirical Pavement Design Guide, Interim Edition, Washington, D.C.
- AASHTO Standard Specifications for Transportation Material and Methods of Sampling and Testing (2002), American Association of State Highways and Transportation Officials, Washington, D.C.
- AASHTO Guide for Design of Pavement Structures (1993), Guide for Design of Pavement Structures, American Association of State Highway and Transportation Officials, Volumen 1
- Al-Qadi I. L. and Appea A. K. (2003). "Eight-Year of Field Performance of A Secondary Road Incorporating Geosynthetics at The Subgrade-Base Interface", Transportation Research Board 82nd Annual Meeting January 12-16, 2003, Washington, D.C
- Al-Qadi, I. L., Dessouky, S. H., Kwon, J. and Tutumluer, E. (2008). "Geogrid in Flexible Pavements: Validated Mechanism", *Transportation Research Record: Journal of the Transportation Research Board*, Vol. 2045, No. 12, pp. 102-109.
- ASTM Annual Book of Standards, Road and Paving Materials; Vehicle Pavement Systems (1999), American Society of Testing Materials, Vol, 04.03, West Conshohsken, PA, 1999.

- ASTM (2009) " Standard Test Method for: Tensile Properties of Geotextiles by the Wide-Width Strip Method.", ASTM International, 100 Barr Harbor Drive, PO Box C700, West Conshohocken, PA 19428-2959, United States, 2009.
- Black P. J. and Holtz R. D. (1999). "Performance of Geotextile Separators Five Years After Installation", Journal of Geotechnical and Geoenvironmental Engineering, Vol. 125, No. 5, May, 1999.
- Berg, R.R., Christopher, B.R., and Perkins, S. (2000). "Geosynthetic Reinforcement of the Aggregate Base/Subbase Courses of Pavement Structures". Geosynthetic Materials Association, Roseville, MN.
- Breidy M. H. (2011). "Development of a Field-Based Fatigue Transfer Function for a Flexible Pavement Section on I-35 in Oklahoma", Thesis (M.S.)- University of Oklahoma
- Chehab, G.R., Palomino, A.M., Tang, X. (2007). "Lab evaluation and specification development for geogrids for highway engineering applications", FHWA-PA-2007-009-050110, Pennsylvania Transportation Institute, University Park, PA.
- Cuelho, E. and Perkins, S. (2009). "Field investigation of geosynthetics used for subgrade stabilization", Report No. FHWA/MT-09-0003/8193, Montana Department of Transportation, July 2009.
- Gabr, M. (2001). "Cyclic plate loading tests on geogrid reinforced roads." Research Rep. to Tensar Earth Technologies, Inc., NC State Univ.
- Giroud, J. P. and Han, J. (2004.a). "Design method for geogrid-reinforced unpaved roads. I: Development of design method." J. Geotech. Geoenviron. Eng., 130(8), 775–786.
- Giroud, J. P. and Han, J. (2004.b). "Design Method for Geogrid-Reinforced Unpaved Roads. II. Calibration and Applications." J. Geotech. Geoenviron. Eng., 130(8), 787–797.
- Giroud, J. P., and Noiray, L. (1981). "Geotextile-reinforced unpaved road design." J. Geotech. Eng., 107(9), 1233–1254.
- Haas R., Wall, J., and Carroll, R.G. (1988) "Geogrid Reinforcement of Granular Bases in Flexible Pavements," Transportation Research Record 1188, TRB, National Research Council, Washington DC, USA, pp. 19-27.).

- Hammitt, G. M. (1970). "Thickness requirement for unsurfaced roads and airfields, bare base support", Project 3782-65. Technical Rep. S-70-5, U.S. Army Engineer Waterways Experiment Station, CE, Vicksburg, Miss.
- Hanes Geo (2008), "Basic Design Approach for Geogrid Base Reinforcement." Hanes Geo Components, Winston-Salem, North Carolina.
- Hatami, K., Mahmood, T., Ghabchi, R. and Zaman, M. (2013). "Influence of Isolation Properties of Geogrids on Their Pullout Performance in a Dense Graded Aggregate". Invited Paper. Indian Geotechnical Journal, Special Issue on Geosynthetic Engineering.
- Hatami, K., Mahmood, T., Zaman, M. and Ghabchi, R. (2012). "Development of ODOT Guidelines for the Use of Geogrids in Aggregate Bases", FINAL REPORT No. FHWAOK-12-04, ODOT SP&R Item 2220, May 2012.
- Henry, K. S., Cortez, E. R., Danyluk, L. S., Brentrup, G., Lamie, N. and Arnold, T. W. (2008). "Construction and Instrumentation of Full-Scale Geogrid Reinforced Pavement Test Sections", ERDC/CRREL TR-08-6, Cold Regions Research and Engineering Laboratory, U.S. Army Engineer Research and Development Center, Hanover, NH.
- IFAI (2013), "2013 Geosynthetics Specifier's Guide" Industrial Fabrics Association International.
- Janoo, V. (1999). "Use of Inductive Coils to Measure Dynamic and Permanent Pavement Strains", U.S. Army Cold Regions Laboratory, Hanover, NH 03755.
- Jersey, S. R., Tingle, J. S., Norwood, G. J., Kwon, J. and Wayne, M. (2012). "Full-Scale Evaluation of Geogrid-Reinforced Thin Flexible Pavements", Journal of the Transportation Research Board No. 2310, Transportation Research Board of the National Academies, Washington D.C., 2012, pp. 61–71.
- Jewell, R.A., Milligan, G.W.E., Sarsby, R.W., and Dubois, D. (1984). "Interaction between soil and geogrids", Proceedings of the Conference on Polymer Grid Reinforcement in Civil Engineering, Thomas Telford Publishing, London: 18–30.
- Kazemian, S., Barghchi, M., Prasad, A., Maydi, H. and Huat, B. B. K. (2010). "Reinforced Pavement above Trench under Urban Traffic Load: Case Study

and Finite Element (FE) Analysis”, *Scientific Research and Essays* Vol. 5, No. 21, pp. 3313-3329.

Kazmee, H.A. (2010). “Effect of gradation on stiffness and flow behavior of aggregate bases: a laboratory and field study”, M.Sc. Thesis, The University of Oklahoma, Norman, OK

ODOT (2009), "2009 Standard Specification for Highway Construction," Oklahoma Department of Transportation, Section 700: Materials, 2009.

Oh, J. H. (2011). “Investigation of Geogrid-Reinforced Flexible Pavement Performance over Expansive Clay.” *Journal of the Korea Society of Hazard Mitigation*, pp. 109-115

Subaramaniam, P. (2011). “Reliability Based Analysis of Slope, Foundation, and Retaining Wall Using Finite Element Method”, Master Thesis, Department of Civil Engineering, National Institute of Technology, Rourkela, June.

Tingle, J. S. and Jersey, S. R. (2009). “Full-Scale Evaluation of Geosynthetic-Reinforced Aggregate Roads” *Transportation Research Record 2116*, Transportation Research Board of the National Academies, Washington D.C., 2009, pp. 96–107.

Tutumluer, E. and Al-Qadi, I. (2009). “Pavement Base Reinforcement with Geogrids-Modeling the Aggregate Interlock Mechanism”, *Geo-Strata*, Geo Institute of ASCE, Vol. 13, No. 3, May/June 2009, pp. 28-30.

United States Department of Agriculture, Natural Resources Conservation Services, “Web Soil Survey”, <http://websoilsurvey.nrcs.usda.gov/app/WebSoilSurvey.aspx>

U.S. Army Corps of Engineers Engineering Technical Letter 1110-1-189 (2003). “Use of Geogrids in Pavement Construction”, U.S. Army Corps of Engineers, Headquarters, Washington, D.C.

Wang, Z. (2009). “Influence of geogrids junction strength on the performance of reinforced aggregate base”, *M.Sc. Thesis*, The University of Oklahoma, Norman, OK.

Warren, K., Brooks, J., and Howard, I. (2008). “Survivability of Foil Strain Gages Mounted on Geosynthetics Under Full-Scale Construction Loads”. *Geosynthetics Research and Development in Progress*: pp. 1-6

Wu, Z. (2013). "Structural Performance of Thin Asphalt Pavement Under Accelerated Pavement Testing", *Pavement and Geotechnical Engineering for Transportation*, pp. 1-18.

Yu, J. (2000). "Flexible Reinforced Pavement Structure - Sensitivity Analysis", A Thesis Submitted to the College of Graduate Studies and Research, University of Windsor, Windsor, ON, Canada.

## **Appendix A**

Database of ODOT latest AADT maps for Central Oklahoma

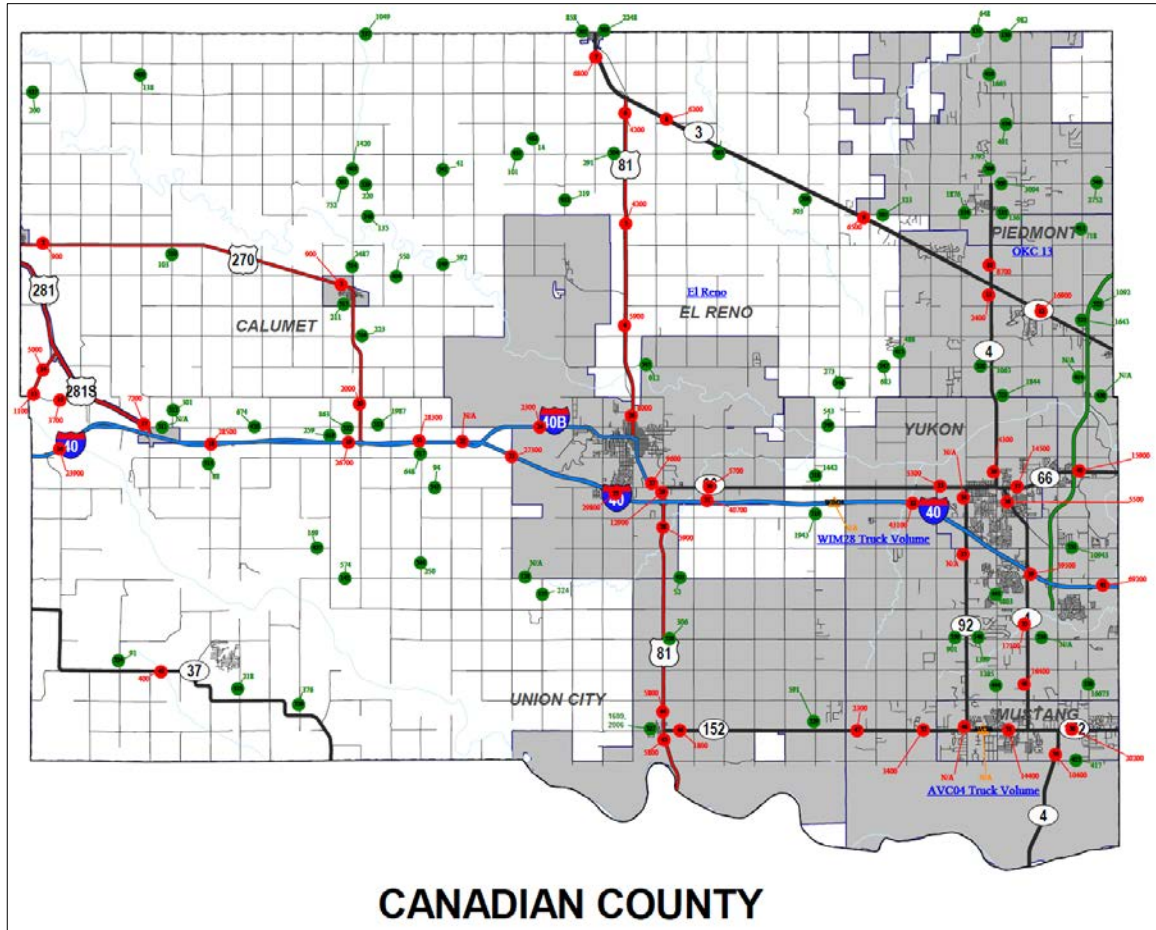


Figure 89. AADT data for Canadian County (2011)

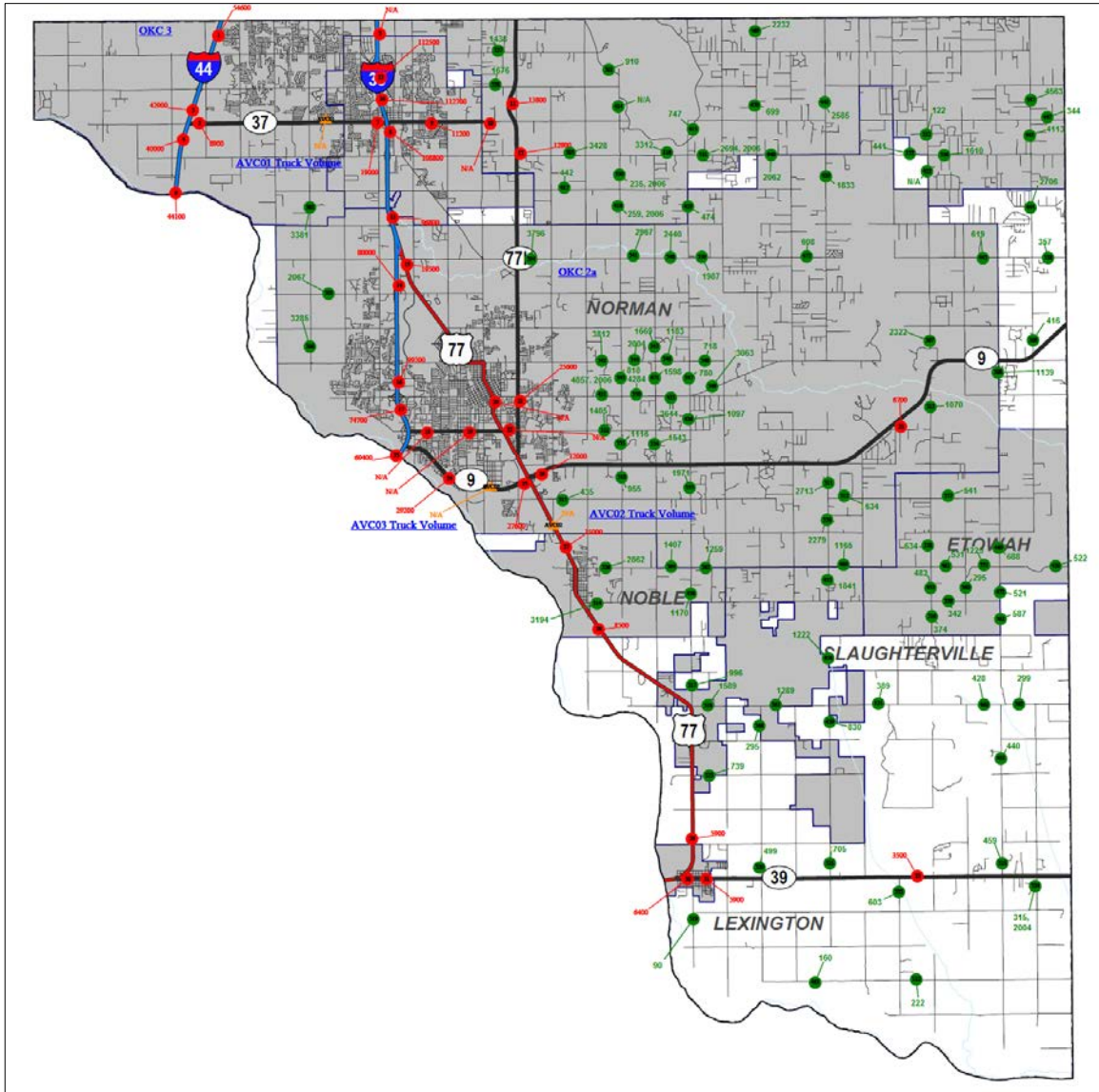


Figure 90. AADT data for Cleveland County (2010)

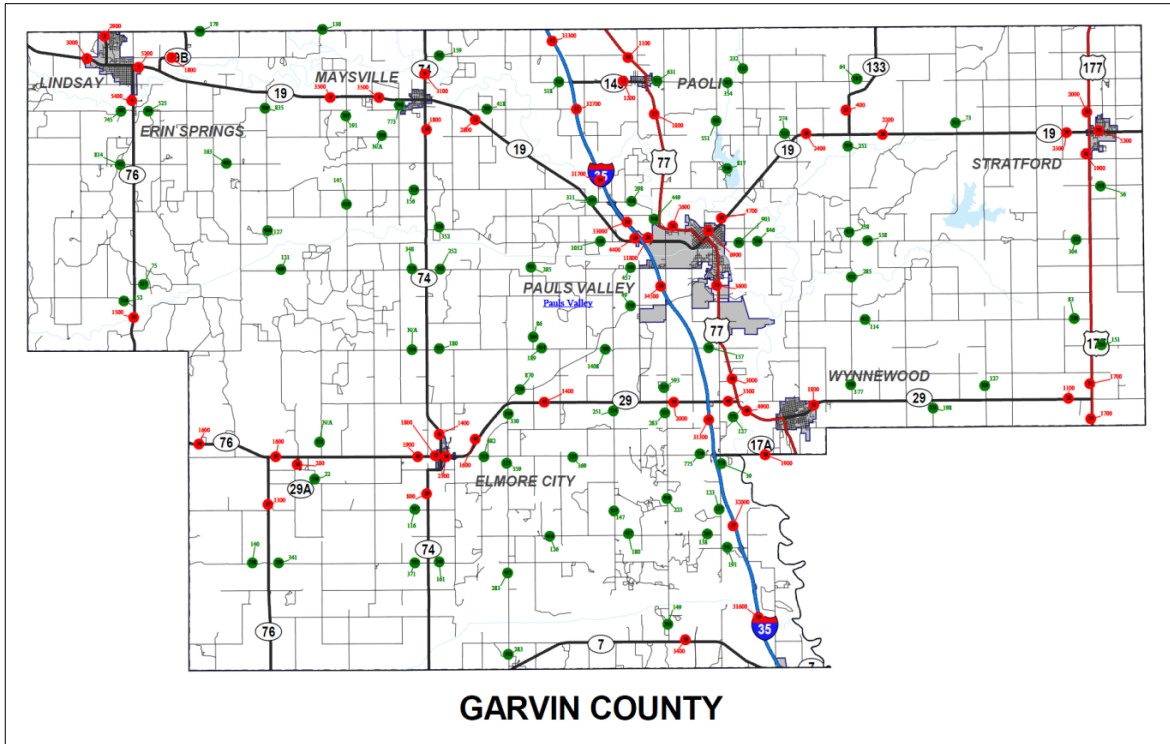


Figure 91. AADT data for Garvin County (2011)

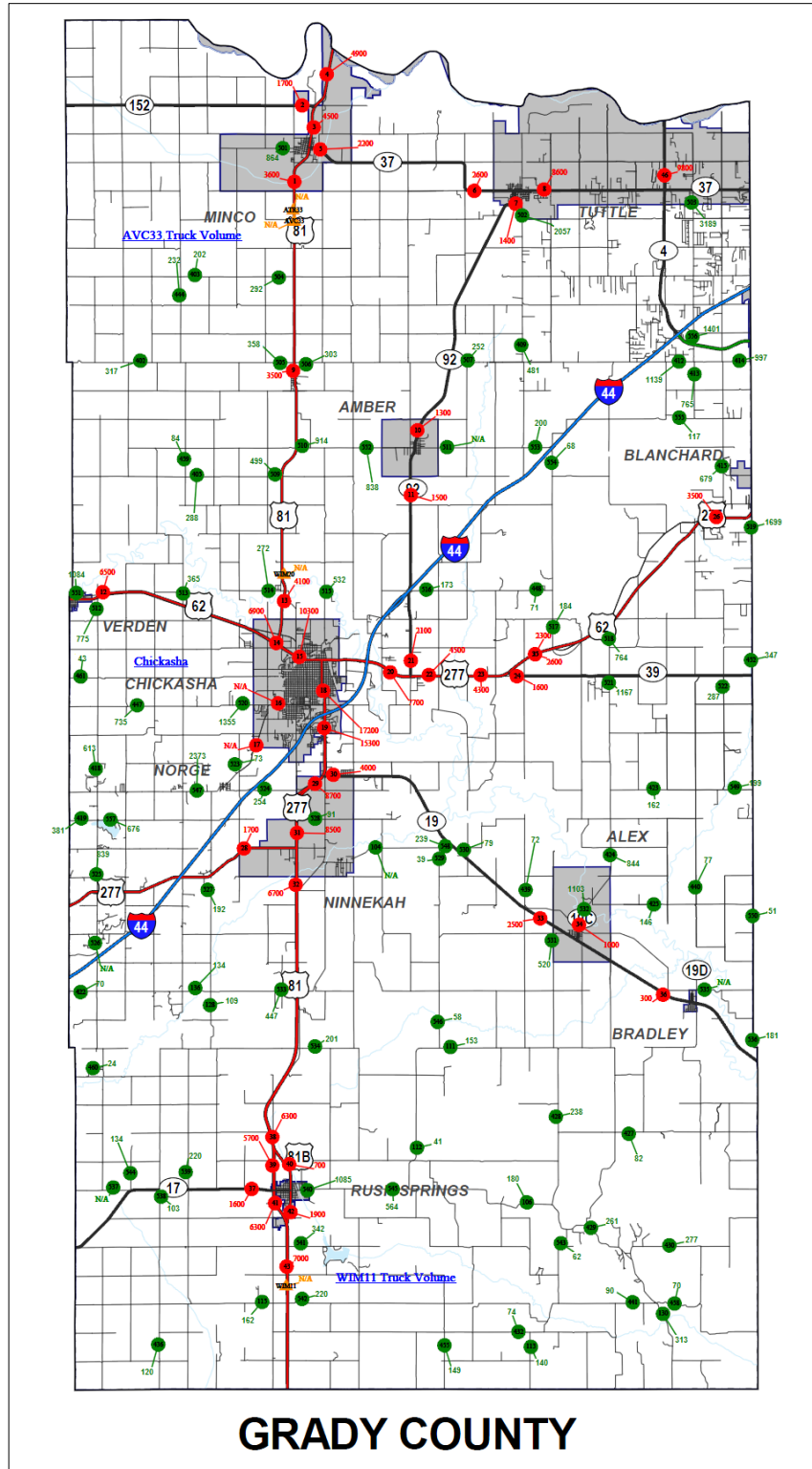
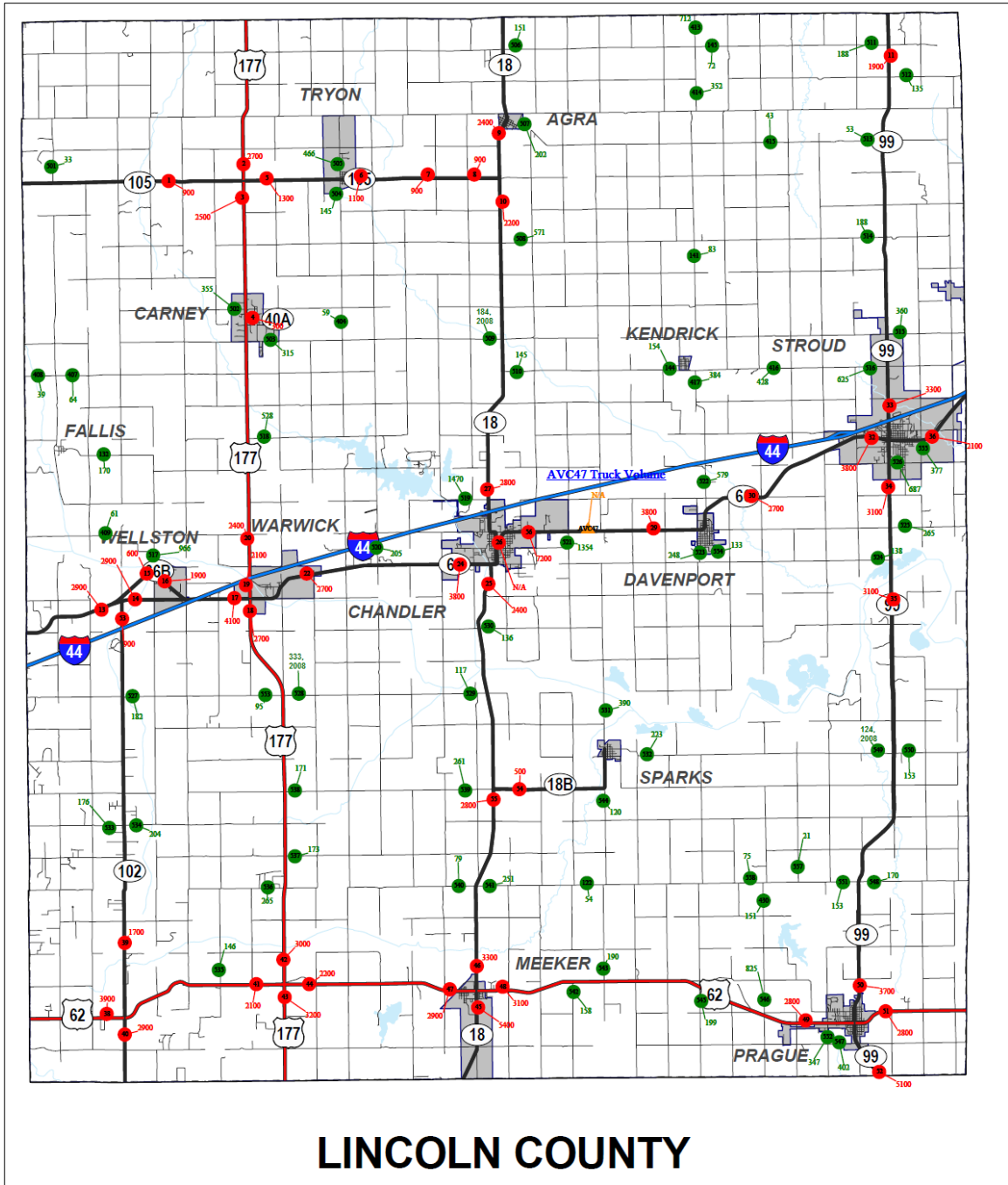


Figure 92. AADT data for Grady County (2010)



# LINCOLN COUNTY

Figure 93. AADT data for Lincoln County (2011)

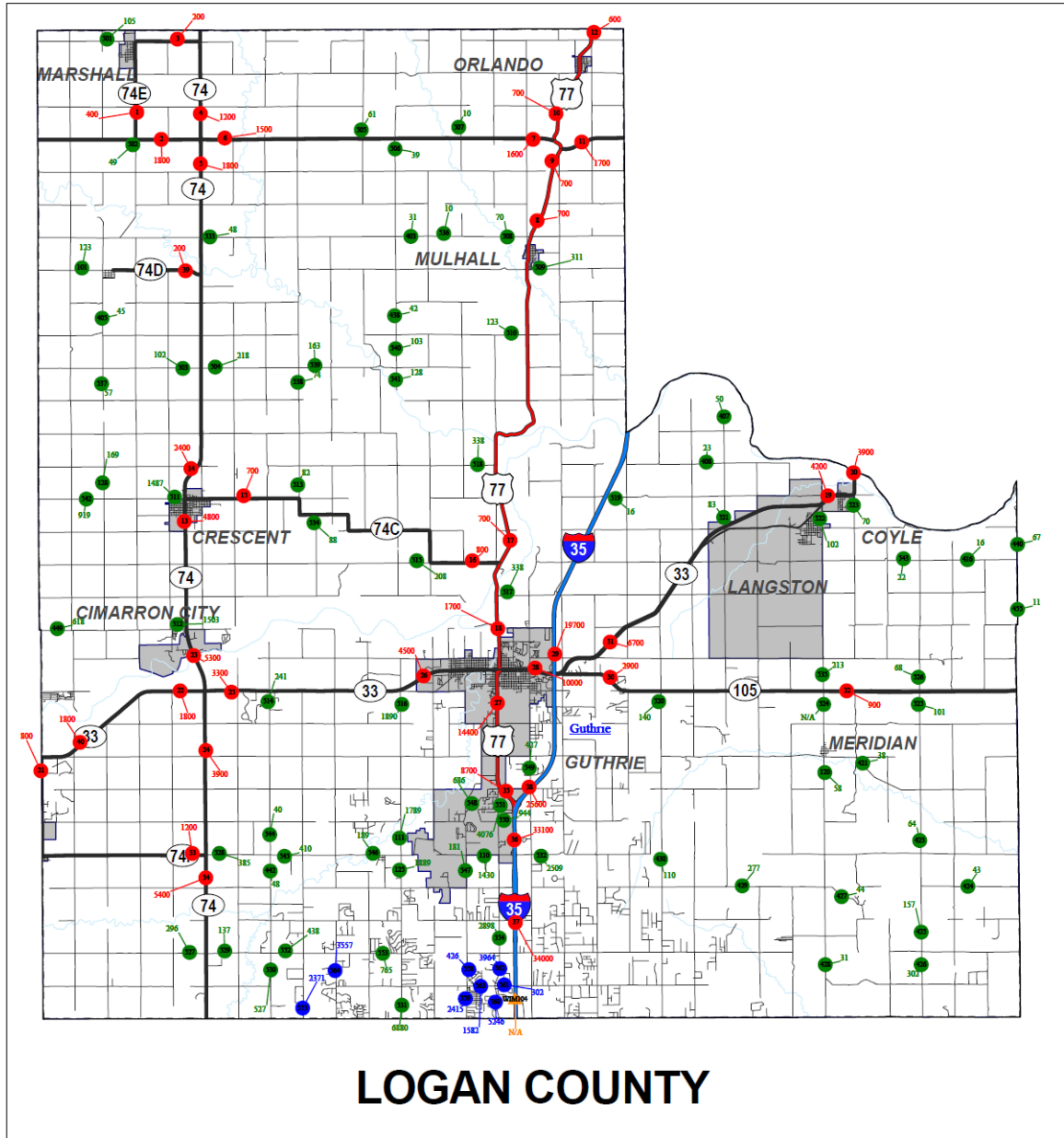


Figure 94. AADT data for Logan County (2011)

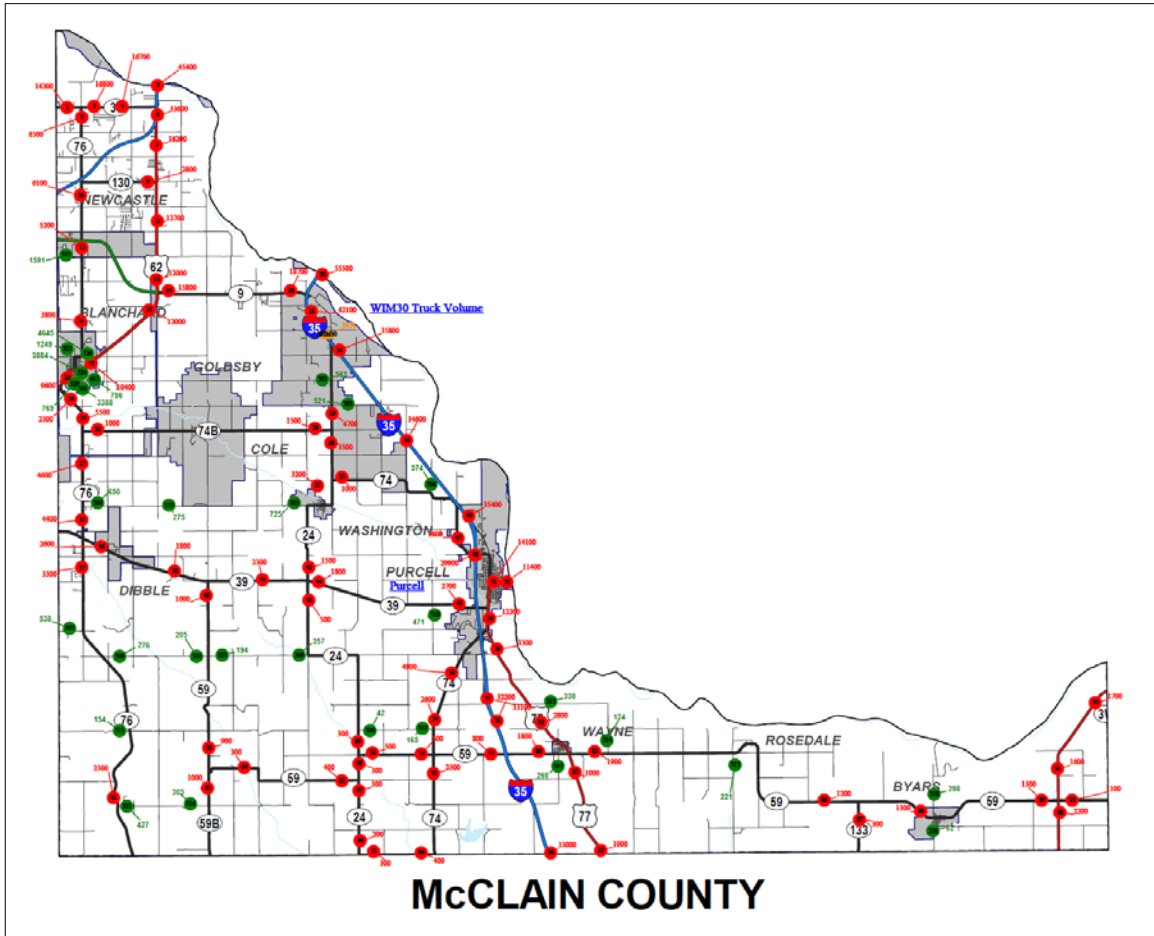


Figure 95. AADT data for McClain County (2007)

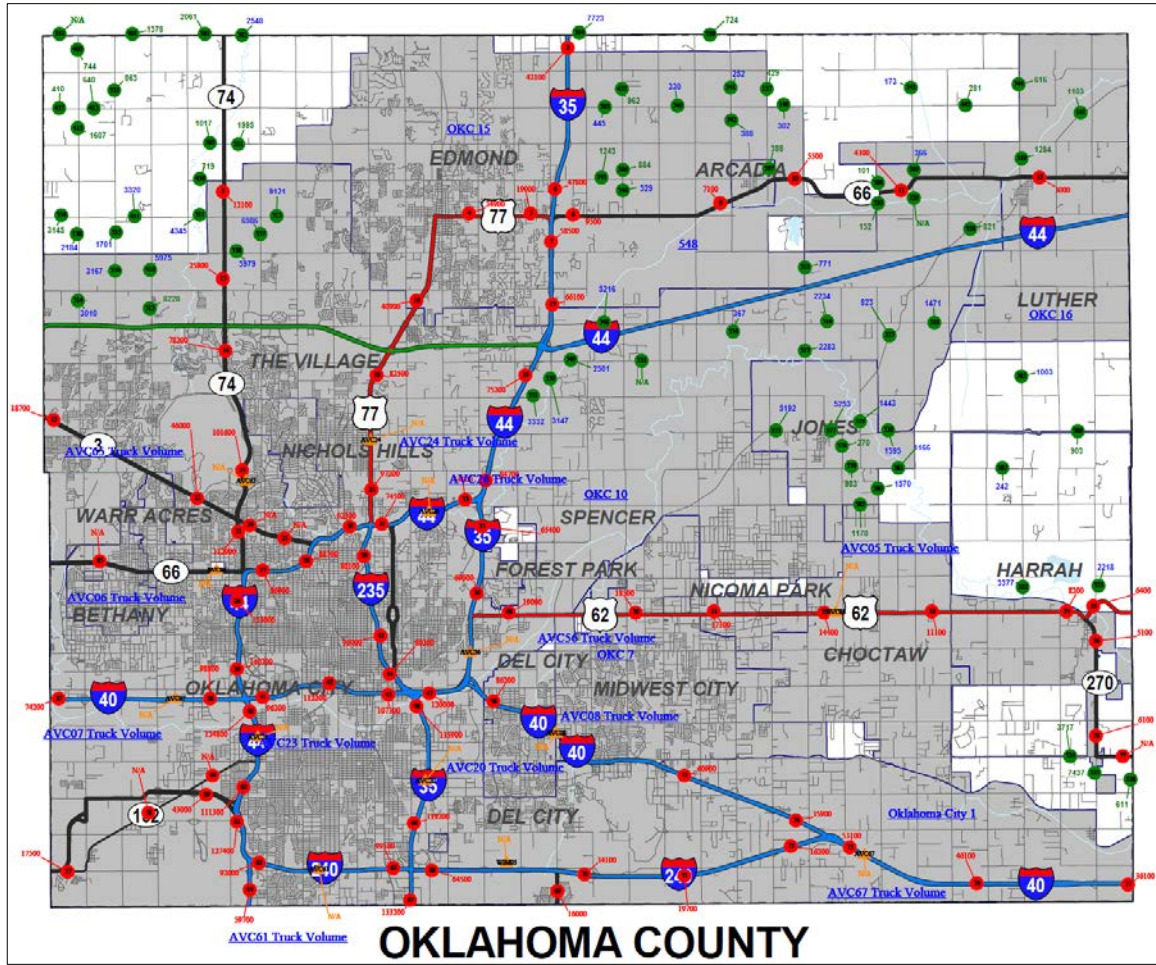


Figure 96. AADT data for Oklahoma County (2006-2010)

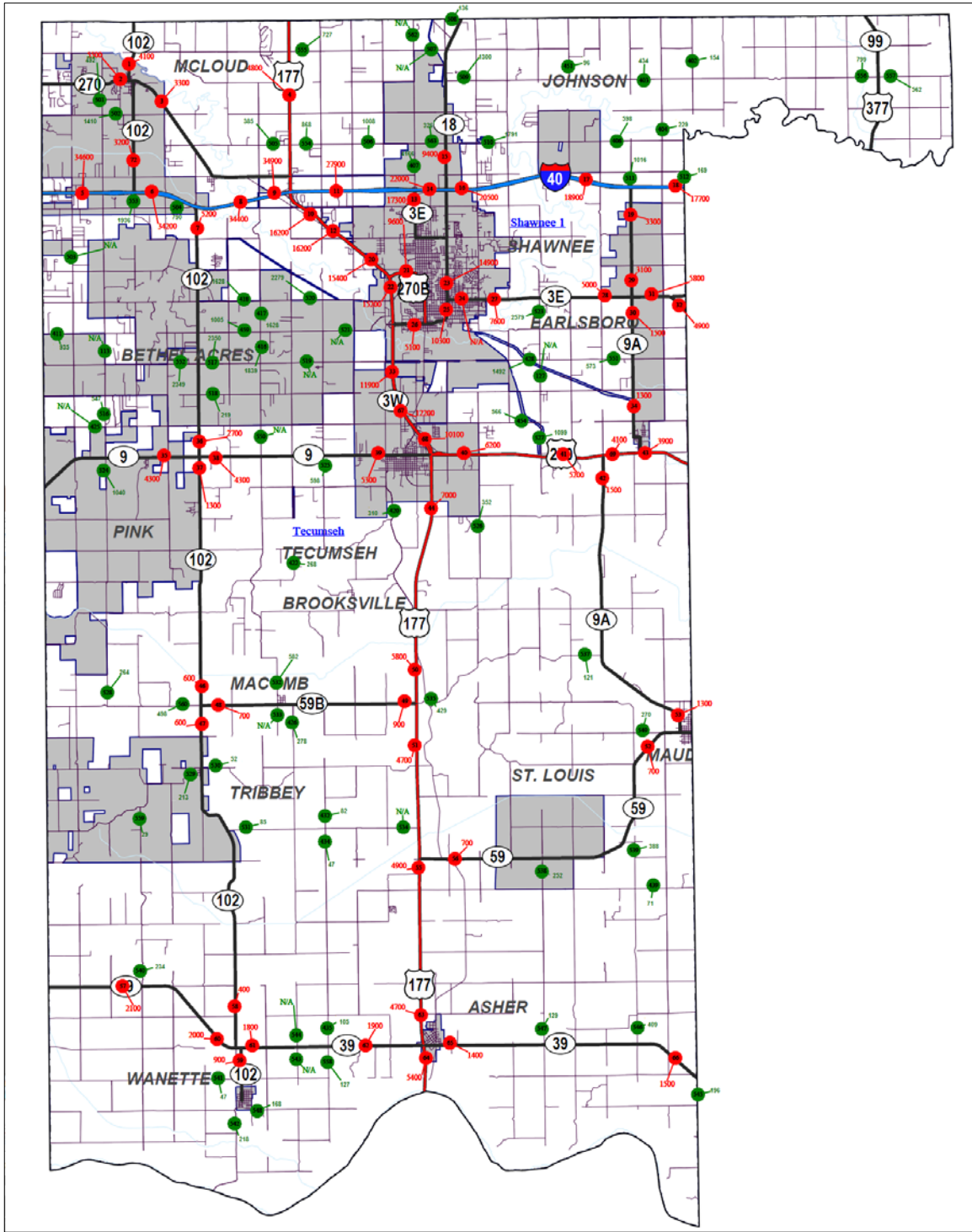


Figure 97. ADT data for Pottawatomie County (2007)

## **Appendix B**

Count sites with maximum AADT for different counties in Oklahoma

(Reduced data)

Table 39. Identification of the maximum AADT per county

| ODOT Divisions | County       | Count Site Number | Location   | Year (Latest) | AADT (Maximum) |
|----------------|--------------|-------------------|--|---------------|----------------|
| 1              | Wagoner      | 510               | .3 miles north of E/W 101                            | 2009          | 5451           |
|                | Cherokee     | 538               |  | 2010          | 3076           |
|                | Adair        | 506               |  | 2010          | 1465           |
|                | Okmulgee     | 404               |  | 2008          | 3206           |
|                | Muskogee     | 525               |  | 2010          | 2611           |
|                | Sequoyah     | 524               |  | 2011          | 4468           |
|                | McIntosh     | 519               |  | 2011          | 3346           |
|                | Haskell      | 504               |  | 2008          | 2142           |
| 2              | Pittsburgh   | 114               | .3 miles south of SH 28                              | 2006          | 2991           |
|                | Latimer      | 523               |  | 2011          | 1800           |
|                | Le Flore     | 523               |  | 2006          | 2630           |
|                | Atoka        | 533               |  | 2006          | 1800           |
|                | Pushmataha   | 516               |  | 2011          | 1242           |
|                | McCurtain    | 518               |  | 2010          | 2998           |
|                | Choctaw      | 511               |  | 2010          | 764            |
|                | Bryan        | 515               |  | 2010          | 2343           |
|                | Marshall     | 518               |  | 2006          | 2811           |
| 3              | Lincoln      | 519               | .3 miles east of N/S 375<br>.3 miles north of EW 113 | 2011          | 1470           |
|                | Okfuskee     | 519               |  | 2011          | 1286           |
|                | Cleveland    | 537               |  | 2010          | 4563           |
|                | Pottawatomie | 407               |  | 2007          | 4166           |
|                | Seminole     | 422               |  | 2008          | 1827           |
|                | Hughes       | 410               | .5 miles north of EW 157                             | 2010          | 839            |
|                | McClain      | 526               |  | 2007          | 4645           |
|                | Garvin       | 560               |  | 2011          | 1408           |
|                | Pontotoc     | 550               |  | 2011          | 4669           |
|                | Coal         | 512               |  | 2011          | 604            |
|                | Johnston     | 516               |  | 2010          | 631            |
| 4              | Grant        | 528               | .5 west of 74 F<br>.5 south of EW 96                 | 2006          | 1062           |
|                | Kay          | 539               |  | 2010          | 2435           |
|                | Garfield     | 524               |  | 2010          | 2381           |
|                | Noble        | 413               |  | 2007          | 546            |
|                | Kingfisher   | 532               |  | 2011          | 1744           |
|                | Logan        | 531               |  | 2011          | 6880           |
|                | Payne        | 511               |  | 2010          | 2416           |
|                | Canadian     | 550               |  | 2011          | 16673          |
|                | Oklahoma     | 515               |  | 2010          | 8228           |

| ODOT Divisions | County      | Count Site Number | Location   | Year (Latest) | AADT (Maximum) |
|----------------|-------------|-------------------|--|---------------|----------------|
| 5              | Roger Mills | 516               |  | 2011          | 622            |
|                | Dewey       | 511               |  | 2006          | 444            |
|                | Blaine      | 505               |  | 2010          | 900            |
|                | Custer      | 549               |  | 2010          | 1871           |
|                | Beckham     | 533               |  | 2007          | 1279           |
|                | Washita     | 502               |  | 2006          | 1168           |
|                | Harmon      | 512               |  | 2011          | 289            |
|                | Greer       | 517               |  | 2006          | 522            |
|                | Kiowa       | 566               |  | 2010          | 3085           |
|                | Jackson     | 507               |  | 2011          | 681            |
|                | Tillman     | 522               |  | 2011          | 598            |
| 6              | Cimaron     | 544               |  | 2006          | 265            |
|                | Texas       | 515               |  | 2010          | 1511           |
|                | Beaver      | 509               |  | 2011          | 549            |
|                | Harper      | 519               |  | 2007          | 880            |
|                | Woods       | 108               |  | 2010          | 522            |
|                | Alfalfa     | 502               |  | 2011          | 749            |
|                | Ellis       | 535               |  | 2010          | 1007           |
|                | Woodward    | 518               |  | 2011          | 1854           |
|                | Major       | 524               |  | 2006          | 1065           |
| 7              | Caddo       | 540               | .3 miles north of EW 197<br>.6 miles north of EW 183<br>.5 miles north of EW 190 | 2010          | 2150           |
|                | Grady       | 503               |  | 2010          | 3189           |
|                | Comanche    | 563               |  | 2011          | 6065           |
|                | Stephens    | 524               |  | 2008          | 2602           |
|                | Murray      | 505               |  | 2007          | 834            |
|                | Carter      | 536               |  | 2011          | 1922           |
|                | Cotton      | 513               |  | 2006          | 348            |
|                | Jefferson   | 401               |  | 2010          | 472            |
|                | Love        | 510               |  | 2011          | 830            |
| 8              | Osage       | 559               | .49 miles east of D 0300   | 2011          | 3571           |
|                | Pawnee      | 523               |  | 2006          | 1546           |
|                | Creek       | 549               |  | 2011          | 4176           |
|                | Washington  | 520               |  | 2011          | 1867           |
|                | Tulsa       | 527               |  | 2011          | 2223           |
|                | Nowata      | 506               |  | 2010          | 543            |
|                | Rogers      | 522               |  | 2011          | 3705           |
|                | Craig       | 400               |  | 2010          | 2189           |

| ODOT Divisions | County   | Count Site Number | Location                | Year (Latest) | AADT (Maximum) |
|----------------|----------|-------------------|-------------------------|---------------|----------------|
|                | Mayes    | 520               | .12 miles north of 69 A | 2010          | 3243           |
|                | Ottawa   | 503               | .1 miles north of E/W 5 | 2006          | 1557           |
|                | Delaware | 507               |                         | 2007          | 4072           |

## **Appendix C**

Central Oklahoma industrial park directory

Table 40. Candidate road with high truck traffic (Industrial park directory)

| INDUSTRIAL PARK NAME                       | CITY         | COUNTY        | ACRES  |
|--|--------------|---------------|--------|
| Ardmore Industrial Airpark                 | Ardmore      | Carter        | 2955   |
| Interstate Industrial Park                 |              |               | 33     |
| New Horizons Park                          |              |               | 190    |
| Westport Industrial Park                   |              |               | 190    |
| Henshaw Industrial Park                    | Broken Arrow | Tulsa/Wagoner | 120    |
| Henshaw South Industrial Park              |              |               | 55     |
| Lynn Lane Business Park                    |              |               | 17     |
| Clinton-Sherman Industrial Airpark         | Burns Flat   | Washita       | 2700   |
| Chickasha Regional Airport Industrial Park | Chickasha    | Grady         | 340    |
| Methvin Industrial Park                    |              |               | 18     |
| Andrew Little Industrial Park              | Cushing      | Payne         | 43     |
| South Industrial Park                      |              |               | 52     |
| Duncan Area Industrial Park                | Duncan       | Stephens      | 347    |
| Duncan Area Industrial Park South          |              |               | 159.91 |
| Durant Industrial Park                     | Durant       | Bryan         | 114    |
| Eaker Field Airport Industrial Park        |              |               | 400    |
| International Business Park                |              |               | 320    |
| Canadian Valley Industrial Park            | El Reno      | Canadian      | 160    |
| El Reno Industrial Park                    |              |               | 50     |
| El Reno Industrial Park II                 |              |               | 73.5   |

| INDUSTRIAL PARK NAME                  | CITY         | COUNTY       | ACRES  |
|---------------------------------------|--------------|--------------|--------|
| Cimarron Industrial Airpark           | Enid         | Garfield     | 133.5  |
| Garfield County Industrial Park       |              |              | 142    |
| Frederick Airport Industrial Park     | Frederick    | Tillman      | 1440   |
| Tinker Business and Industrial Park   | Midwest City | Oklahoma     | 70     |
| Davis Field Industrial Park           | Muskogee     | Muskogee     | 550    |
| East Pointe West Bus And Ind Park     |              |              | 119.9  |
| Muskogee Industrial Complex           |              |              | 400    |
| Muskogee Port Industrial Park         |              |              | 388.27 |
| Okmulgee Airport Industrial Park      | Okmulgee     | Okmulgee     | 589    |
| Okmulgee South Industrial Park        |              |              | 260    |
| MidAmerica Industrial Park            | Pryor Creek  | Mayes        | 9000   |
| North Airport Industrial Park         | Shawnee      | Pottawatomie | 262    |
| Shawnee Industrial Park               |              |              | 20     |
| Shawnee Municipal Airport (Airport)   |              |              | 40     |
| Wolverine Industrial Park             |              |              | 160    |
| Airport Industrial Park               | Stillwater   | Payne        | 50     |
| O'Haver Industrial Park               |              |              | 60     |
| Oklahoma Technology and Research Park |              |              | 160    |
| Stillwater Industrial Park            |              |              | 800    |
| Woodward Industrial Airpark           | Woodward     | Woodward     | 720    |

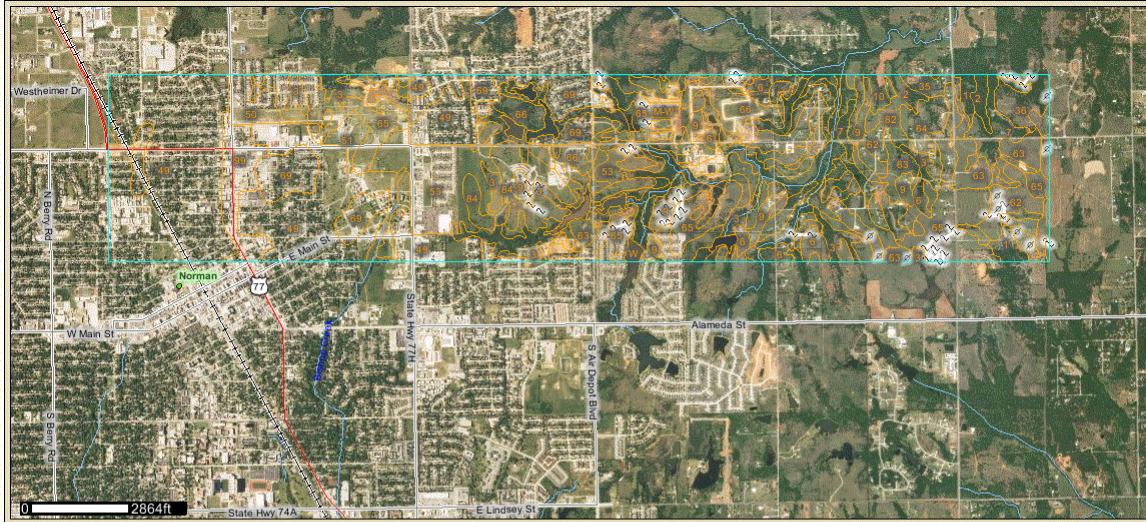
## **Appendix D**

Locations of candidate roads for a field test section in this study together with their subgrade properties



Table 41. Locations of high AADT candidate roads in Central Oklahoma

| ODOT Divisions | City          | Count Site # | Location      | Year | AADT |
|----------------|---------------|--------------|---------------|------|------|
| 3              | Oklahoma City | 116          | SE 149th St   | 2010 | 3312 |
|                |               | 505          |               |      | 3428 |
|                | McCloud       | 443          | 192nd Ave NE  |      | 4113 |
|                |               | 537          |               |      | 4563 |
|                | Norman        | 502          | S Western Ave |      | 3381 |
|                |               | 504          | E Franklin Rd |      | 3796 |
|                |               | 506          | 60th Ave NW   |      | 3285 |
|                |               | 435          | Alameda St    |      | 3644 |
|                |               |              |               |      | 4284 |
|                |               | 542          | E Robinson St |      | 3812 |
|                |               | 549          | Alameda DR    |      | 3063 |
|                | Nobel         | 514          | E Maguire Rd  |      | 3194 |



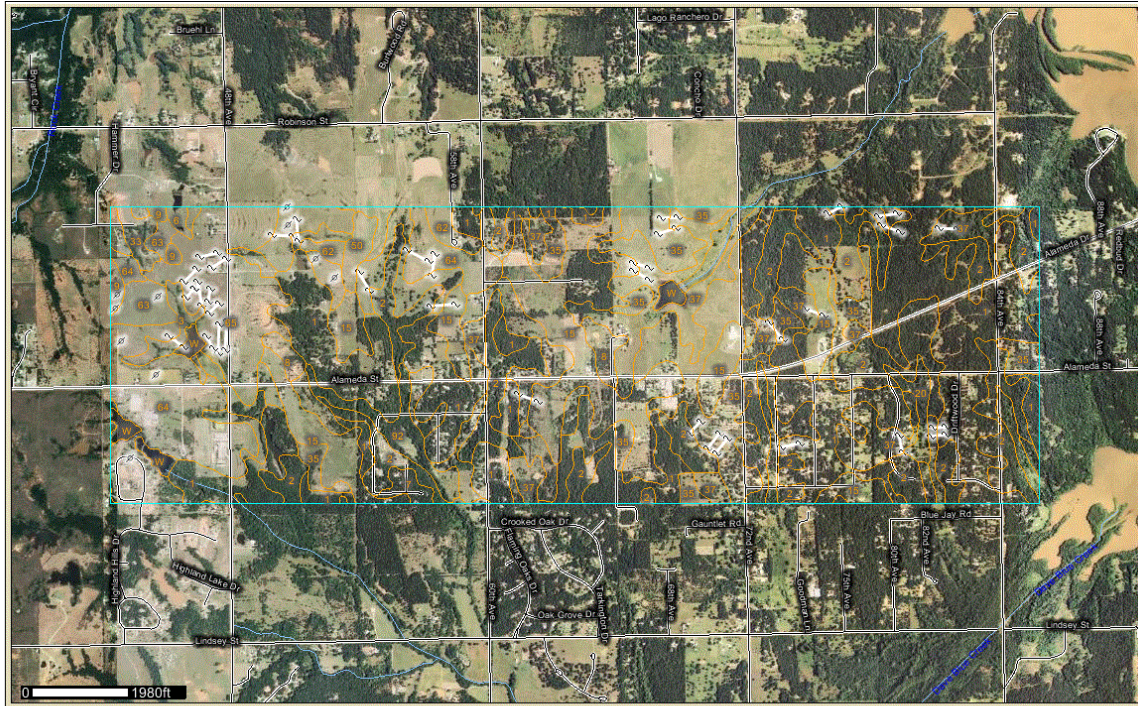
**Report — Engineering Properties**

Absence of an entry indicates that the data were not estimated. The asterisk '\*' denotes the representative texture; other possible textures follow the dash.

**Cleveland County, Oklahoma**

| Map unit symbol and soil name                   | Depth     | USDA texture                      | Classification       |               | Fragments  |             | Percentage passing sieve number— |        |        |       | Liquid limit | Plasticity index |
|---|-----------|-----------------------------------|----------------------|---------------|------------|-------------|----------------------------------|--------|--------|-------|--------------|------------------|
|   |           |                                   | Unified              | AASHTO        | >10 inches | 3-10 inches | 4                                | 10     | 40     | 200   |              |                  |
|   | <i>In</i> |                                   |                      |               | <i>Pct</i> | <i>Pct</i>  |                                  |        |        |       | <i>Pct</i>   |                  |
| 2—Harrah fine sandy loam, 5 to 8 percent slopes |           |                                   |                      |               |            |             |                                  |        |        |       |              |                  |
| Harrah  | 0-6       | *Fine sandy loam                  | CL-ML, ML, SC-SM, SM | A-4           | 0          | 0           | 95-100                           | 95-100 | 94-100 | 36-60 | 15-26        | NP-7             |
|   | 6-14      | *Loamy fine sand, Fine sandy loam | CL-ML, ML, SC-SM, SM | A-2, A-4      | 0          | 0           | 95-100                           | 95-100 | 94-100 | 15-60 | 0-26         | NP-7             |
|   | 14-51     | *Sandy clay loam, Fine sandy loam | SC-SM, CL, CL-ML, SC | A-4, A-6      | 0          | 0           | 95-100                           | 95-100 | 90-100 | 36-65 | 20-37        | 5-16             |
|   | 51-80     | *Sandy clay loam, Fine sandy loam | SC, SC-SM, CL, CL-ML | A-2, A-4, A-6 | 0          | 0           | 70-100                           | 70-100 | 60-100 | 25-65 | 20-37        | 5-16             |

Figure 99. Subgrade soil properties along East Robinson Street, Norman, Oklahoma  
(Source: USDA-WSS)



**Report — Engineering Properties**

Absence of an entry indicates that the data were not estimated. The asterisk "\*" denotes the representative texture; other possible textures follow the dash.

**Cleveland County, Oklahoma**

| Map unit symbol and soil name                   | Depth     | USDA texture                      | Classification       |               | Fragments  |             | Percentage passing sieve number— |        |        |       | Liquid limit | Plasticity index |
|---|-----------|-----------------------------------|----------------------|---------------|------------|-------------|----------------------------------|--------|--------|-------|--------------|------------------|
|   |           |                                   | Unified              | AASHTO        | >10 inches | 3-10 inches | 4                                | 10     | 40     | 200   |              |                  |
|   | <i>In</i> |                                   |                      |               | Pct        | Pct         |                                  |        |        |       | Pct          |                  |
| 2—Harrah fine sandy loam, 5 to 8 percent slopes |           |                                   |                      |               |            |             |                                  |        |        |       |              |                  |
| Harrah  | 0-6       | *Fine sandy loam                  | CL-ML, ML, SC-SM, SM | A-4           | 0          | 0           | 95-100                           | 95-100 | 94-100 | 36-60 | 15-26        | NP-7             |
|   | 6-14      | *Loamy fine sand, Fine sandy loam | CL-ML, ML, SC-SM, SM | A-2, A-4      | 0          | 0           | 95-100                           | 95-100 | 94-100 | 15-60 | 0-26         | NP-7             |
|   | 14-51     | *Sandy clay loam, Fine sandy loam | SC-SM, CL, CL-ML, SC | A-4, A-6      | 0          | 0           | 95-100                           | 95-100 | 90-100 | 36-65 | 20-37        | 5-16             |
|   | 51-80     | *Sandy clay loam, Fine sandy loam | SC, SC-SM, CL, CL-ML | A-2, A-4, A-6 | 0          | 0           | 70-100                           | 70-100 | 60-100 | 25-65 | 20-37        | 5-16             |

Figure 100. Subgrade soil properties along Alameda Street, Norman, Oklahoma  
(Source: USDA-WSS)